SUBTLE HETEROGENEITY OF HIGH-AFFINITY CHOLINE TRANSPORTER EXPRESSION AND LOCALIZATION IN LIMBIC PROJECTIONS OF THE CHOLINERGIC BRAINSTEM TEGMENTUM

by

Ericka C. Holmstrand

B.S. Neuroscience, Brown University, 2000

Submitted to the Graduate Faculty of

University of Pittsburgh School of Arts & Sciences

in partial fulfillment

of the requirements for the degree of

Doctor of Philosophy

University of Pittsburgh

2010

UNIVERSITY OF PITTSBURGH

School of Arts & Sciences

This dissertation was presented

by

Ericka C. Holmstrand

It was defended on

September 21, 2010

and approved by

J. Patrick Card, Ph.D., Professor, Department of Neuroscience

Anthony A. Grace, Ph.D., Professor, Departments of Neuroscience, Psychiatry, and Psychology

Bita Moghaddam, Ph.D., Professor, Departments of Neuroscience and Psychiatry

Robert A. Sweet, M.D., Professor, Departments of Psychiatry and Neurology

Philip Winn, Ph.D., Professor, Strathclyde Institute of Pharmacy and Biomedical Science

Dissertation Advisor: Susan R. Sesack, Ph.D., Departments of Neuroscience and Psychiatry

SUBTLE HETEROGENEITY OF HIGH-AFFINITY CHOLINE TRANSPORTER EXPRESSION AND LOCALIZATION IN LIMBIC PROJECTIONS OF THE CHOLINERGIC BRAINSTEM TEGMENTUM

Ericka C. Holmstrand, Ph.D.

University of Pittsburgh, 2010

The high-affinity choline transporter (CHT) supplies the substrate, choline, for the synthesis of acetylcholine (ACh) within cholinergic neurons. Choline uptake mediated by this protein has been studied for over 30 years and many of the regulatory mechanisms governing its function are well characterized. Early studies, as well as more recent investigations, focused on specific populations of cholinergic axons in the brain, namely the cholinergic innervations of cortical, striatal, and hippocampal regions. Details of the expression and subcellular localization of the high-affinity choline transporter within the projections of the pedunculopontine (PPT) and laterodorsal (LDT) tegmental cholinergic neurons have not been examined. The studies described herein compare the cholinergic axons within two limbic regions that are innervated by the ascending projections from these brainstem nuclei. These experiments were designed to characterize: 1) the relative amount and pattern of subcellular localization of the high-affinity

choline transporter protein in the axon varicosities of this projection system; 2) the co-expression of the high-affinity choline transporter and the vesicular acetylcholine transporter in these two populations of axon varicosities; and 3) the organization and possible collateralization of projections of the cholinergic neurons that provide cholinergic innervation to these regions. The results of these studies indicate that the expression and localization of the high-affinity choline transporter differs only subtly across brain regions innervated by the brainstem tegmental cholinergic neurons, and suggest that these differences may be accounted for by a pattern of specific innervation arising from distinct subsets of pedunculopontine and laterodorsal tegmental cholinergic neurons.

TABLE OF CONTENTS

LIST OF TABLES

LIST OF FIGURES

PREFACE

This dissertation is the culmination of several years' work at the University of Pittsburgh. Throughout my graduate studies, I have been supported and encouraged by many individuals in both within the scientific community and outside of the University as well. First, I would like to acknowledge my thesis advisor, Dr. Susan R. Sesack, for her unwavering support and encouragement of me as I struggled to develop workable projects and to unite my experiments in a common theme. In addition to providing a supportive research environment for me to explore new ideas, Dr. Sesack has been a source of tremendous emotional support and valuable perspective during the often frustrating process of learning to design, direct, and interpret my own research.

In developing and interpreting these experiments, all of the members of my committee have influenced my thinking scientifically, and I am grateful to have had their insight and involvement in my graduate experience. In particular, I would like to thank the chair of my thesis committee, Dr. J Patrick Card, for his advice throughout my graduate education, and for his practical and collegial manner during our committee meetings and other interactions.

Many faculty members, post-doctoral researchers, and graduate students have assisted me with advice, technical expertise, and access to equipment and other resources during my graduate study. In particular, Dr. Robert Sweet and Dr. Kenneth Fish generously and enthusiastically assisted me with the design and implementation of the dual immunofluorescence study detailed

in Chapter 3. Although the pilot projects that I worked on in their labs did not lead to larger final experiments, I greatly appreciated the generosity and patience of Dr. Bita Moghaddam and Alicia Lisowitz, as well as that of Dr. Gonzalo Torres, Marisol Quiroz, and Loreto Egaña, as they supported and aided my experimental efforts. My interactions with members of the departmental neuroanatomy group helped me to identify solutions to technical problems and analytical approaches to my experiments, in addition to providing a fun community of researchers with whom to discuss science in a collegial setting.

I also have to thank many of the graduate students & post-doctoral researchers who have become my good friends over the last seven years. The years I have spent living and working in Pittsburgh have been some of the most enjoyable in my life, and I feel lucky to have been a part of the neuroscience community here, and to have experienced the warmth and friendship of the larger community of Pittsburgh.

Finally, to Drew Celley, who has supported and encouraged me through my toughest moments, kept me on this path, and who continues to be my source of strength and joy. I could not have completed this journey without you, and I am reminded daily of how lucky I am to have your friendship and our partnership in my life.

1.0 INTRODUCTION

This thesis examines the pattern of expression and subcellular localization of the high-affinity choline transporter (CHT) within cholinergic axons arising from the brainstem tegmental cholinergic system. The characteristics of CHT in these axons are compared across two important components of the limbic system, the anteroventral nucleus of the thalamus (AVN) and the ventral tegmental area (VTA). The differences in CHT observed across these regions are further characterized in relation to the pattern of innervation of these regions by brainstem cholinergic neurons.

1.1 CHOLINERGIC SYSTEMS IN THE MAMMALIAN CNS

Acetylcholine (ACh) is a phylogenetically ancient chemical transmitter, and has been adapted for an impressive range of functional roles by different species and at different sites within the vertebrate nervous system (Cooper et al 2003). In mammals, ACh serves as the excitatory transmitter at the neuromuscular junction and is also utilized extensively throughout the autonomic and central nervous systems. ACh exerts its effects through a large number of ionotropic and metabotropic receptor subtype and so can have vastly different effects on post-synaptic cells. ACh is synthesized and released by many different groups of neurons in the brain, as illustrated in Figure 1, including interneurons that provide local innervation in the

striatum, and projection neurons in the forebrain and the brainstem (Mesulam et al 1983; Woolf 1991) that provide cholinergic innervation to most cortical and subcortical structures.

The projections of different cholinergic groups are organized such that the brain regions innervated by each major group are largely non-overlapping. For simplicity, these projections systems can be divided into two loose groups. Cholinergic neurons in several forebrain nuclei (e.g. diagonal band nuclei, nucleus basalis of Meynert, medial septum) provide the majority of acetylcholine innervation to the olfactory bulb, cerebral cortex and hippocampal formation, (Mesulam et al 1983; Woolf 1991). ACh release in frontal cortical regions modulates cognitive processing and is important for directing attention towards information that is relevant to on-going, goal-directed behavior (Himmelheber et al 2000; 2001). In contrast, the majority of ACh innervation of the thalamus and midbrain originates from a second group of neurons in the brainstem mesopontine tegmentum. Cholinergic neurons located within the pedunculopontine tegmental (PPT) and laterodorsal tegmental (LDT) nuclei have ascending projections to subcortical limbic structures. Limbic targets of PPT and LDT cholinergic axons contribute to cognitive and emotional processing through their anatomical interconnection with other cortical and subcortical limbic areas. Ascending cholinergic innervation from the PPT/LDT is present in many areas that are heavily interconnected with each other (Woolf & Butcher 1986). The brainstem cholinergic system can therefore influence a variety of cognitive and behavioral processes, and represents a powerful modulatory force in the brain (Winn 1998; 2008).

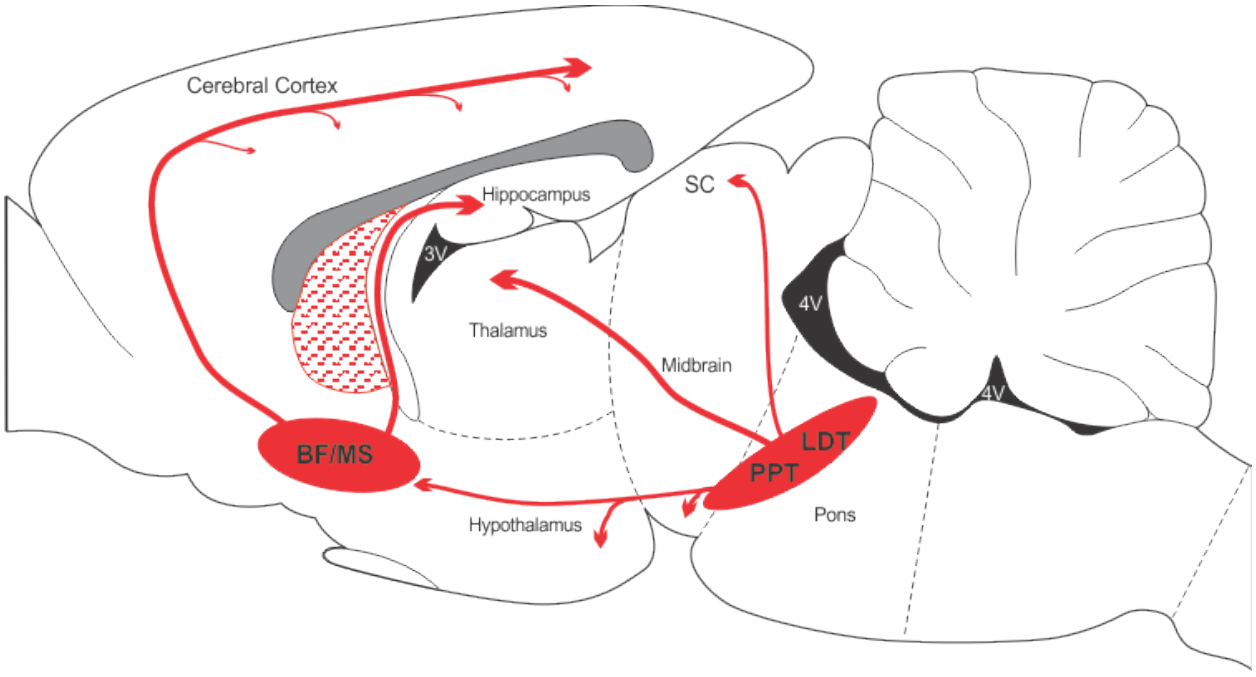

Figure 1 Major sources of cholinergic innervation to limbic structures in the mammalian nervous system.

Separate groups of ACh-synthesizing cells modulate neuronal activity in different forebrain and midbrain structures. Cholinergic cells in the basal forebrain (**BF**), medial septum (MS) provide ACh innervation of the cortical mantle and hippocampal formation, respectively. The brainstem PPT/LDT nuclei have ascending cholinergic projections that innervate a broad variety of subcortical brain regions, such as the thalamus, hypothalamus, superior colliculus, and ventral midbrain. In contrast, the ACh in the striatum (stippled region) is released by a network of intrinsic interneurons. Illustration is modeled after (Woolf 1991), using a base sagittal plane illustration from (Paxinos & Watson 1997).

1.2 BRAINSTEM TEGMENTAL CHOLINERGIC NEURONS

As indicated above, the brainstem PPT and LDT cholinergic neurons provide a substantial proportion of the ascending cholinergic innervation to subcortical structures in the midbrain and forebrain. The cellular and physiological characteristics of these neurons, and their anatomical connectivity with other brain regions, indicate that there are heterogenous sub-populations of cholinergic neurons within the larger grouping of the PPT/LDT.

1.2.1 Morphological Characteristics and Anatomical Organization

Cholinergic neurons in the brainstem tegmentum are typically large, multipolar neurons radiating multiple primary dendrites (Hallanger et al 1987; Hallanger & Wainer 1988; Jones 1995). These cells are distributed in two densely packed groups within the brainstem, in the lateral portion of the PPT, where ACh neurons are clustered around the lateral margin of the brachium of the superior cerebellar peduncle (Woolf 1991; Lavoie & Parent 1994), and, more caudally, within the ventral portion of the periaqueductal gray matter designated as the LDT. This nucleus is bordered rostrally by the dorsal tegmental nucleus and both dorsally and medially by the dorsal raphé nucleus. Cholinergic neurons are also found in a ventral extension of the LDT, scattered within the medial longitudinal fasciculus (*mlf)* and in the dorsolateral reticular field that lies immediately ventral to this fiber tract. A third group of ACh cells are found

scattered within the medial PPT (or PPT *pars dissipata*, PPTd) a region of the dorsolateral tegmentum that is bounded laterally and dorsally by the superior cerebellar peduncle (*scp)* (Lavoie & Parent 1994). Cholinergic neurons are more loosely distributed throughout the PPTd, and are intermingled with numerous non-cholinergic cells, some of which are glutamatergic (Clements & Grant 1990). Although non-cholinergic neurons are found in the lateral PPT and the LDT as well, they account for a larger proportion of cells in the PPTd (Rye et al 1987).

PPT and LDT neurons provide ACh innervation to a large number of subcortical areas, including many thalamic and hypothalamic nuclei, the lateral septum, and basal forebrain (Satoh & Fibiger 1986; Hallanger et al 1987; Hallanger & Wainer 1988; Cornwall et al 1990; Bina et al 1993). Through these subcortical projections, PPT/LDT neurons can have pronounced effects over a range of behaviors (Inglis & Winn 1995). For example, cholinergic projections to the thalamus indirectly influence neural activity in cortical regions, as the thalamic relay nuclei targeted by PPT/LDT cholinergic projections contain the cell bodies of the major excitatory afferents to the neocortex (Groenewegen & Witter 2004). ACh release in the thalamus results in the activation of thalamocortical neurons, thereby influencing cortical excitability indirectly (Hu et al 1988; Paré et al 1990; Curro Dossi et al 1991). Cholinergic projections from the brainstem that target the intralaminar thalamic nuclei can alter neural processing in cortico-subcortical circuitry by modulating the activity of thalamostriatal projection neurons (Erro et al 1999). Additionally, projections to the locus coeruleus, raphé nuclei, and midbrain substantia nigra *pars compacta* (SNc) and ventral tegmental area (VTA) modulate, respectively, the activity of norephinephrine (NE), serotonin (5-hydroxytryptamine; 5-HT), and dopamine (DA) projection neurons that innervate widespread areas in the cerebral cortex, thalamus, hippocampus, and other forebrain structures (Mesulam et al 1983; Woolf & Butcher 1986; Woolf 1991).

The projections of the PPT and LDT are organized in a loose topography, such that the PPT projects more heavily to sensorimotor-associated structures (e.g. relay nuclei of the thalamus, the SNc (Beninato & Spencer 1987; Clarke et al 1987)), while the projections of the LDT more commonly target limbic-related regions, such as the midline and intralaminar nuclei of the thalamus (Satoh & Fibiger 1986), and the VTA (Oakman et al 1995). Similarly, the reciprocal projections of many regions innervated by the cholinergic brainstem neurons show a preferential targeting of the nucleus from which its input arises (Semba & Fibiger 1992; Steininger et al 1992). The functional topography of PPT and LDT projections is not strict, as most targets of ascending PPT/LDT axons receive projections from both brainstem tegmental nuclei. Rather, some structures have afferent populations that are more heavily drawn from either the PPT or the LDT (Satoh & Fibiger 1986; Hallanger & Wainer 1988; Oakman et al 1995).

In addition, axon collaterals of single PPT/LDT neurons have been shown to project to multiple targets, indicating that ACh release might be coordinated across disparate brain regions (Woolf & Butcher 1986). In particular, it has been reported that almost all cholinergic neurons in the cholinergic mesopontine tegmentum send a projection to the thalamus, implying that the innervation of non-thalamic targets results from the collateralization of ascending cholinergic axons (Oakman et al 1999). PPT/LDT neurons can innervate multiple thalamic nuclei (Steriade et al 1990a; Bolton et al 1993) and separate studies have demonstrated collateralized input to both a thalamic target and the basal forebrain (Losier & Semba 1993), cerebral cortex (Jourdain et al 1989), olfactory bulb (Cornwall & Phillipson 1989), superior colliculus (Billet et al 1999), or the VTA (Bolton et al 1993). Despite these observations, the organization of collateral

projections from PPT/LDT neurons to specific combinations of discrete thalamic nuclei and non-thalamic targets is far from fully understood.

1.2.2 Heterogeneity of Physiological Characteristics in PPT/LDT cells

The best-characterized PPT/LDT neurons are the large, ACh synthesizing cells with ascending projections throughout the forebrain. Neurons that utilize glutamate or GABA as a neurotransmitter are interspersed among the cholinergic cells, and these transmitters may be co-released by ACh neurons as well (Clements & Grant 1990; Lavoie & Parent 1994; Ford et al 1995; Grofova & Zhou 1998; Parent et al 1999; Jia et al 2003; Hur & Zaborszky 2005). Cholinergic PPT/LDT neurons express NADPH-diaphorase (Lavoie & Parent 1994; Lolova et al 1996; Nemcova et al 2000), a nitric oxide synthase, and actively generate nitric oxide as a signaling agent (Williams et al 1997), although ACh neurons are not unique in the tegmentum in expression of this enzyme (Scherer-Singler et al 1983). Finally, some ACh neurons colocalize various neuropeptides, including substance P (Vincent et al 1983; Sutin & Jacobowitz 1990), corticotrophin releasing factor, and atriopeptin (Crawley et al 1985; Standaert et al 1986). Although some targets of ACh and peptide co-expressing neurons have been identified (Crawley et al 1985), the specific projections of the ACh/neuropeptidergic neurons have not been thoroughly explored.

Electrophysiological recordings in the rat and cat indicate that the component neurons of the PPT and LDT have heterogeneous firing rates and responses to stimulation. Cells with fast or slow spontaneous firing rates have been identified (Steriade et al 1990a), and at least three separate groups of neurons have been postulated on the basis of ionic currents and firing patterns

(Kang et al 1990; Reese et al 1995b). Furthermore, the correlation of activity in PPT/LDT neurons with behavioral states (i.e. wake (W), slow-wave sleep (SWS), and rapid eye movement sleep (REM)) reveals at least three sub-populations of tegmental neurons within the PPT and LDT (Steriade et al 1990a; Datta & Siwek 2002). Many neurons show elevated firing during W and REM sleep, some display progressive increases in activity across stages, with REM firing > SWS > W, and still others have behavioral state-independent spontaneous rates of activity.

Unfortunately, these physiologically-defined groups do not strictly correspond to distinct neurochemical phenotypes (Leonard & Llinás 1990), but there are indications that most mesopontine tegmental cholinergic neurons display tonic firing patterns, increased activity in W and REM states, and an absence of low-threshold calcium currents that underlie some neuronal bursting behavior. Some of these neurons may be capable of firing bursts of action potentials (Wilcox et al 1989), through the activation high-threshold calcium currents (Kang et al 1990; Leonard & Llinás 1990), and so might fire differentially based on their relative depolarization state, but this possibility is still contentious. Although cholinergic PPT/LDT neurons are all thought to have relatively fast (>10 Hz) spontaneous firing rates, the tonic firing rates observed within this physiological category still displays some variability across neurons, indicating that some cholinergic PPT/LDT cells probably fire action potentials at higher resting rates than others (Steriade et al 1990a).

Although in vitro and in vivo recordings have provided invaluable information on the activity of brainstem neurons, it is, as yet, practically impossible to determine the biophysical properties of a neuron, its behaviorally correlated responses, its innervation targets, and its neurochemical phenotype within the a single experiment. The variable physiological characteristics of PPT/LDT neurons imply that there may be significant heterogeneity along a

number of dimensions within this group of cells that is only beginning to be understood (Steriade et al 1990b). Nevertheless, it is clear that subgroups of PPT/LDT neurons are likely to mediate different functional roles in their projections to the forebrain through unique activity patterns and distinctive receptor targets.

1.2.3 Ascending Projections from the Cholinergic PPT/LDT: Functional Effects in Distinct Innervation Targets

The major function generally ascribed to ascending cholinergic projections from the tegmental brainstem is the promotion of arousal. Stimulation of the brainstem projections to the thalamus generally increases the responsiveness of thalamocortical neurons to inputs from other regions (Steriade et al 1997) (e.g. glutamatergic corticothalamic afferents, hypothalamic inputs, etc.) and increases *c*-Fos expression in selected thalamic nuclei, confirming a general activating effect of PPT signaling (Ainge et al 2004). Furthermore, the increased activity in the PPT/LDT that appears during W and REM states mediates a switch in the mode of thalamic firing, producing the characteristic changes in electroencephalographic recordings that are used to define sleep states (Steriade et al 1990a; Williams et al 1997; Huitron-Resendiz et al 2005).

Overall, the excitatory effects of brainstem cholinergic input to the thalamus are thought to facilitate the entry of sensory information into the cortico-subcortical circuits that connect distinct cortical regions with topographically specific parts of the basal ganglia and thalamus, and that mediate complex behaviors such as cognition and goal-oriented behavioral selection (Inglis & Winn 1995; Ding et al 2010). In addition, the projections to the intralaminar nuclei in the thalamus can potentially influence cortical activation globally, as the thalamocortical projections of these nuclei are diffuse throughout the cortex (Berendse & Groenewegen 1991;

Groenewegen & Witter 2004; Vertes et al 2006). Similarly, in non-thalamic targets of brainstem tegmental ACh innervation, the net effect of cholinergic stimulation appears to be increased excitability of primary circuit neurons and decreases in inhibitory tone impinging on these cells (Kobayashi & Isa 2002). In the case of projections to the monoamine systems, increased excitability is noted with stimulation of the PPT/LDT, leading to greater monoaminergic tone in the forebrain regions innervated by these cells (Mesulam 1995a; Gronier & Rasmussen 1998; Mena-Segovia et al 2008). These effects are typically blocked by systemic or local administration of cholinergic antagonists, indicating that the activating effects of PPT/LDT activity are mediated, at least in part, by the cholinergic neurons in these areas (Hu et al 1988; Forster & Blaha 2000; Grillner et al 2000; Forster & Blaha 2003).

In awake animals, many PPT/LDT neurons respond in a time-locked manner to environmental stimuli in one or more modalities, including auditory, visual, somatosensory, and/or nociceptive systems (Grant & Highfield 1991; Pascoe & Kapp 1993; Reese et al 1995a; Kayalioglu & Balkan 2004; Pan & Hyland 2005). The sensory responsiveness of these neurons appears to facilitate detection of novel or behaviorally relevant environmental stimuli by forebrain systems (Kobayashi & Isa 2002), and these projections may have significance for the direction of attentional resources toward salient events in the outside world (Florio et al 1999; Mena-Segovia et al 2008; Wilson et al 2009).

1.2.4 Diversity of Cholinergic Signaling Mechanisms in Innervation Targets of PPT/LDT Neurons

While PPT/LDT is thought to generate a common “arousal” signal in forebrain systems, the actions of acetylcholine at a cellular level are likely to differ across regions receiving

tegmental cholinergic inputs. Specifically, ACh can exert its effects on a wide variety of receptors expressed by different cellular components of an innervated region. Nicotinic acetylcholine receptors (nAChRs) on post-synaptic dendrites or neuronal cell bodies mediate direct depolarization of neurons in the innervated region. In addition, activation of nAChRs on presynaptic axon terminals can increase neurotransmitter release by non-cholinergic afferents (McGehee et al 1995; Wonnacott 1997; MacDermott et al 1999; Schilström et al 2000). Depending on the specific subunit identity, the activation of G-protein coupled muscarinic acetylcholine receptors (mAChRs) can exert excitatory or inhibitory effects on neuronal firing, primarily through the activation or inactivation of potassium conductances (Cooper et al 2003). mAChRs are frequently localized to extrasynaptic sites on dendrites and cell bodies, and are expressed on some presynaptic terminals as well (Sikes & Vogt 1987; Sherman & Friedman 1990; Amadeo et al 1995; Zhou et al 2003; Oda et al 2007).

The localization of AChRs to non-synaptic sites indicates that volume transmission is a significant mode of communication utilized by cholinergic modulatory systems. Axo-axonic synapses are infrequently observed in regions where presynaptic modulation of transmitter release by acetylcholine has been demonstrated (Wonnacott 1997; Jones & Wonnacott 2004). Similarly, mAChRs on somatodendritic profiles are not usually associated with direct synaptic innervation. The expression of ACh receptors at these sites, some distance from cholinergic axon varicosities, implies that ACh must diffuse away from the point of its release to reach its receptor targets (reviewed in Descarries et al., 1997). Further evidence that volume transmission is used by cholinergic systems comes from the observation that central cholinergic axon varicosities often fail to form synapses despite the presence of synaptic vesicles within these profiles. The synaptic incidence, or proportion of axon terminals displaying the morphological

specializations associated with classical synapses, can be significantly lower than 100% and varies across brain regions, indicating that the release of ACh from non-synaptic sites may be more prominent in some regions than in others (Descarries et al 1997; Turrini et al 2001). Cholinergic axons within discrete thalamic nuclei show different rates of synapse formation (Hallanger et al 1990; Parent & Descarries 2008), even though the majority of thalamic cholinergic input comes from the brainstem PPT/LDT. Importantly, the cholinergic innervation of some brain regions appears to be entirely synaptic (Parent & Descarries 2008), indicating that the low synaptic incidence reported in other regions is not due to experimental factors limiting the ability to detect synaptic structures. The hetereogeneity of these axons and the great diversity in subunit composition and cellular localization of AChRs in different brain regions implies that ACh signaling probably differs considerably between targets of the same cholinergic group.

The collective differences in the anatomical organization of PPT/LDT cholinergic projections, in co-transmitter content, and in the physiological characteristics of these cells support the view that within the larger PPT/LDT complex, subsets of cholinergic neurons exist that might influence activity in their target structures in unique ways. Due to these differences, we hypothesized that the expression and regulation of the high-affinity choline transporter might show similar heterogeneity in the projections of the PPT/LDT as well.

1.3 HIGH-AFFINITY CHOLINE TRANSPORTER

ACh released from cholinergic axons must be enzymatically degraded by acetylcholinesterase, unlike the monoamine neurotransmitters (DA, NE, and 5-HT) that are primarily cleared from the extracellular space by specific reuptake transporters (Cooper et al

2003). The hydrolysis of ACh produces choline and acetate ions that then diffuse through the extracellular space. Extracellular choline is taken up by cholinergic neurons via the high-affinity choline transporter (CHT) and resynthesized into ACh.

CHT is a Na^+/Cl^- dependent membrane transporter that provides the substrate, choline, for acetylcholine (ACh) synthesis (Apparsundaram et al 2000; Okuda et al 2000; Löffelholz & Klein 2006). The expression of this protein is, with few exceptions (Lecomte et al 2005), limited to cholinergic neurons (Misawa et al 2001; Ferguson et al 2003; Kus et al 2003) and closely resembles that of the vesicular acetylcholine transporter (VAChT) and the acetylcholine synthetic enzyme choline acetyltransferase (ChAT). The highly matched expression pattern of CHT with ChAT and VAChT is consistent with its role in supporting ACh synthesis.

1.3.1 Cellular Expression of CHT

Although the expression of CHT is a strong indicator of cholinergic phenotype, high-affinity choline uptake characteristic of that mediated by CHT is detectable in some non-ACh-synthesizing cells, such as retinal photoreceptors (Masland & Mills 1980), skin (Haberberger et al 2002), and vascular smooth muscle (Lips et al 2003). Such ectopic expression of CHT indicates that transcription and translation of the gene is not necessarily exclusive to cholinergic neurons, but can be utilized by cells that have a high biological demand for choline.

Loss of CHT by genomic deletion does not preclude some synthesis of ACh (Matthies et al 2006), as the precursor choline may be acquired through low-affinity uptake transporters (Michel et al 2006) or derived from hydrolysis of membrane phospholipids (Zhao et al 2001). Still, the ability of cholinergic neurons to maintain elevated and/or sustained cholinergic signaling depends upon functional CHT expression. Loss of CHT at the mammalian

neuromuscular junction is fatal after birth (Ferguson et al 2004; Ferguson & Blakely 2004) due to paralysis of the diaphragm and subsequent asphyxiation. CHT heterozygotes (+/-) appear to have normal baseline levels of ACh, but neurotransmitter release quickly becomes depleted under conditions that require sustained elevations in ACh release (Bazalakova et al 2007). Finally, blockade of CHT with hemicholinium-3 (HC-3), a potent inhibitor of high-affinity choline uptake, results in decreased quantal ACh content (Van der Kloot et al 2000; Van der Kloot et al 2002).

At central cholinergic synapses, the consequences of CHT hypofunction are not as serious as for the NMJ. In fact, there is apparent variability in the levels of CHT protein among different sets of cells with cholinergic phenotype, identified by positive immunoreactivity for the vesicular acetylcholine transporter (VAChT) or the ACh synthesizing enzyme, choline acetyltransferase (ChAT). In the rat median eminence, CHT immunoreactivity is strikingly absent from fibers that contain both ChAT and VAChT (Misawa et al 2001). In the primate CNS, subpopulations of ChAT+/CHT- neurons have been described, and the relative size of these populations varies across different cholinergic neuronal groups (0-20% of all ChAT+ neurons within selected sets of ACh cells) (Kus et al 2003). Although absence of immunolabeling is not necessarily indicative of a total lack of expression of CHT protein, the varying degrees of colocalization observed suggest that levels of CHT protein may be heterogenous, even among the neurons of a single cholinergic group.

The proposed heterogeneity of CHT protein expression levels in relation to other cholinergic proteins is made possible by the specific genomic organization of genes necessary for the expression of cholinergic phenotype. The expression of VAChT and ChAT is coordinated through the targeted location of their corresponding genes into a single, “cholinergic

gene locus" (Erickson et al 1994; Eiden 1998). In contrast, CHT is transcribed from a separate chromosome (Eiden 1998; Ferguson & Blakely 2004), and mRNA levels are regulated independently from those of VAChT and ChAT (Slotkin et al 1994; Bissette et al 1996; Brock et al 2007). Although many factors that upregulate the expression of VAChT and ChAT also increase CHT expression (Berse et al 2005), differential regulation of gene expression can occur (Lecomte et al 2005). Increases in functional CHT appear at later developmental time points than developmental increases in ChAT (Zahalka et al 1993), and during the regeneration of damaged nerves, CHT is transcribed in significant quantities only after a new synaptic contact has been established (Oshima et al 2004). It appears that in developing axons, ChAT expression increases prior to upregulation of CHT, indicating that other sources of choline may suffice to meet the demand for acetylcholine synthesis in neurons with only low levels of ACh release (e.g. prior to the establishment of synapses). Furthermore, increased expression of CHT can compensate for ChAT hypofunction in mature animals (Brandon et al 2004), and the increases in functional choline uptake that are observed in cortical tissue from Alzheimer's patients probably represent compensatory mechanisms in the face of reduced cholinergic tone (Slotkin et al 1990; Slotkin et al 1994).

Recent evidence indicates that expression of CHT may be reduced or absent from some cholinergic synapses, and that synaptic strength can influence the level of CHT protein in axon terminals. CHT immunoreactivity is lost at "silent synapses" that lack post-synaptic nicotinic acetylcholine receptors (nAChRs) in ganglionic preparations from α3 nAChR knock-out mice (Krishnaswamy & Cooper 2009) suggesting that the activation of post-synaptic mechanisms resulting, in retrograde signaling to the presynaptic axon, are necessary to support continued expression and trafficking of CHT to cholinergic release sites.

Interestingly, ultrastructural examination of cholinergic axon varicosities in central cholinergic systems has revealed that many cholinergic axon varicosities fail to display synaptic contacts in the rat cortex (Umbriaco et al 1982; Turrini et al 2001), thalamus (Levey et al 1987; Hallanger et al 1990; Parent & Descarries 2008) and midbrain dopaminergic VTA (Omelchenko & Sesack 2006; Holmstrand et al 2010). The non-synapsing boutons contain synaptic vesicles, mitochondria, and transmitter-associated protein immunoreactivity such as ChAT or VAChT, and so are presumed to be active sites of transmitter release. Furthermore, non-synaptic release of neurotransmitters into the extracellular fluid environment (i.e. volume transmission) is accepted as a major mode of neurochemical signaling. At non-synaptic release sites, transmitter diffuses away from its parent axon to act on extrasynaptic receptors within the vicinity of the site of release, or at considerable distance from its axonal source (Agnati et al 1995; Bjelke et al 1995). Volume transmission is thought to be a particularly important mode of signaling for modulatory transmitters, such as ACh and monoamines (Fuxe et al 1988; Descarries et al 1997; Zoli et al 1998; Fuxe et al 2010).

The absence of classical synapses at these sites of release raises interesting questions concerning the expression of CHT in these axons. If activation of post-synaptic receptors is necessary for the continued axonal expression of CHT in central as well as autonomic cholinergic axons, then cholinergic pathways that release ACh from non-synaptic sites may not contain reduced amounts of CHT, and may rely on other sources to maintain adequate levels of ACh. Alternatively, the intracellular mechanisms regulating the trafficking of CHT may differ according to the type of cholinergic neurons considered, or the region into which they release ACh.

1.3.2 Membrane Trafficking of CHT

Newly synthesized CHT protein is modified post-translationally and trafficked predominantly to axons. Within cholinergic axons, CHT is localized to small synaptic vesicles (Ferguson et al 2003; Nakata et al 2004) and endosomal membranes (Ribeiro et al 2007a). Surprisingly, relatively little CHT is found in the plasma membrane under conditions of minimal neuronal activity. A predominantly vesicular localization of CHT has been observed at the neuromuscular junction (Nakata et al 2004), and in numerous brain regions, including the brainstem facial nucleus, striatum, interpeduncular nucleus, and VTA (Ferguson et al 2003; Holmstrand et al 2006; Holmstrand et al 2010). Expression of CHT in cultured cells yields a similar subcellular distribution of the protein (Krishnaswamy & Cooper 2009).

The localization of CHT to synaptic vesicle membranes enables the protein to be delivered to the plasma membrane as a consequence of ACh release (see Figure 2). Exocytosis of synaptic vesicles increases the high-affinity choline uptake in synaptosomes (Roskoski 1978) and *in vitro* slice (Antonelli et al 1981) and *in vivo* preparations (Apparsundaram et al 2005); the increases in choline transport are due to concomitant increases in the number of transporters situated in the plasma membrane (Ferguson et al 2003; Apparsundaram et al 2005). Increased ACh synthesis, required to support sustained cholinergic release through the refilling of depleted vesicular stores of ACh following high-frequency neuronal firing, is met by the increased capacity of high- affinity choline uptake that occurs as a result of the fusion of CHT containing synaptic vesicles during periods of high frequency neuronal activity.

CHT is removed from the plasma membrane via clathrin-dependent endocytosis (Ribeiro et al 2003), the same process by which synaptic vesicles are efficiently recycled at the synapse. However, the rate at which CHT is endocytosed through this mechanism can be modulated by

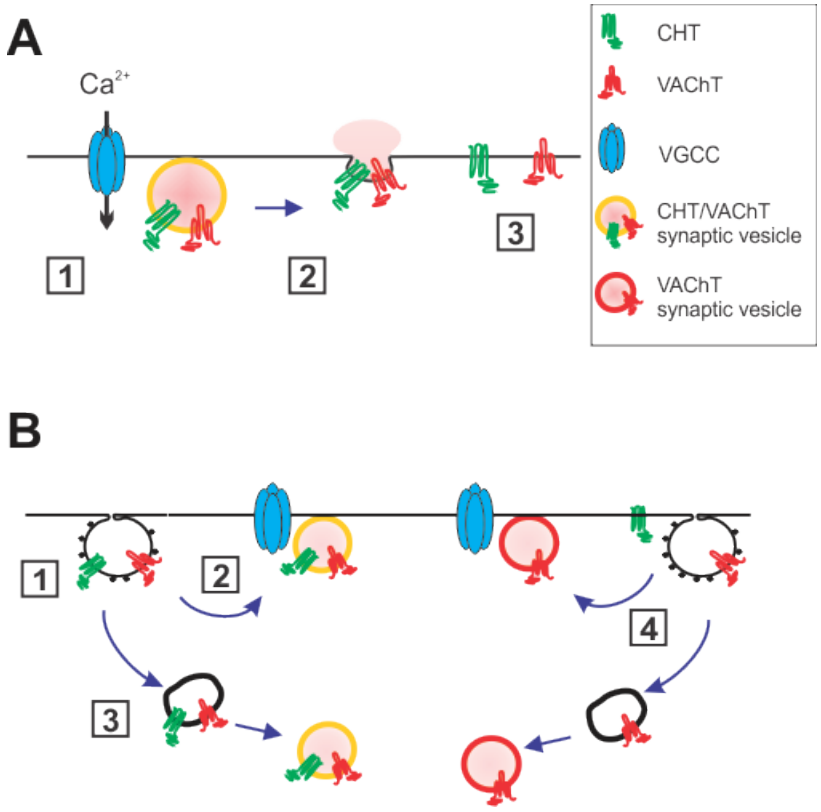

Figure 2 Plasma membrane trafficking of CHT

A CHT is delivered to the plasma membrane through fusion of synaptic vesicles containing both CHT and VAChT. Readily releasable vesicles are docked at the plasma membrane in close proximity to voltage-gated calcium channels (1). Ca^{2+} entry through these channels causes docked vesicles to fuse with the plasma membrane, releasing ACh during exocytosis and exposing the luminal surface of CHT to the extracellular space (2). The fusion of vesicular membrane with the plasmalemma results in the transfer of CHT to a functional pool mediating high-affinity choline uptake (3). **B** CHT is removed from the plasma membrane through clathrin mediated endocytosis (1). Recycled synaptic vesicles may be returned to the readily releasable pool (2) or trafficked through endosomal pathways to the reserve pool (3). Alternatively, CHT may be retained in the plasma membrane even as VAChT is endocytosed, resulting in VAChT+/CHT- synaptic vesicles (4).

intracellular signaling cascades. Phosphorylation by PKC, or inhibition of protein phosphatase 1/2A, promotes the internalization of CHT and decreases choline uptake (Ferguson & Blakely 2004; Gates et al 2004). Similarly, exposure to peroxynitrite or hydrogen peroxide appears to decrease choline uptake by accelerating the endocytosis of CHT, while leaving the rate of exocytosis unaltered (Pinthong et al 2008). Subcellular trafficking of CHT may be further regulated through interaction with other proteins (Ribeiro et al 2007b) such as vesicular-sorting proteins (SEC14-like protein, (Ribeiro et al 2007b)) and amyloid β (Aβ) (Bales et al 2006; Wang et al 2007) a protein implicated in the pathology of Alzheimer's disease.

The current view of CHT membrane trafficking is that only a small fraction of transporter molecules comprise a "recycling pool" of CHT that is inserted into the membrane, endocytosed, then redelivered to the plasma membrane within minutes (Ribeiro et al 2007a). New transporters are constitutively recruited to this pool, as evidenced by the complete restoration of choline transport within 2 hours of exposure to an irreversible antagonist of CHT (Ivy et al 2001). These pools of CHT-containing synaptic vesicles are believed to correspond to the "readily releasable" and "reserve" pools that have generally been described in other types of axon terminals (Pieribone et al 1995; Brodin et al 1997; Ferguson & Blakely 2004). The addition of new CHT molecules to the recycling pool of vesicles is presumably offset by removal of transporters from the membrane or readily releasable pool, producing stable rates of high-affinity choline uptake. However, increased choline transport is predicted to result from the accelerated recruitment of CHT-containing reserve pool vesicles to the readily releasable pool, thereby increasing the number of transporters that are cycling through the plasma membrane and vesicular compartments (Ivy et al 2001). The ultrastructural distribution of CHT may therefore be an indicator of recent synaptic activity or increases in tonic cholinergic tone (Grailhe et al 2009).

Elevations in neuronal activity mobilize reserve-pool vesicles to the releasable pool, thereby transiently increasing the number of transporters in the plasma membrane and the functional capacity of high-affinity choline uptake in highly active terminals (Figure 3). During periods of relative quiescence, endocytosis of CHT may exceed the rate of its delivery to the membrane, reestablishing lower equilibrium levels of choline uptake as the demand for ACh synthesis decreases. In terminals with higher expression of CHT, the amount of CHT in the recycling pool of vesicles would be elevated, leading to an increased level of CHT in the plasma membrane under baseline firing conditions. Increased activity in these terminals would result in a larger upregulation of choline transport as well (Figure 3B).

The utility of CHT localization as an indicator of synaptic activity is uncertain, however, because the rate of CHT internalization through endocytosis can be altered independently from the rate of its delivery to the plasma membrane. Although a few molecular players that influence the trafficking of CHT have been identified, much remains to be discovered. For instance, although phosphorylation of the transporter decreases choline uptake by promoting the endocytosis of CHT (Breer & Knipper 1990; Gates et al 2004), the cellular mechanisms that can alter phosphorylation of CHT at central synapses are only beginning to be identified. Activation of protein kinases through receptor-mediated mechanisms could also potentially modulate the capacity of high-affinity choline uptake at the level of individual cholinergic boutons.

It is difficult to say whether CHT density in the plasma membrane of different sets of cholinergic terminals would be relatively uniform across different brain regions or would vary due to differing local signaling environments or activity patterns. Still, in the cholinergic systems studied so far, activity dependent increases of CHT are extremely robust (Haga & Noda 1973; Simon & Kuhar 1975; Murrin & Kuhar 1976; Antonelli et al 1981; Krištofiková et al 1998).

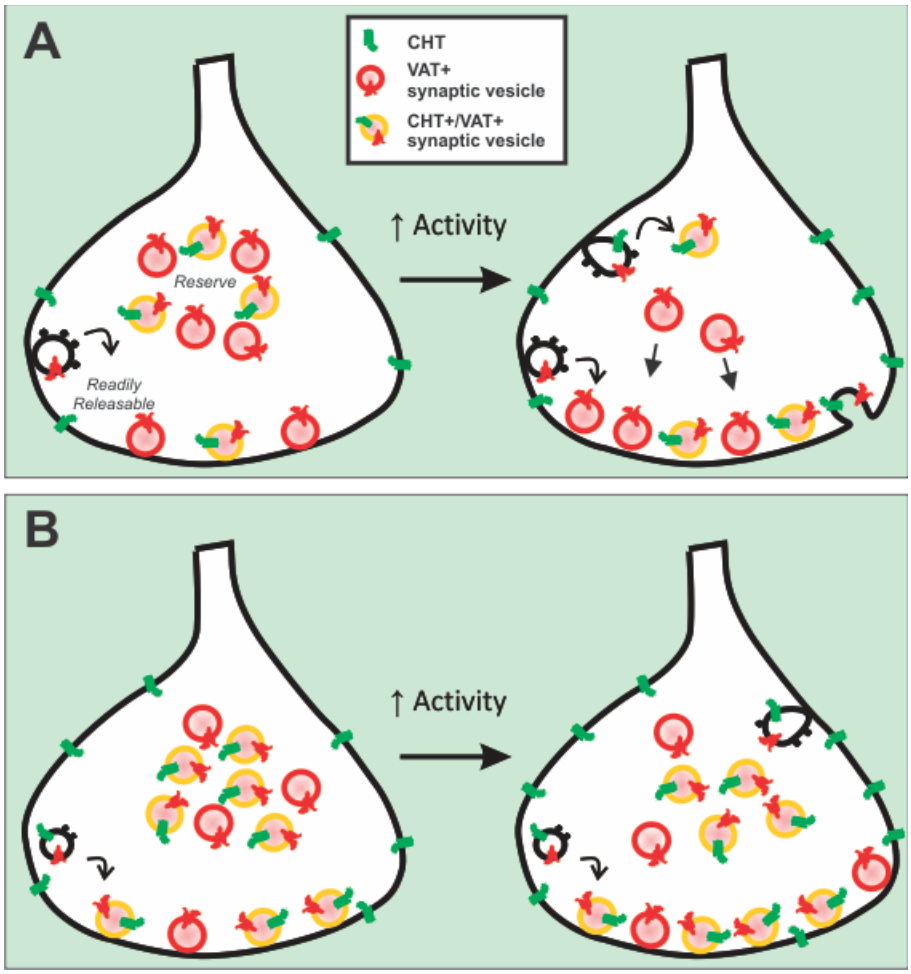

Figure 3 Membrane levels of CHT are upregulated by elevations in neuronal activity.

A Increases in ACh release lead to increased numbers of transporters in the plasma membrane through activity-dependent trafficking mechanisms. Sustained neuronal firing results in the recruitment of reserve pool vesicles to the readily releasable pool, increasing the number of transporters that are actively cycling between the plasma membrane and vesicular compartments. **B** The total level of CHT protein contained within synaptic vesicles affects the functional capacity of high-affinity choline transport. Axon terminals with more CHT-containing vesicles (compare B to A) have more CHT cycling through the readily releasable pool, higher levels of plasma membrane associated CHT, and consequently more choline uptake. When stimulated, axons with higher expression of CHT recruit more transporter containing vesicles to the readily releasable pool, resulting in larger increases in choline uptake.

This evidence indicates that the level of membrane CHT is primarily driven by relative levels of neuronal activity, and that higher overall levels of CHT protein probably support more active cholinergic release sites. The idea that CHT could serve as an indicator of activity in cholinergic varicosities suggests that different levels of total and membrane CHT should be detectable in brain regions innervated by distinct groups of cholinergic neurons. Additionally, given the possible differences in neurochemical signaling impinging on cholinergic axon varicosities locally, it seems reasonable that the rate of endocytosis of CHT may also differ across brain regions due to the specific activation of intracellular signaling molecules. In fact, relative differences in the regulation of membrane levels of CHT, or in high-affinity choline uptake, are detectable across brain regions under certain experimental (Wecker & Dettbarn 1979; Stanton & Johnson 1987) and pathological conditions . However, the majority of investigations into CHT function have been conducted in reduced preparations from cortical, hippocampal, or striatal tissue. In contrast, very little is known about the function of this protein within the projections of the tegmental brainstem cholinergic neurons.

Our laboratory's long-standing interest in the VTA initially drove our interest in the cholinergic afferents to this region. In addition, the observation that LDT cholinergic neurons tend to preferentially innervate limbic structures in the midbrain and forebrain (in contrast to the PPT ACh projections) led us to focus our investigation of CHT immunoreactivity on limbic innervation targets. Furthermore, we tried to maximize the possibility of detecting a difference in CHT localization in the axonal populations examined by comparing the cholinergic innervation of the VTA to that of the anteroventral nucleus of the thalamus (AVN), a region that is also associated with the limbic system, but is sufficiently different in its connectivity from the VTA to support hypothesized differences in cholinergic modulation.

1.3.3 Cholinergic Innervation of the Anteroventral Thalamus

In the rat, the anteroventral nucleus of the thalamus (AVN) has a remarkably dense cholinergic innervation that arises exclusively from brainstem cholinergic neurons (Sofroniew et al 1985; Gonzalo-Ruiz et al 1995). This stands in contrast to other limbic nuclei in the thalamus (Heckers et al 1992), which can receive substantial cholinergic input from the basal forebrain cholinergic groups ((Cornwall & Phillipson 1989); but see Parent et al., 1988 for species differences in basal forebrain cholinergic innervation of the limbic thalamus). As in most thalamic nuclei, stimulation of the PPT or LDT results in transient depolarization of thalamocortical neurons in the AVN that is mediated through primarily dendritic nicotinic ACh receptors. Evidence from in situ hybridization and radioligand binding studies indicate that these are likely to be $\alpha_4\beta_2$ nAChRs (Wada et al 1989; Tribollet et al 2004; Rasmussen & Perry 2006). A longer-lasting increase in the excitability of thalamocortical cells, mediated by muscarinic ACh receptors, follows the brief nicotinic depolarization (Paré et al 1990; Steriade et al 1997; Groenewegen & Witter 2004). Muscarinic receptors are also present on the axons of selected glutamatergic afferents to the AVN, but mAChR inhibitory autoreceptors are unlikely to be expressed on cholinergic axons innervating this region (Sikes & Vogt 1987). Furthermore, a complex pattern of M2 and M3 subtypes of mAChR expression within the AVN suggests that ACh may have different effects in distinct subregions of this nucleus (Sikes & Vogt 1987; Oda et al 2007). Cholinergic projections from the brainstem can also inhibit GABA neurons in the reticular nucleus of the thalamus that provide the only source of inhibitory synaptic input to the rat AVN (Wang et al 1999; Oda et al 2007) and appear to modulate selected inhibitory inputs to the AVN at the terminal level as well (Curro Dossi et al 1992). The sum of these effects is

increased firing of thalamocortical neurons in these nuclei, and the subsequent excitation of cortical circuitry.

Functionally, the AVN plays an important role in hippocampal-dependent memory, particularly with respect to spatial memory and learning processes. It is heavily interconnected with the posterior cingulate cortex and the hippocampal region (including projections to the post- and parahippocampal cortices, and from the presubiculum and subiculum) (Woolf & Butcher 1986; Bentivoglio et al 1993; Oda 1997; Oda et al 2003), and it receives a prominent input from the mammillary nuclei in the hypothalamus (Dekker & Kuypers 1976; Paré et al 1990; Shibata 1992). The specific cortical projections of the AVN fit within a topographically organized thalamocortical projection from the dorsal thalamus, in which more lateral structures such as the AVN project to posterior associative cortical areas, while the medial thalamic nuclei communicate with more anterior regions of cortex (Reep 1984; Vertes 2006). Natural or experimental lesions of the AVN result in amnesiac symptoms while leaving many other aspects of cognition unaltered (Mitchell & Dalrymple-Alford 2006; Wolff et al 2008). Damage to the AVN results in impairment of spatial-memory dependent tasks, such as the Morris Water maze, and suggests a specific inability to use allocentric cues to navigate the environment (Aggleton et al 1996; Warburton & Aggleton 1999; Aggleton et al 2009). These effects are distinct from the deficits encountered following midline thalamic lesions (Gibb et al 2006; Mitchell & Dalrymple-Alford 2006), reflecting the specific mediation of limbic functions by segregated circuits with distinct thalamic components (Vogt et al 1992; Morgane et al 2005).

1.3.4 Cholinergic Innervation of the Ventral Tegmental Area

Dopamine released in the limbic forebrain exerts a powerful influence over behavior, and pathophysiological changes in the midbrain DA system are thought to underlie many core features of both substance abuse disorders and schizophrenia (Yeomans 1995; Weiss & Koob 2001). DA projections to the ventral striatum, prefrontal and anterior cingulate cortices, and the amygdala originate in the midbrain VTA (Sesack et al 2003; Lammel et al 2008). Interestingly, the specific limbic regions that are directly connected to the AVN receive little DA input. DA innervation of the thalamus is generally poor in the rat, with the exception of medial structures such as the mediodorsal and parafascicular nuclei (Sanchez-Gonzalez et al 2005; Garcia-Cabezas et al 2009). These medial thalamic nuclei innervate the same cortical and striatal regions that are most heavily targeted by VTA DA axons (Hökfelt et al 1974; Lindvall et al 1974; Berger et al 1985; Berger et al 1991), suggesting complex but specific functional organization in differing limbic circuits. It is unknown whether the segregation of these limbic circuits extends as well to their cholinergic afferent innervation, a question that is specifically explored in this thesis.

The limbic circuitry that is targeted by VTA DA neurons mediates such well-known functions as motivation and the selection of appropriate goal-oriented behavior (Reep 1984; Gabbott et al 2005; Morgane et al 2005; Vertes 2006) Perhaps the most appreciated actions of this transmitter are its contributions to cognitive processes like working memory and action selection within the context of reward-reinforced learning (Cooper 2002; Schultz 2007). DA neurons fire characteristic “bursts” of action potentials in response to unexpected rewards; this mode of firing results in dramatically increased levels of extracellular DA in the ventral striatum (Grace & Bunney 1984; Ljungberg et al 1992; Suaud-Chagny et al 1992; Overton & Clark 1997). These reward-related responses can be conditioned to external stimuli that predict an

imminent or response-contingent reward (Ljungberg et al 1992; Yun et al 2004; Pan & Hyland 2005). This process of associative learning enables the animal to choose behavioral strategies that have proved effective in procuring natural rewards such as food in the past, and to base the selection of current behavior on salient aspects of the external environment (Schultz 2002). Furthermore, when such behavior fails to produce an expected reward, the DA system responds with a decrease in activity below baseline, which may attenuate repetition of the ineffective action (Schultz et al 1993). This pattern of physiological activity has lead researchers to consider DA as a signal of reward prediction error (Schultz 2002; Okada et al 2009).

Through ascending projections to the VTA, the characteristic sensory-evoked excitation of PPT/LDT neurons is translated into increased excitability of DA neurons (Mena-Segovia et al 2008). Furthermore, evoked activity in the PPT/LDT is necessary for an animal to acquire associations between external cues and reward-reinforced behavioral responses (Lepore & Franklin 1996; Florio et al 1999; Pan & Hyland 2005), just as the reward-evoked and cue-conditioned responses of VTA DA neurons are required for such learning (Yun et al 2004). Accordingly, disruption of the brainstem cholinergic input to the VTA can significantly inhibit motivated behavior (Wilson et al 2009) and has often been noted to lead to increased omission of appropriate responses on cue-driven operant tasks (Florio et al 1999; Chilton et al 2004).

ACh axons in the VTA are of moderate density, and form synapses with both dopaminergic and GABAergic dendrites and neurons (Omelchenko & Sesack 2006). Cholinergic projections from the LDT to the VTA facilitate the release of DA in the ventral striatum (Forster & Blaha 2000) by specifically enhancing the behaviorally relevant burst-firing of DA neurons that drives dramatic increases in DA release in response to reward-predictive cues (Floresco et al 2003; Lodge & Grace 2006). Direct application of cholinergic agonists to the

midbrain DA cell-containing regions also results in net excitation of DA neurons that is mediated through multiple cellular processes (Mansvelder et al 2003).

Briefly, activation of nAChRs expressed on cell bodies and dendrites directly depolarizes DA neurons. Secondly, nAChRs on presynaptic axon terminals can potentiate glutamate release onto DA neurons as well (Schilström et al 1998; Schilström et al 2000; Jones & Wonnacott 2004), and enhance synaptic plasticity at these excitatory synapses (Mansvelder & McGehee 2000). These choline-sensitive receptors are present in the VTA and can alter the processing of salient environmental stimuli to guide behavior (Schilström et al 1998; Chilton et al 2004; Jones & Wonnacott 2004; Keller et al 2005). Activation of α7 nAChRs can induce long-term potentiation (Mansvelder et al 2003), a form of synaptic plasticity, at excitatory synapses impinging on DA neurons, thereby contributing to the acquisition of learned stimulus-response associations. Interestingly, the nAChRs mediating this enhancement of presynaptic glutamate release (α7 nAChRs) show sensitivity to both ACh and choline as agonists, a property that is not shared by other AChR subtypes (Alkondon et al 1997; Mike et al 2000; Alkondon & Albuquerque 2006), presenting the possibility that the rate of high-affinity choline uptake may have secondary effects on cholinergic modulatory processes in this region. Finally, mAChRs on VTA DA neurons (probably the M5 subtype) mediate a slower and prolonged excitation that significantly increases DA release in the ventral striatum (Yeomans 1995; Gronier & Rasmussen 1998; Forster & Blaha 2000; Gronier et al 2000; Miller & Blaha 2004), and the cholinergic afferents to the VTA may also express cholinergic autoreceptors that depress ACh release when activated.

1.4 EXPERIMENTAL HYPOTHESES AND DESIGN

PPT/LDT neurons display heterogeneity in their projection targets and co-transmitter content, and may vary in their firing rates, afferent input, and activity patterns as well; therefore, we hypothesized that neurons in this central cholinergic system might display differential expression or localization of CHT. We tested this hypothesis by comparing the level and pattern of immunoreactivity for CHT between distinct regions that receive cholinergic innervation from these brainstem nuclei.

1.4.1 Choice of Regions for Comparison

As discussed in the preceding section, acetylcholine released from the ascending projections of PPT/LDT neurons alters the sensitivity of cholinoceptive neurons to afferent input, both by directly exciting these neurons at somatodendritic receptors, and by modulating transmitter release from non-cholinergic axon terminals. However, the functional roles of the AVN and the VTA appear to be different, and the cellular heterogeneity observed in the brainstem tegmental cholinergic nuclei suggests that ACh modulation might differ considerably between these innervation targets. As the expression and localization of CHT have not been characterized in this cholinergic projection system, we undertook immunohistochemical studies to determine if the distribution of this transporter is similar in PPT/LDT projections to that observed in other cholinergic axons. We also tested the hypothesis that the subcellular distribution of CHT can differ between unique targets of the same cholinergic system by comparing CHT-immunoreactivity in axons innervating the AVN to those in the VTA. We

chose to compare these specific regions in order to maximize the chances of detecting such hypothesized differences.

There are many prominent ways in which the AVN and VTA differ. Obviously, the AVN is a thalamic nucleus containing glutamate neurons that convey information to certain limbic cortical regions through direct point-to-point connections (Groenewegen & Witter 2004). In contrast, VTA DA neurons modulate the neural processing of convergent excitatory and inhibitory inputs in limbic structures distinct from those that communicate with the AVN (Bamford et al 2004a; Bamford et al 2004b; Wolf et al 2004; Kroener et al 2009; Kehagia et al 2010). While the AVN has a clear role in supporting spatial learning and memory (Warburton & Aggleton 1999; Jenkins et al 2002; Gibb et al 2006; Sziklas & Petrides 2007; Yasoshima et al 2007; Wolff et al 2008; Aggleton et al 2009), the output of the VTA impacts appetitively motivated behavior and associative learning (Cooper 2002; Yun et al 2004; Geisler & Zahm 2005). Furthermore, differences in the density of ACh innervation and the spatial distribution of AVN versus VTA afferents within the PPT/LDT, combined with the cellular heterogeneity observed within the brainstem tegmental cholinergic nuclei, suggests that the cholinergic modulation of the AVN and VTA could arise from neurons with different intrinsic properties. Finally, the differences in AChR subunit expression between the AVN and the VTA lends further support to the hypothesis that these regions may differ along other dimensions of cholinergic signaling as well. Interestingly, the presynaptic α7 nAChRs in the VTA can be desensitized by exposure to micromolar concentrations of choline present in the extracellular fluid (Uteshev et al 2003; Alkondon & Albuquerque 2006), presenting the possibility that the regulation of high-affinity choline uptake may have secondary effects on cholinergic transmission in the midbrain. In contrast, cholinergic transmission in the AVN does not appear

to contain choline-sensitive nAChRs (Morley et al 1977; Morley & Garner 1986; 1990; Tribollet et al 2004; Guseva et al 2006). We aimed to detect gross differences in CHT immunoreactivity that might arise from the collective differences in these two by comparing the axon terminals in the AVN to those in the VTA.

Unlike other "limbic" thalamic nuclei such as the mediodorsal nucleus or parafascicular nucleus (Cornwall & Phillipson 1989), the AVN receives cholinergic innervation exclusively from the tegmental brainstem neurons (Gonzalo-Ruiz et al 1995); cholinergic cells in the basal forebrain group do not contribute to its innervation, at least in the rat (Parent et al 1988). Similarly, midbrain DA regions (SNc and VTA) are innervated by only the PPT/LDT cholinergic neurons (Woolf 1991). By selecting these regions for examination, we ensured that any differences observed reflected true heterogeneity in the projections of the brainstem ACh neurons.

1.4.2 Experimental Framework

As previously stated, the PPT/LDT cholinergic system is perhaps the least well-studied group of cholinergic neurons within the CNS, and the characteristics of CHT expression and subcellular trafficking have not been described for this system. The lack of data for this system stems in part from the small size of its terminal fields and the resulting difficulty of extracting sufficient tissue for use in synaptosomal preparations or traditional protein analytical methods.

In order to overcome these experimental issues, we used immunohistochemical methods to characterize CHT expression in the axons of PPT and LDT neurons. By utilizing fixed brain tissue and both fluorescence and electron microscopy, these experiments had the additional

advantage of preserving the native spatial distribution of CHT within cholinergic axons in innervated regions.

1.4.3 Experimental Questions

Our experiments aimed to characterize CHT in the axons of PPT and LDT neurons. To this end, we examined: 1) the level of expression and the subcellular localization of CHT within these axonal populations; 2) the occurrence of colocalization of CHT and VAChT within axons in the AVN and VTA, and the relative levels of expression of these two proteins; and 3) the source population(s) of cholinergic axons to the AVN and VTA.

1.4.4 Ultrastructural localization of CHT

Immunohistochemistry has been used to examine the ultrastructural distribution of CHT immunoreactivity in presumed cholinergic axon varicosities from a number of CNS regions, including the neuromuscular junction (Lips et al 2002; Nakata et al 2004), striatum, and facial nucleus (Ferguson et al 2003). All of these studies utilized silver-enhanced immunogold histochemistry, a reaction that produces discrete electron-dense particles at the site of antibody binding. In contrast to diffusible reaction products such as immunoperoxidase, the immunogold method allows a high degree of spatial resolution (accurate to ~20 nm) (Umeda et al 1997; Mathiisen et al 2005; Miner et al 2006), making it the preferred method for studies of the precise subcellular localization of proteins. In all prior reports, the majority of CHT-*ir* appeared to be

confined to an intracellular compartment and associated with small clear synaptic vesicles (Lips et al 2002; Ferguson et al 2003; Ferguson & Blakely 2004; Nakata et al 2004). A minority (5-20%) of CHT immunogold-silver particles could be found in association with the plasma membrane of immunoreactive axonal structures, indicating that the functioning pool of transporters at any given time represents a small fraction of the total CHT protein.

Given the similar distribution of CHT-*ir* across the different cholinergic neurons examined thus far, we hypothesized that this pattern of a predominantly cytoplasmic subcellular localization of CHT would also be true in the axon varicosities of brainstem cholinergic neurons. However, we also wished to know if axonal populations arising from a common cholinergic group would display similar characteristics despite innervating different anatomical structures. We therefore used immunogold-silver histochemistry to compare the total immunoreactivity for CHT and the amount of CHT associated with the plasma membrane between axons examined in the AVN and VTA from the same group of animals.

1.4.5 Expression and Localization of CHT Relative to VAChT

Although CHT is robustly expressed in most cholinergic neurons and axons in the rat CNS, this protein may not be strictly necessary for proper cholinergic function at brain synapses (Matthies et al 2006). CHT-immunoreactivity is absent from some choline acetyltransferase (ChAT) and vesicular acetylcholine transporter (VAChT) immunoreactive (VAChT-*ir*) neurons (Misawa et al 2001), and its constituitive expression can be extinguished in some cells by genomic deletion of post-synaptic nicotinic receptors (Krishnaswamy & Cooper 2009). In other

regions of the brain, qualitative observations indicate that CHT immunoreactivity appears to vary among otherwise homogenous populations of axon terminals (Ferguson et al 2003).

Although cholinergic cell bodies in the primate PPT/LDT show 100% colocalization of ChAT and CHT (Kus et al 2003), the colocalization of CHT with other cholinergic markers has not been examined in the axonal compartments of these cells in any species. Consequently, dual fluorescence immunohistochemistry combined with spinning disk confocal microscopy was used to examine and compare the rate of colocalization of CHT and VAChT in the AVN and the VTA. Given the central role of choline uptake in the maintenance of a synaptic pool of releasable ACh (Ferguson & Blakely 2004), we hypothesized that a majority of the immunofluorescent puncta in both regions would demonstrate co-localized VAChT and CHT immunoreactivities. However, we also expected that the rate of colocalization observed in VAChT-*ir* puncta would be lower in the VTA, based on preliminary observations that levels of CHT immunoreactivity were qualitatively lower in this region, and thus might fall below our detection level. We examined the colocalization of VAChT immunoreactivity within CHT-*ir* puncta, to determine if there might be sites of high-affinity choline uptake that may not primarily subserve ACh synthesis (e.g. sites that remove choline from the extracellular space in order to facilitate the excitation of presynaptic nAChRs), as evidenced by low or absent VAChT immunofluorescence. Although the occurrence of such CHT-*ir* puncta was entirely speculative, the experimental design would allow us to detect such sites if they exist.

In addition, we examined the relationship between VAChT immunoreactivity and CHT immunoreactivity within these regions in order to determine if CHT expression is primarily driven by the relative levels of vesicular ACh. We expected that VAChT levels would significantly predict levels of CHT immunoreactivity within these axons, as larger reserves of

vesicular ACh (as indirectly evidenced by VAChT immunoreactivity levels) are expected to require higher levels of choline uptake to maintain adequate ACh synthesis. Finally, we compared this relationship between the AVN and the VTA to determine if CHT expression might vary in relation to VAChT expression across different innervation targets of the PPT and LDT ascending cholinergic system, possibly due to differences in the local extracellular environment of these cholinergic terminals.

1.4.6 Determination of the Source of Cholinergic Axons Projecting to the AVN and VTA

The hypothesized differences in CHT expression within axon varicosities in the AVN and VTA could result from separate populations of afferents from the PPT/LDT. The overall distribution of afferents to the AVN and VTA, as demonstrated in single retrograde tracing studies, appears to differ, as the VTA is innervated by both the PPT and LDT (Satoh & Fibiger 1986; Woolf & Butcher 1986; Hallanger & Wainer 1988; Oakman et al 1995; Holmstrand & Sesack 2004; Omelchenko & Sesack 2005), but the AVN innervation originates predominantly from the LDT (Woolf & Butcher 1986; Gonzalo-Ruiz et al 1995). However, cholinergic neurons from the brainstem tegmentum are known to send collaterals to thalamic nuclei and other subcortical structures (Woolf & Butcher 1986; Cornwall & Phillipson 1988b; Parent et al 1988; Jourdain et al 1989; Bolton et al 1993; Losier & Semba 1993; Billet et al 1999), and some studies assert that all cholinergic neurons in this region innervate the thalamus, in addition to any other projections that they might have (Oakman et al 1999). To determine if axons in the VTA arise from collaterals of PPT/LDT neurons projecting to the AVN, we combined dual retrograde tract-tracing with immunohistochemistry for VAChT, and examined the PPT and LDT for

evidence of colocalization of both tracers in cholinergic and non-cholinergic neurons within these nuclei.

2.0 ULTRASTRUCTURAL LOCALIZATION OF HIGH-AFFINITY CHOLINE TRANSPORTER IN THE RAT ANTEROVENTRAL THALAMUS AND VENTRAL TEGMENTAL AREA: DIFFERENCES IN AXON MORPHOLOGY AND TRANSPORTER DISTRIBUTION.

This chapter contains the published manuscript detailing the results of Aim 1. This report has been previously published in the following peer-reviewed publication:

> Holmstrand, EC, Asafu-Adjei, J, Sampson, AR, Blakely, RD, and Sesack, SR. 2010. *Journal of Comparative Neurology* 518(11): 1908-1924.

With the exception of minor changes, such as matching the formatting of the dissertation and updating figure numbering and titles, it is unchanged in form from that article.

2.1 INTRODUCTION

The Na+/Cl- dependent high-affinity choline transporter (CHT) supplies substrate for the synthesis of acetylcholine (ACh) in central and peripheral cholinergic neurons (Yamamura & Snyder 1972; Haga & Noda 1973; Yamamura & Snyder 1973; Wecker & Dettbarn 1979; Löffelholz & Klein 2006; Takashina et al 2008). Due to its high affinity for choline, this protein can meet the demand for local ACh synthesis during prolonged activation of cholinergic neurons

(Simon & Kuhar 1975; Simon et al 1976). Blockade of choline transport leads to subsequent depletion of ACh in brain synaptosomes, and at the neuromuscular junction (Guyenet et al 1973; Zapata et al 2000; Bazalakova et al 2007). Expression of the transporter is therefore necessary to successful cholinergic transmission and ultimately to survival in mammals (Ferguson et al 2004).

The regional and cellular expression of CHT mRNA and the localization of CHT protein closely match that of other selective markers of cholinergic phenotype in the rodent and primate nervous system (Misawa et al 2001; Ferguson et al 2003; Kus et al 2003). Nevertheless, the transcription and translation of CHT are dissociable from those of the synthetic enzyme, choline acetyltransferase (ChAT) and the vesicular acetylcholine transporter (VAChT) (Erickson et al 1994; Eiden 1998; Lecomte et al 2005). Furthermore, CHT shows a different expression profile from these other markers during development (Lecomte et al 2005), following injury (Oshima et al 2004), and in some pathological conditions (Slotkin et al 1990; Slotkin et al 1994).

At the ultrastructural level, CHT is localized mainly to synaptic vesicles in the cytoplasmic compartment of axon terminals, with only a small proportion associated with the plasma membrane (Ferguson et al 2003; Nakata et al 2004). This subcellular localization suggests the existence of a recruitable pool of cytoplasmic transporters, consistent with decades of biochemical research showing that high-affinity choline uptake can be dramatically increased through the rapid insertion of new transporters into the plasma membrane, a process mediated by the fusion of CHT-containing synaptic vesicles with the plasmalemma (Haga & Noda 1973; Simon & Kuhar 1975; Murrin & Kuhar 1976; Roskoski 1978; Antonelli et al 1981; Ferguson et al 2003; Ferguson & Blakely 2004). Membrane-bound CHT is also internalized through clathrin-dependent endocytosis (Ribeiro et al 2003). The number of membrane bound transporters is therefore determined by the rates of exo- and endocytosis. Furthermore, the rate

of endocytosis can be influenced by the activity of protein kinases and phosphatases in the axon terminal (Breer & Knipper 1990; Vogelsberg et al 1997; Gates et al 2004). It therefore seems likely that external signaling events in the vicinity of cholinergic terminals could potentially influence the number of active transporters in the plasma membrane, independent of any action on the rate of acetylcholine release (Breer & Knipper 1990).

Functional investigations of high-affinity choline uptake in synaptosomes have focused largely on striatal, hippocampal, and cortical tissues. Both the basal rate of choline uptake and modulation of high-affinity choline uptake have been shown to differ between striatal and cortical tissue (Wecker & Dettbarn 1979; Stanton & Johnson 1987). This is not surprising given that the cholinergic innervation of the striatum and cortex arise from separate systems. The characteristics of high-affinity choline uptake have not been described for the projections of the brainstem pedunculopontine (PPT) and laterodorsal tegmental (LDT) cholinergic neurons; therefore, it is not known whether the low level of membrane incorporation of CHT is a property of this system as well.

PPT and LDT cholinergic cells provide ascending modulation to a variety of subcortical structures. These neurons are the predominant source of ACh to the thalamus (Sofroniew et al 1985; Hallanger & Wainer 1988), and the midbrain ventral tegmental area (VTA) (Gould et al 1989; Gonzalo-Ruiz et al 1995). They also project to the basal forebrain cholinergic system (Losier & Semba 1993), and thus can theoretically influence signaling in a diverse and large group of forebrain structures. It has been suggested that PPT/LDT cholinergic neurons modulate forebrain processing of environmental stimuli, thus facilitating externally directed behavioral responses (Kobayashi & Isa 2002).

We wished to examine the ultrastructural distribution of CHT protein in the projections of cholinergic PPT/LDT neurons in intact animals. We chose to examine the terminal fields of these neurons in the VTA because of their demonstrated role in general motivational processes (Ikemoto & Panskepp 1996; Pan & Hyland 2005) and their relevance to nicotine addiction in particular (Lança et al 2000; Corrigall et al 2002; Laviolette & van der Kooy 2003; Pidoplichko et al 2004). For comparison, we examined cholinergic terminals in the anteroventral nuclei of the thalamus (AVN) for two reasons. First, the cholinergic innervation of this particular thalamic nucleus is relatively dense (Sofroniew et al 1985; Heckers et al 1992; Holmstrand et al 2006) and probably arises exclusively from the brainstem cholinergic system (Shibata 1992; Gonzalo-Ruiz et al 1995), at least in the rat (see (Parent et al 1988)). Secondly, the AVN is an important component of the limbic system and so is linked functionally with the VTA, even though there are no direct connections between the two regions (Shibata 1992; Geisler & Zahm 2005). We examined CHT-containing axonal profiles in these nuclei at the ultrastructural level and compared the morphology, synaptology, and both the overall density of CHT immunogold reactivity and the specific membrane density of CHT in cholinergic axons innervating these regions. Preliminary accounts of this investigation were previously reported in abstract form (Holmstrand et al 2006; Holmstrand et al 2008).

2.2 MATERIALS AND METHODS

2.2.1 Subjects

All animal procedures were carried out with approval from the Institutional Animal Care and Use Committee at the University of Pittsburgh. Male Sprague-Dawley rats (Hilltop Lab Animals, Inc., Scottdale, PA) weighing 300-400 g were deeply anesthetized with sodium pentobarbital (60 mg/kg i.p.) and pretreated for 15 minutes with sodium diethyldithiocarbamate (DEDTC, Spectrum Chemical Corp., Gardena, CA; 1 mg/kg i.p.) to prevent silver enhancement of endogenous zinc ions in axon terminals (Veznedaroglu & Milner 1992). A cohort of paired animals were then perfused using a transcardial approach with 50 mL of heparinized saline (1000 U/mL), followed by 500 mL of 3% paraformaldehyde and 0.15% glutaraldehyde in 0.1 M phosphate buffer, pH 7.4 (PB). The brains were removed and cut in the coronal plane to yield 3-4 mm thick blocks. Tissue was then post-fixed overnight in the same fixative at 4°C. Brains were sectioned through the anterior thalamus and the midbrain to a thickness of 50 μm and collected in PB. Sections were treated with 1% sodium borohydride in PB for 30 minutes and rinsed extensively.

2.2.2 Immunohistochemistry

Sections were labeled by immunoperoxidase or immunogold-silver using a polyclonal antibody raised in rabbit against the C-terminus 15 amino acid sequence that is conserved in the human, mouse and rat CHT protein. Several lines of evidence support the specificity of this

antibody (Ferguson et al 2003). The antiserum labels a band of the predicted molecular weight for CHT by Western blot analysis of mouse whole tissue or brain synaptosomes and from PC12 cells transfected with human CHT. This immunoreactive band is absent from kidney and from PC12 cells transfected with empty vector. Immunohistochemical labeling with the polyclonal rabbit antibody conforms to the expected distribution of cholinergic neurons and fibers throughout the mouse and rat brain and at the neuromuscular junction, and is co-localized with other markers of cholinergic phenotype but not other transmitters. Pre-adsorption with the immunizing peptide abolishes this labeling (Ferguson et al 2003). Finally, immunolabeling is absent from CHT -/- mice (Ferguson & Blakely 2004).

Sections for immunoperoxidase visualization of CHT were rinsed in 0.1 M Tris-buffered saline, pH 7.6 (TBS) and incubated for 30 minutes in a blocking solution containing 1% bovine serum albumin (BSA), 5% normal donkey serum (NDS, Jackson Immunoresearch Laboratories, Inc., West Grove, PA), and Triton X-100 (Sigma, St. Louis, MO) at 0.2% or 0.04% for light or electron microscopy, respectively. Sections were then transferred to blocking solution containing the polyclonal rabbit anti-CHT at 1:1000 and incubated overnight at 4°C. After rinsing, sections were incubated for 30 minutes in biotinylated donkey anti-rabbit IgG (Jackson Immunoresearch) diluted at 1:400 in blocking solution. Excess secondary antibody was removed with several rinses in TBS, and sections were incubated in ABC solution (Vectastain kit, Vector Laboratories, Burlingame, CA) for 30 minutes. Peroxidase product was developed by incubation in 0.022% diaminobenzidine (Sigma) and 0.003% hydrogen peroxide for 3 minutes. Sections for light microscopy were rinsed extensively in TBS and 0.01 M phosphate buffered saline prior to mounting on Superfrost microscope slides (Fisher Scientific, Pittsburgh, PA). After drying, slides were dehydrated through a series of increasing ethanol concentrations, defatted in xylene,

and coverslipped with Cytoseal-60 mounting medium (Richard Allen Scientific, Kalamazoo, MI). Immunoperoxidase labeled sections for electron microscopy were prepared as detailed below.

Sections for pre-embedding gold-silver immunostaining were treated according to the recommended protocol included with the Aurion RGent SEM kit (Electron Microscopy Sciences, Hatfield, PA). Sections were rinsed in 0.02 M phosphate buffered saline, pH 7.4 (PBS) and permeabilized in 0.05% Triton X-100 for 10 minutes. Non-specific antigenic sites were blocked by a 30 minute incubation in PBS containing 5% BSA, 5% NDS, and 0.1% fish gelatin (GE Healthcare Life Sciences, Waukesha, WI). Sections were then rinsed in an incubation buffer containing 0.2% acetylated BSA (Aurion BSAc, Electron Microscopy Sciences) and incubated overnight at 4°C in incubation buffer containing primary antibody (rabbit anti-CHT, 1:1000). Sections were rinsed extensively in incubation buffer and placed in vials containing secondary antibody (Aurion donkey anti-rabbit 0.8 nm gold conjugate, 1:50, Electron Microscopy Sciences) and 5% NDS in the same buffer. Secondary antibody binding occurred overnight at 4°C. After rinsing in incubation buffer and PBS, antibody complexes were fixed by incubation for 10 minutes in 2% glutaraldehyde in PBS. Following several rinses in PBS, gold particles were silver-enhanced using the Aurion RGENT SEM kit, according to the manufacturer's instructions and using the optional enhancement conditioning solution (Aurion ECS, Electron Microscopy Sciences). Silver enhancement proceeded from 45-75 minutes and was terminated by several rinses in ECS, followed by 0.1 M PB.

2.2.3 Tissue Preparation for Light and Electron Microscopy

Brightfield micrographs were captured on an Olympus BX-51 microscope (Olympus America Inc., Center Valley, PA) equipped with a CCD camera (Hamamatsu, Bridgewater, NJ). Acquired images were imported into Adobe Photoshop (Adobe Systems Incorporated, San Jose, CA) and modified to match brightness and contrast.

Immunoperoxidase and immunogold-silver reacted tissue was processed for electron microscopy by incubation in 2% osmium tetroxide in 0.1 M PB for 1 hour, dehydrated through a series of increasing ethanol concentrations, treated with propylene oxide, and infiltrated with an epoxy resin (EMBed-812, Electron Microscopy Sciences). Sections were then flat-embedded between sheets of commercial plastic (Aclar, Electron Microscopy Sciences). Ultrathin (60-70 nm) sections were cut through the regions of interest on a Leica Ultracut ultramicrotome (Leica Microsystems, Bannockburn, IL) and mounted on either copper mesh grids or carbon coated copper slot grids (Electron Microscopy Sciences). Sections were then counterstained with 5% uranyl acetate and lead citrate and examined on a transmission electron microscope (Morgagni, FEI Company, Hillsboro, Oregon) equipped with a CCD camera (Advanced Microscopy Techniques, Danvers, MA). Digital micrographs of labeled axonal profiles were captured at 14,000 – 28,000x magnification and adjusted for exposure and contrast in Adobe Photoshop.

2.2.4 Image Analysis

In cholinergic projections to the cortex, it has been shown that the synaptic incidence extrapolated from single section observations is equal to the rate of synapse formation obtained

from the analysis of serial ultrathin sections (Umbriaco et al 1982). However, this relationship has not yet been established for the projections of the PPT/LDT cholinergic cells. We therefore evaluated the rate of synapse formation observed in serial section data and compared this to an extrapolated synaptic incidence calculated from data obtained only from single sections.

For each rat, two Vibratome sections were examined through each region. For most CHT immunolabeled profiles, we were able to obtain a series of micrographs from adjacent ultrathin sections, and we used these profiles to determine if each displayed a synaptic specialization (n = 637, Data set #1, Table 1). We also used this first data set to determine whether each CHT labeled profile contained at least one dense-cored vesicle or none.

To further analyze the extent of synapse formation, we utilized a second data set of single sections through CHT immunoreactive profiles from 3 of the 6 animals (n = 410, Data set #2, Table 1) and applied a well-accepted method for post hoc size correction to generate an extrapolated synaptic incidence (Beaudet & Sotelo 1981). By comparing the values obtained from the serial sections with that extrapolated from single section analysis, we could determine if this extrapolation method can accurately estimate synaptic incidence in these brain regions. More specifically, we recorded the minimum diameter (D), and length of the synaptic junction (d) for each of these profiles. We also measured the thickness of our sections (w) using the minimal fold method (Small 1968). We computed the means of these measurements for each region, and applied the following equation:

$$P = (d/D)*(2/\pi) + (w/D);$$

where *P* is the probability of observing a synapse in a single section through an axonal profile if all profiles form one synapse (Beaudet & Sotelo 1981). In other words, *P*(true synaptic incidence) = single-section synaptic incidence*. We therefore divided the rate of synapse

formation we observed in our single section sample by this probability (*P*) to generate the extrapolated synaptic incidence.

For the analysis of CHT immunogold localization, we used a third data set consisting of single sections through each profile from both Data sets #1 and #2 (n = 1047, Data set #3, Table 1). To avoid bias in the selection of a single image through the serial micrographs from Data set #1, we chose the image that was photographed first, regardless of its position within the series. In this case, we assumed that the first encounter with a profile constituted a random event.

Using a commercial image analysis software program (SimplePCi, Hamamatsu), we measured immunoreactive profiles and recorded the number of gold particles in the cytoplasm and associated with the plasma membrane. From these data, we derived the following measurements: (1) profile area, 2) profile perimeter, 3) total gold density of CHT immunogold particles, defined as the total number of gold particles per unit profile area, and 4) membrane density of CHT immunogold particles, defined as the number of membrane associated gold particles per unit profile perimeter. Membrane gold particles were defined as those immediately in contact with the plasmalemma or separated by no more than 20 nm, based on estimates of gold particle and immunoglobulin size (Umeda et al 1997; Mathiisen et al 2005).

Silver-enhanced gold particles were observed at high density in axonal profiles that clearly contained synaptic vesicles. The presence of a lower density of gold-silver particles in some dendrites suggested a certain degree of background staining, which varied between animals. Therefore, when there was any concern regarding specific gold labeling in axons, these profiles were followed in a short series of adjacent sections. Profiles that contained fewer than 10 gold particles per square micron were excluded from our sample unless consistent

Table 1 Sampling scheme for ultrastructural analysis

		Number of profiles analyzed		
Animal	**Region**	**Data set 1 serial sections**	**Data set 2 single sections**	**Data set 3 all profiles**
1	AVN	30	68	98
	VTA	26	65	91
2	AVN	7	93	100
	VTA	0	93	93
3	AVN	89	0	89
	VTA	107	0	107
4	AVN	48	44	92
	VTA	39	47	86
5	AVN	80	0	80
	VTA	56	0	56
6	AVN	79	0	79
	VTA	76	0	76
Total		637	410	1047

immunolabeling was observed in at least 3 serial micrographs.

Non-specific background labeling was similar in the two regions, averaging 1.6 ± 1.3 gold particles per μm^2 in the AVN versus 1.7 ± 1.4 gold particles per μm^2 in the VTA. Specific gold-silver labeling in the final data set was determined to be at least 2.5 times above background levels, with the majority of profiles well beyond this minimum level.

2.2.5 Statistical Analysis

Serial micrographs from the first data set (Table 1) were examined for the *presence of synaptic specializations and dense-cored vesicles*. The probabilities of synapse presence and dense-cored vesicle presence were modeled using generalized linear mixed models based on the Bernoulli distribution, with the logit as the link function. Brain region was treated as a fixed effect. Animal pair was also treated as a fixed effect to account for the fact that animal tissue was processed in pairs. To account for the correlation among observations within an animal and among observations within each Vibratome section, animal and section nested in animal were treated as independent normally distributed random effects.

The remaining dependent measures were analyzed from the third data set of all labeled profiles (Table 1). A linear mixed model was used to model the *profile area of CHT-immunoreactive structures*, with brain region and animal pair treated as fixed effects. To account for the correlation among observations within an animal and among observations within each Vibratome section, animal and section nested in animal were treated as independent normally distributed random effects.

A generalized linear mixed model, based on a Poisson distribution, was used to model *total gold density of CHT immunogold positive profiles*, with the log as the link function and the

natural logarithm of profile area as an offset variable. Brain region and animal pair were treated as fixed effects. To account for the correlation among observations within an animal and among observations within each Vibratome section, animal and section nested in animal were treated as independent normally distributed random effects.

Membrane density of CHT immunogold positive profiles was modeled in a manner similar to that of *total gold density of CHT immunogold positive profiles*. The only difference arose from the fact that the model for membrane density used the natural logarithm of profile perimeter as an offset variable and included total gold density and the interaction between brain region and total gold density as fixed effects, in addition to brain region and animal pair.

The analysis of profile area was implemented in SAS PROC MIXED (Version 9.2, SAS Institute Inc., Cary, NC), while all other analyses were implemented in SAS PROC GLIMMIX. The Kenward-Roger degrees of freedom method was used in each analysis. When testing for the significance of fixed effects in a mixed model, the Kenward-Roger method is generally recommended to approximate the denominator degrees of freedom in subsequent F tests (Littell et al 2006). This method corrects for the fact that the estimated variability of the fixed effects parameter estimates tends, on average, to be lower than the actual variability of these estimates.

All statistical tests were conducted at the 0.05 significance level.

2.3 RESULTS

2.3.1 Light Microscopic Detection of CHT

Immunoperoxidase staining was used to examine the distribution of CHT in the AVN and VTA (Figure 4). The AVN division of the thalamus contained dense puncta immunoreactive for CHT that were suggestive of axon varicosities. Such profiles were notably absent from the adjacent anterodorsal thalamic nucleus (Figure 4A). In the VTA, similar axon-like immunoreactive puncta were observed, although the innervation appeared to be less dense (Figure 4B).

2.3.2 Ultrastructural Detection of CHT

Immunoperoxidase labeling for CHT was observed mainly in unmyelinated axonal profiles in the AVN and VTA (Figure 5). By qualitative estimation of both light and electron micrographs, it appeared that the AVN contained a higher density of CHT-labeled profiles (Figure 4, inserts; Figure 5); however, this was not quantified further. In the VTA, occasional myelinated axons were also found to contain CHT. The efferent fibers of the oculomotor nerve pass through the VTA without synapsing, and given that these are cholinergic premotor axons, we restricted our examination to only the unmyelinated profiles likely to represent brainstem cholinergic axons. Immunogold-silver labeling for CHT was also localized primarily to unmyelinated axonal profiles in the AVN and VTA (Figure 6). With either staining method, CHT-labeled axon varicosities in both regions formed axodendritic synapses with either symmetric or asymmetric morphology and contained mainly small-clear and occasional dense-

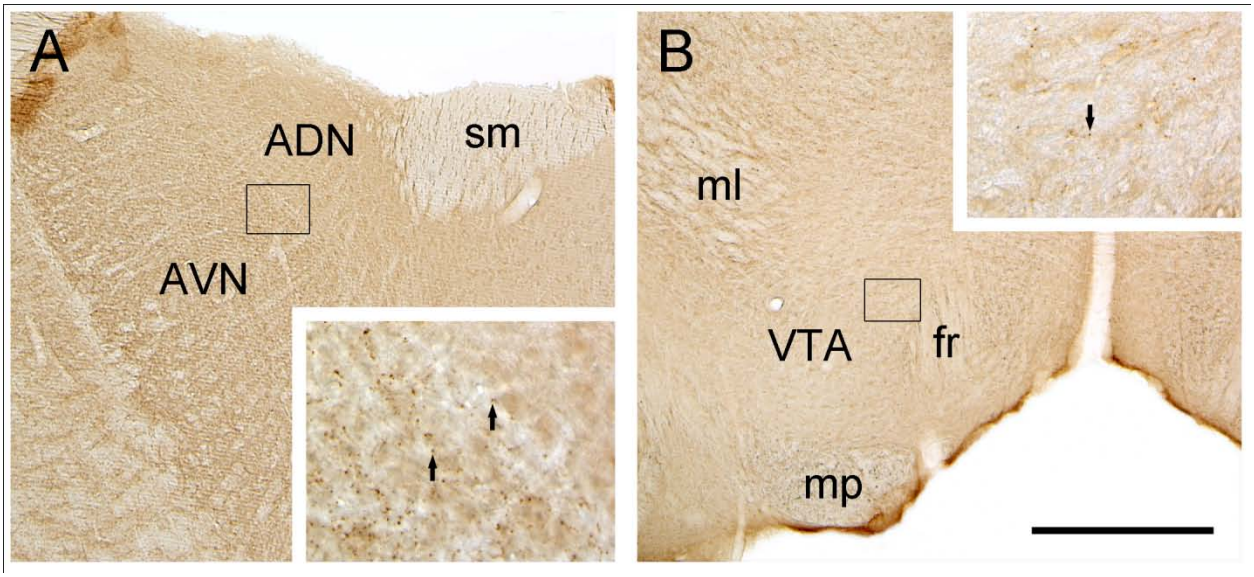

Figure 4 Light micrographic images illustrating immunoperoxidase labeling for CHT in the AVN and VTA.

In **A**, immunoreactivity for CHT appears to be denser in the AVN than in the anterodorsal thalamic nucleus (ADN). The boxed region shown at higher magnification in the insert straddles the two divisions and illustrates immunolabeled puncta (arrows) representing probable axon varicosities. Note the absence of these puncta in the adjacent ADN. **B** shows relatively uniform CHT staining in the VTA. The boxed region shown at higher magnification in the insert illustrates immunoreactive puncta (arrow) that appear at lower density than in the AVN. Abbreviations: fr, fasciculus retroflexus; ml, medial lemniscus; mp, mammillary peduncle; sm, stria medullaris. Scale bar represents 500 µm in A and B, 100 µm in inserts.

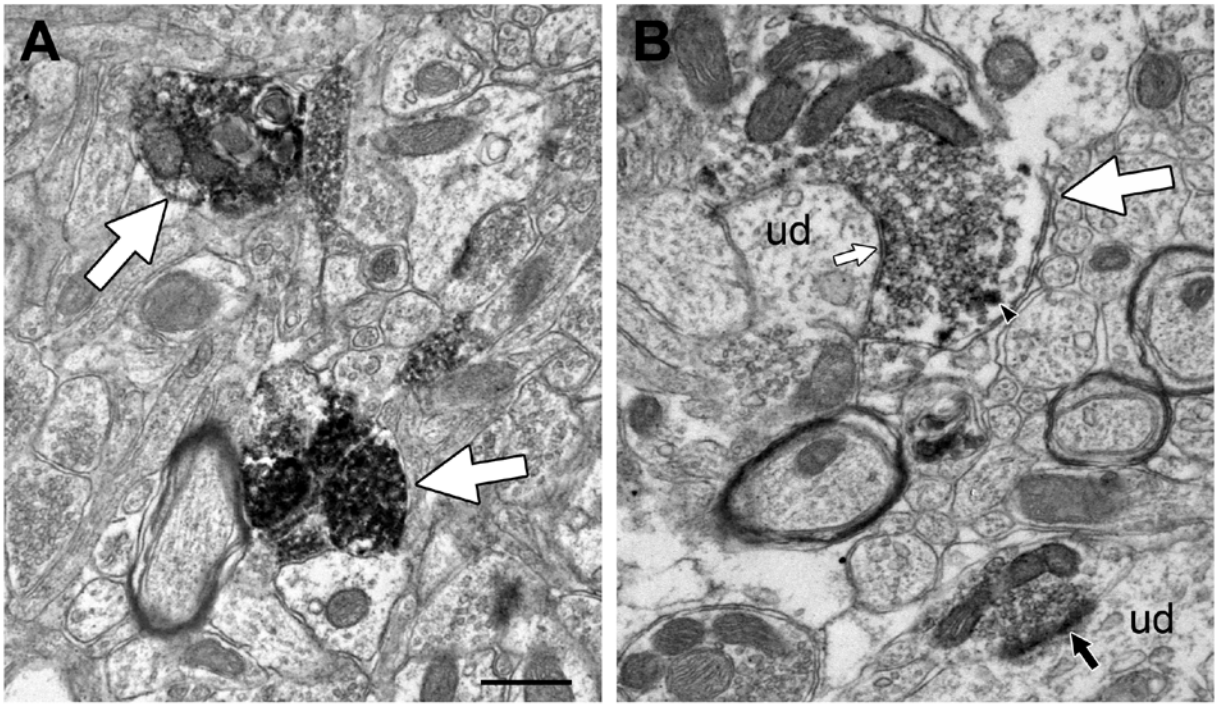

Figure 5 Electron micrographs showing representative immunoperoxidase labeling for CHT in axonal profiles.

In CHT immunoreactive profiles (large white arrows), the reaction product typically appears to be denser in labeled AVN (**A**) profiles than those observed in the VTA (**B**), although a range of immunoreactive densities is evident. CHT positive profiles also appear to be more numerous in the AVN than in the VTA, consistent with the observations made at the light microscopic level. The lightly labeled CHT varicosities in the VTA form symmetric (small white arrow) or asymmetric (black arrow) synapses onto unlabeled dendrites (ud). One of these also contains a dense-cored vesicle (arrowhead). The heavy peroxidase reaction product in AVN profiles makes it difficult to identify dense-core vesicles in this region. Scale bar represents 0.5 µm.

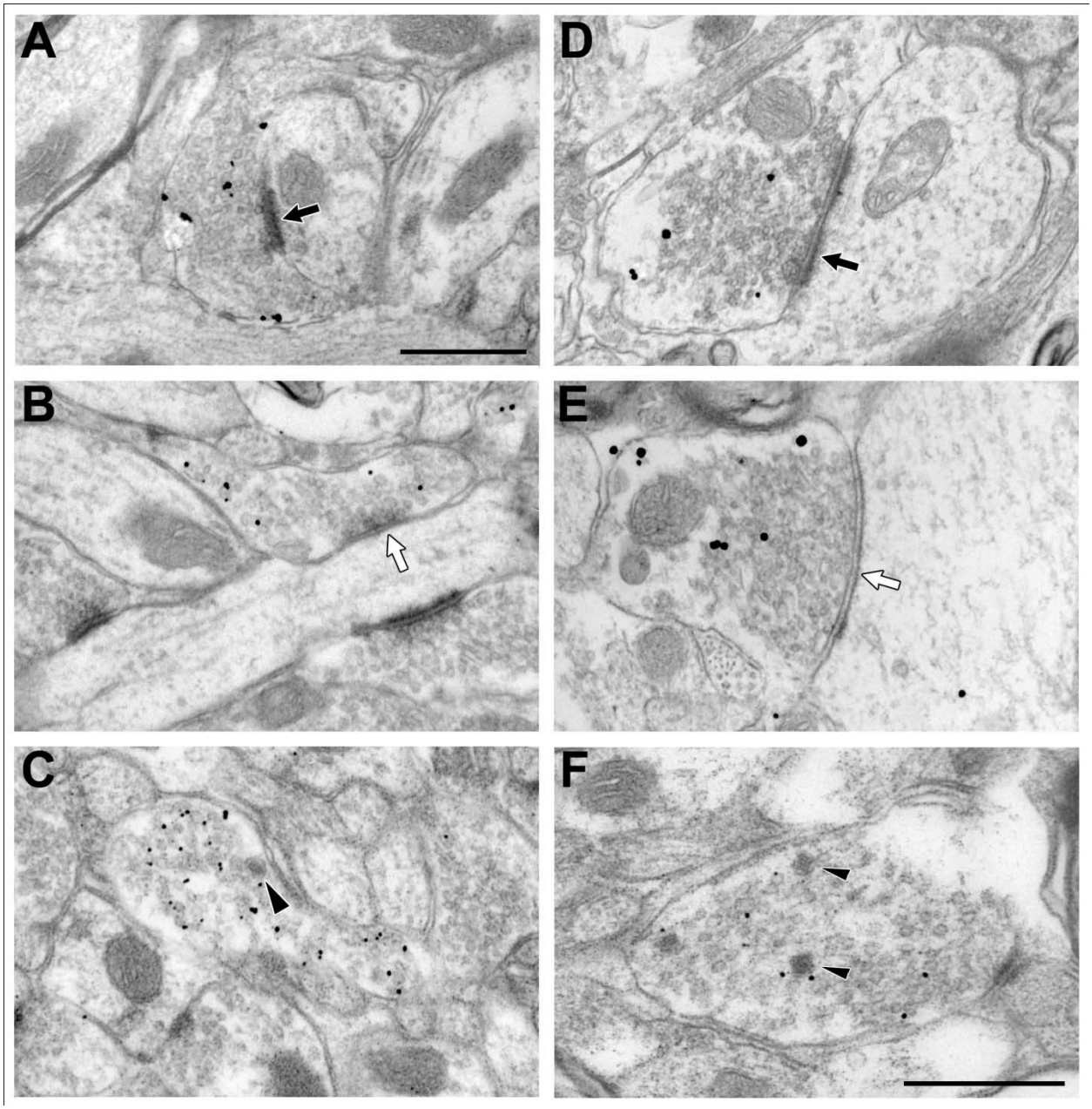

Figure 6 Morphology of CHT-immunoreactive profiles in the AVN and VTA.

Electron micrographs showing the morphological features of CHT-positive profiles in the AVN (**A-C**) and VTA (**D-F**). CHT labeled profiles form both asymmetric (black arrows, **A & D**) and symmetric (white arrows; **B & E**) types of synaptic contacts with unlabeled dendrites in the regions examined. Occasionally, dense-cored vesicles are observed in labeled profiles (arrowheads in **C & F**). Scale bar represents 0.5 µm.

cored vesicles (Figures 5, 6). These morphological features were more easily visualized with the immunogold-silver method, and this approach was therefore used to investigate regional differences in the frequency of observation of synaptic specializations and dense-cored vesicles (see below). By either immunoperoxidase or immunogold labeling methods, CHT-containing axons in the AVN appeared to be smaller and more densely labeled than profiles in the VTA. These apparent differences were also compared quantitatively using immunogold-silver labeling for CHT.

2.3.3 Morphological Features of CHT-labeled Axon Varicosities in the AVN and VTA

For the more exhaustive approach of counting synapses in serial sections, we included only profiles for which 3 or more serial micrographs were available to examine. This subset of CHT-labeled profiles was also used for statistical comparison between the AVN and VTA. The majority of this data came from 5 of the 6 rats (Data set #1, Table 1); sections from animal 2 were collected only on mesh grids and yielded few sets of serial micrographs. In the AVN, 333 CHT-immunoreactive axon varicosities were examined in serial ultrathin sections, and of these, 120 (36%) formed synaptic specializations of the symmetric or asymmetric type. In the VTA, 304 CHT-labeled profiles were analyzed in serial, and 144 of these (47%) were synaptic. There was a significant effect of region on the synaptic incidence of the profiles examined ($t_{(633)}$= -2.69, p = 0.0074), indicating that CHT axons in the VTA were more commonly observed to form synapses than those in the AVN. There was no significant effect of animal pair. Furthermore, there were no apparent differences across region in the extent to which CHT-labeled profiles formed symmetric (33% in the AVN versus 34% in the VTA) or asymmetric (60% in the AVN versus 54% in the VTA) synapse types; the remaining synapses had indeterminate morphology.

From single sections (Data set #2, Table 1), we observed 51 synapses from a total of 205 CHT-labeled varicosities (25%) in the AVN. In the VTA, we observed 60 synapses from a total of 205 CHT-labeled profiles examined (29%). These profiles had a mean diameter of 0.38 µm (AVN) and 0.58 µm (VTA), with a mean synapse length of 0.32 µm (AVN) and 0.47 µm (VTA). The mean section thickness in these micrographs was 65 nm (AVN) and 69 nm (VTA). Using the equation described in the methods, we obtained an extrapolated synaptic incidence of 35% in the AVN, compared to 36% observed in our serial sections. For the VTA, the extrapolated synaptic incidence was 47%, identical to the rate observed in our serial sections. The close agreement of the extrapolated synaptic incidence with results obtained from serial ultrathin section analysis suggests that extrapolation from single sections is an appropriate method for application to the brainstem cholinergic projection system, and may be used in place of the more labor-intensive serial examination.

CHT-positive varicosities were also analyzed in serial sections to determine whether dense-cored vesicles were present. In the AVN, 13% (44/333) of CHT-labeled profiles contained at least one dense-cored vesicle, compared to 29% (87/304) in the VTA. This regional difference was also statistically significant ($t_{(17.5)}$= -2.58, p = 0.0191), confirming that dense-cored vesicles were more commonly observed in the VTA CHT-positive population. There was no significant effect of animal pair.

2.3.4 Size of CHT-labeled Axon Terminals in the AVN and VTA

To quantify possible regional differences in the size and immunolabeling density of CHT-positive profiles, a larger data set was utilized in which profiles were collected from both serial and single section analyses (Data set #3, Table 1). For the AVN, 538 CHT-positive axon varicosities were measured, and their mean size was 0.41 μm^2 (± 0.13 SD). In the VTA, 509 profiles had a mean size of 0.63 μm^2 (± 0.12 SD). Figure 7 shows the distribution of observed profile areas and illustrates that similar ranges of areas were observed for both regions and that the distributions were overlapping. However, a large proportion of AVN profiles had small areas (> 90% in the first three bins), whereas VTA profiles were more likely to be of moderate area, as evidenced by the rightward shift of the VTA distribution compared to that of the AVN (Figure 7A). Statistically, there was a significant regional difference in profile area ($t_{(20.6)} = -4.18$; $p = 0.0004$), indicating that the population of CHT-positive varicosities in the AVN is on average smaller than that in the VTA. There was also a significant effect of animal pair ($F_{(2, 20.6)} = 6.49$; $p = 0.007$). The reason for this is not clear, but it might reflect the fact that animals within pairs were more likely to be the same age and weight and might even have been litter mates. Alternatively, the significant effect of animal pair might be due to differences in tissue shrinkage during the fixation, dehydration, and/or plastic embedding processes that would be expected to occur, as animal pairs were processed at different times.

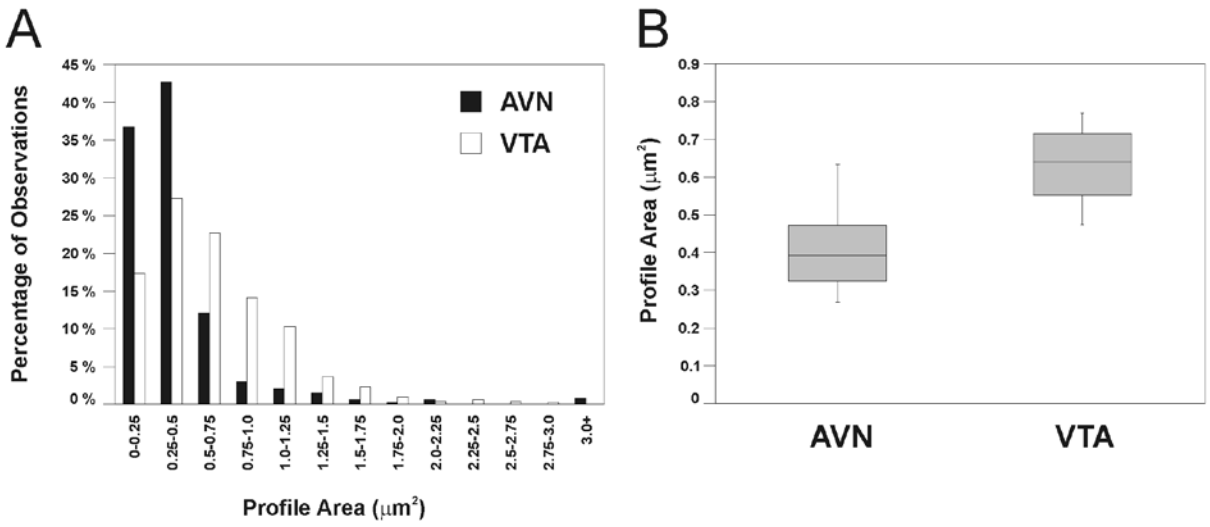

Figure 7 Cross-sectional area of CHT-*ir* profiles in the rat AVN and VTA.

Frequency distribution (**A**) and quartile plots (**B**) of CHT-labeled axon profile areas observed in the AVN and VTA. **A**: Histogram illustrating the frequency of areas measured for profiles immunoreactive for CHT in the rat AVN (black bars) or VTA (white bars). Each bar represents the percentage of the total sample of immunoreactive profiles having a particular area. **B**: Box plots illustrating the range of mean profile areas (between whiskers) as well as the median values (central line) and the middle 50% of values observed in each region (shaded boxes). Mean profile areas were computed by averaging profile areas within each region for each rat.

2.3.5 Total Gold and Membrane Gold Densities of CHT-labeled Axon Terminals in the AVN and VTA

CHT-labeled varicosities in the AVN appeared to contain more total gold-silver particles than those in the VTA, although a considerable range was also evident (Figures 6, 8). In the AVN, CHT-positive axon varicosities had a mean total gold density of 43.5 (± 17.0 SD) gold particles per unit area versus a density of 22.8 (± 4.4 SD) in the VTA. As shown in Figure 9, A&B, this difference reflects a larger proportion of profiles with low total gold in the VTA as compared to the AVN. The total gold density of CHT-labeled axonal profiles was significantly different between the AVN and VTA populations ($F_{(1, 20)} = 18.89$, $p = 0.0003$). There was also a significant effect of animal pair ($F_{(2, 20)} = 4.45$, $p = 0.0252$), indicating that total gold density was more similar within than across pairs. This is not surprising given that tissue from paired cohorts were processed at separate times using different batches of immunoreagents.

The greater density of total gold labeling might be expected to raise the probability of gold-silver particles contacting the plasma membrane (compare for example, Figure 8A and 8D). Therefore the set of all CHT-labeled profiles was also analyzed for membrane gold density, which had mean values of 1.05 (± 0.42 SD) and 0.55 (± 0.09 SD) gold particles per unit perimeter in the AVN and VTA, respectively. As shown in Figure 9 C,D, this apparent difference reflects a larger proportion of profiles with high membrane gold densities in the AVN versus the VTA. The difference in membrane gold density was significant between regions ($F_{(1,25.14)} = 24.32$, $p < 0.0001$); the effect of animal pair was not significant. As expected, total gold density also had a significant effect on membrane gold density ($F_{(1, 1041)} = 684.00$, $p < 0.0001$). However, there was also a significant interaction effect of region and total gold density on the membrane gold density ($F_{(1, 1041)} = 21.94$, $p < 0.0001$), indicating that although membrane

gold density was dependent on total gold density in both regions, the relationship between these variables differed significantly between regions. In other words, total gold density drove membrane gold density in a region-specific manner.

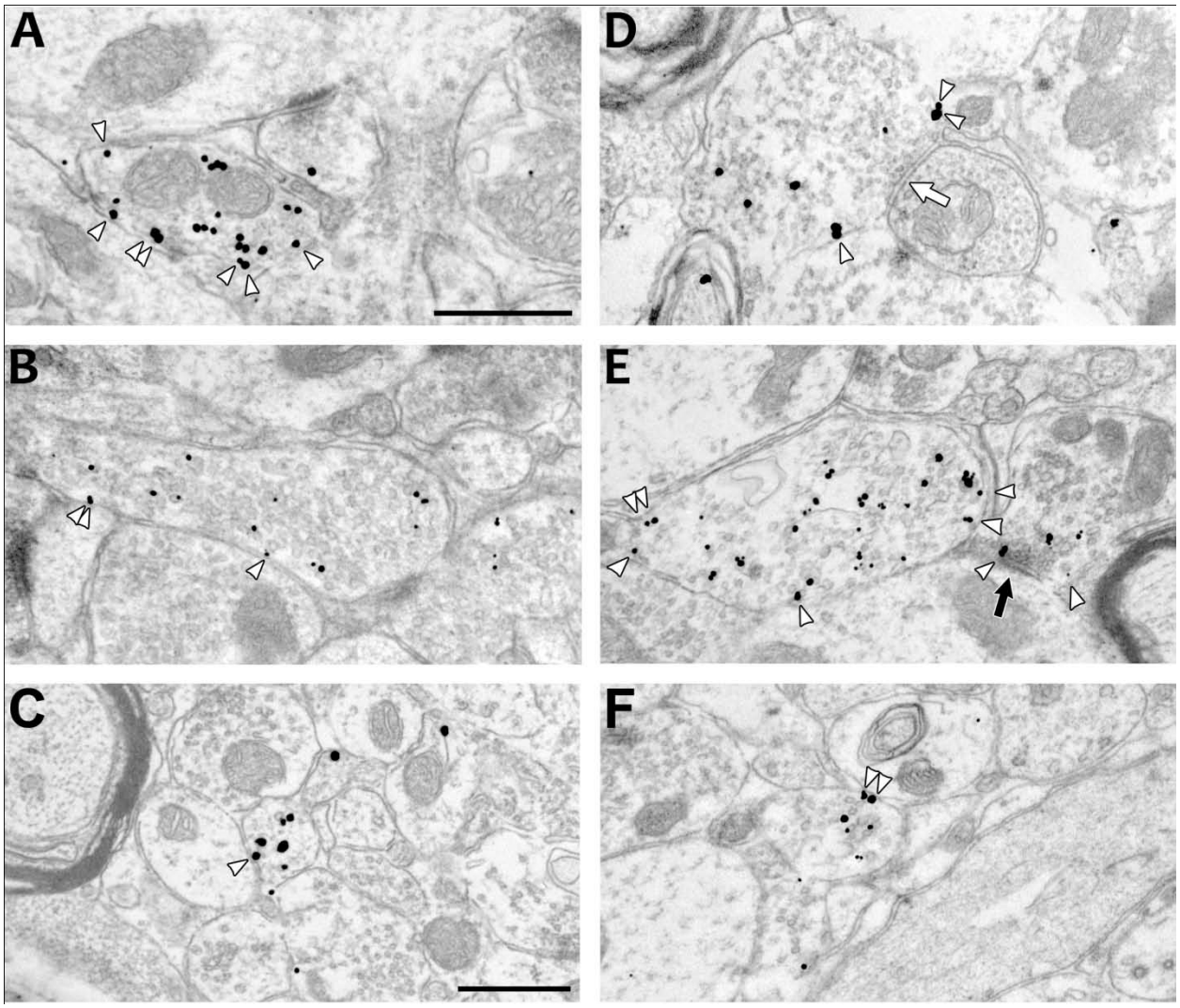

Figure 8 CHT immunogold labeling in axon varicosities from the rat AVN and VTA.

Electron micrographs illustrating CHT positive-profiles labeled by immunogold-silver in the AVN (**A-C**) and VTA (**D-F**) and displaying a range of sizes and also total gold and membrane gold densities. Arrowheads indicate gold-silver particles counted as being in association with the plasma membrane. Occasional symmetric (white arrow in **D**) or asymmetric (black arrow in **E**) synapses onto dendrites are exhibited by CHT-immunoreactive axons. Scale bars represent 0.5 µm. Scale bar in **A** represents 0.5 µm in **A** and **B**; scale bar in C represents 0.5 µm in **C**-**F**.

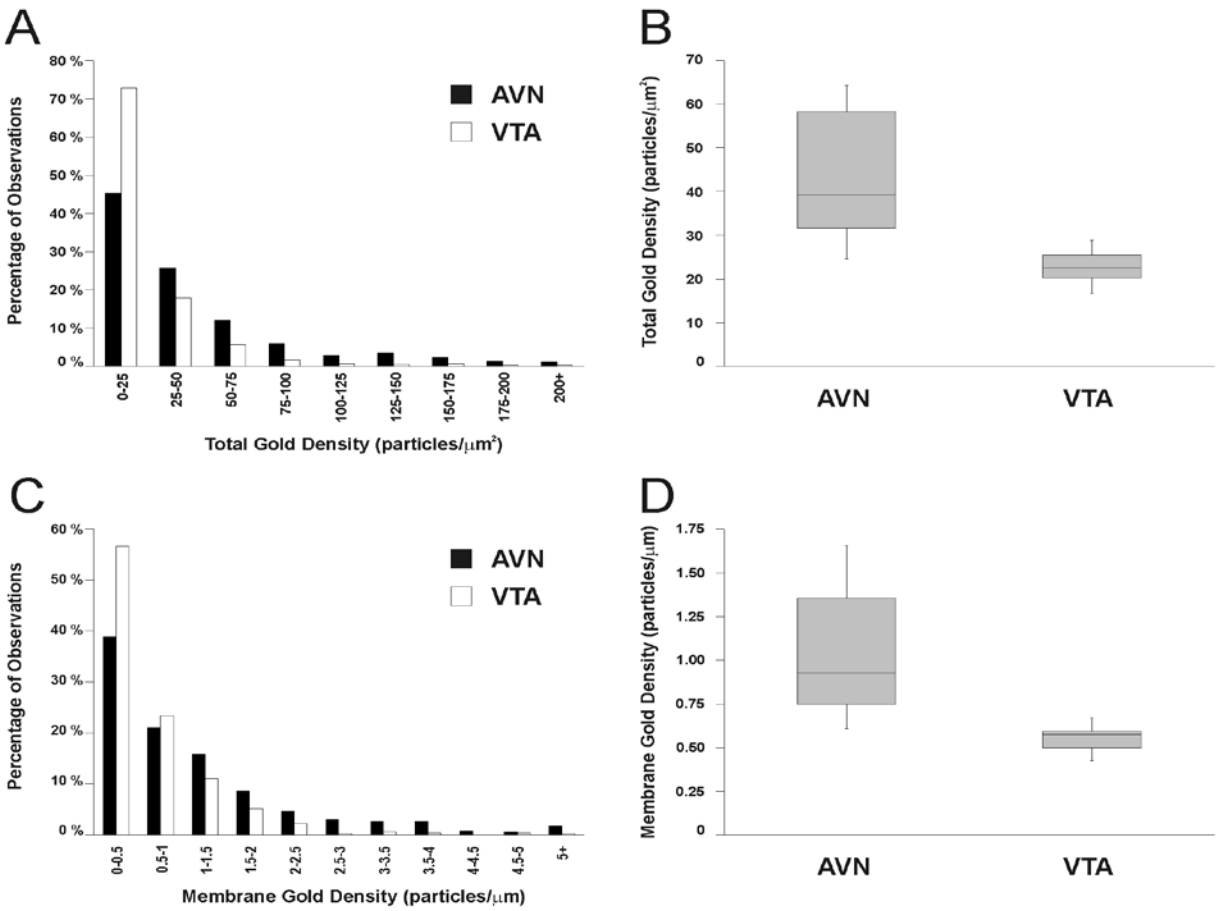

Figure 9 Total Gold Density and Membrane Gold Density of CHT-*ir* profiles in the rat AVN and VTA.

Frequency distributions (**A&C**) and quartile plots (**B&D**) of values observed for the total gold density (# gold particles/profile area; **A&B**) and membrane gold density (# membrane associate gold particles/profile perimeter; **C&D**) in the sample of CHT-labeled axonal profiles in the AVN and VTA. **A&C**: Histograms illustrating the frequency of total gold density (**A**) or membrane gold density (**C**) measured for profiles immunoreactive for CHT in the rat AVN (black bars) or VTA (white bars). Each bar represents the percentage of the total sample of immunoreactive profiles having a particular density. **B&D**: Box plots illustrating the range of mean total gold density and mean membrane gold density (between whiskers in **B** and **D**, respectively) as well as the median values (central lines) and the middle 50% of values observed in each region (shaded boxes). Mean total gold density and mean membrane gold density were computed by averaging total gold density and membrane gold density, respectively, within each region for each rat.

2.4 DISCUSSION

This study represents the first ultrastructural investigation of the distribution of CHT in the rat thalamus and midbrain as representative target areas of the brainstem mesopontine cholinergic system. The morphology and synaptology of the axons displaying CHT immunoreactivity in both regions were relatively well matched to profiles identified by other markers of cholinergic projections in the published literature. Nevertheless, direct comparison of CHT immunolabeled boutons in the rat AVN versus the VTA revealed some important differences, both in the morphological characteristics of these axon varicosities, and in the density and localization of the transporter. Labeled axons in the AVN were smaller and less frequently formed synaptic specializations with neuronal elements than those in the VTA. AVN profiles were also less frequently observed to contain dense-cored vesicles. Finally, AVN varicosities contained more total CHT immunogold particles than their VTA counterparts and showed a higher density of transporters associated with the plasma membrane.

2.4.1 Limitations of the Methods

The principal limitation of immunoelectron microscopy is the potential for false negative results based on restricted penetration of immunoreagents. The efficiency of the preembedding immunogold-silver method in particular is limited by incomplete penetration of gold-conjugated

secondary antibodies, and the need to minimize exposure to detergents that degrade phospholipid membranes. To reduce false negatives, we therefore examined tissue from only the first few microns of each section. We also used a stringent but consistent inclusion criterion to avoid false positives (see Materials and Methods). Therefore, we acknowledge that our sampling may have excluded some cholinergic axons that express low levels of CHT. As profiles in the VTA generally displayed a lower level of staining overall, this may have resulted in a more restricted sample population in this region. Nevertheless, the analysis involved thalamic and midbrain sections from the same animals exposed to the same batches of immunoreagents and subjected to the same sampling scheme. Moreover, the range of observed values overlapped considerably for both regions. Hence, the reported findings are likely to reflect true regional differences.

An additional limitation of the preembedding immunogold-silver method of antigen detection is the relative inefficiency of labeling membrane proteins in the synapse (Baude et al 1995; Bernard et al 1997). While this method localizes extrasynaptic membrane proteins well, the density of the synaptic space and associated structures reduces the ability of antibodies to gain full access to all available epitopes, hence increasing the likelihood of false negative staining specifically at this site. To determine with certainty the presence of transporters within synaptic membranes, post-embedding methods must be employed. However, we found that the antigenicity of CHT was not preserved following plastic embedding, thus preventing application of this more sensitive method. Therefore, our results concerning differences in the membrane density of CHT are applicable only to the extrasynaptic portions of the axonal membrane.

Finally, we must acknowledge that the low level of immunogold-reactivity associated with the plasma membrane may reflect a preferential association of the primary antibody with cytoplasmic transporters and reduced epitope recognition of membrane-bound transporters. This

could occur if association with the phospholipid membrane induced allostearic changes in the structure of the intracellular tail of CHT, or if the tail structure is otherwise different between the two states (e.g. through phosphorylation or interaction with scaffolding proteins). It should be noted that our sample included axonal profiles from each region that showed greater numbers of membrane transporters than cytoplasmic transporters, demonstrating that the heavily cytoplasmic staining is not artifactual. Nonetheless, we cannot exclude the possibility of a physical bias in immunoreactivity.

2.4.2 Population Characteristics of AVN and VTA CHT-Positive Varicosities

Our sample of CHT-positive boutons most likely represents cholinergic axons arising from the ascending projections of the tegmental cholinergic cell groups. To date, CHT expression in the brain has only been reported in cholinergic neurons (Okuda & Haga 2003), and the pattern of immunoreactivity closely matches that of VAChT and ChAT (Misawa et al 2001; Kus et al 2003). Hence, immunoreactivity for CHT serves as an exclusive marker of cholinergic axons. Furthermore, the AVN and VTA appear to receive cholinergic innervation predominantly from neurons in the brainstem mesopontine tegmentum (Sofroniew et al 1985; Jones & Beaudet 1987; Gonzalo-Ruiz et al 1995; Yeomans 1995). Although a minor projection from basal forebrain cholinergic cells to the AVN has been proposed (Hallanger et al 1987; Parent et al 1988), the majority of the cholinergic innervation to this region is believed to arise from the brainstem (Heckers et al 1992). Furthermore, the AVN is not immunoreactive for the nerve growth factor (NGF) receptor (Yan & Johnson Jr. 1989), a selective marker of basal forebrain cholinergic axons (Woolf et al 1989). The VTA is innervated by some neurons in the basal

forebrain (Tomimoto et al 1987; Grove 1988; Geisler & Zahm 2005), but these have never been demonstrated to be cholinergic. Moreover, the VTA regions that receive these projections are also devoid of NGF immunoreactivity (Yan & Johnson Jr. 1989), and other authors have asserted that the PPT and LDT represent the sole source of cholinergic afferents to the VTA (Yeomans et al 1993).

The morphology and synaptology of CHT-labeled axons in the thalamus and midbrain closely match previous descriptions of cholinergic boutons within these regions, including the relatively small size, content of small clear vesicles, and predominant formation of axodendritic synapses (Hallanger et al 1990; Garzon et al 1999; Oda et al 2003; Omelchenko & Sesack 2006). The presence of numerous dense-cored vesicles in these varicosities appears not to have been reported previously, most likely due to the masking effect of heavy immunoperoxidase product in prior studies.

Our sample of CHT-labeled varicosities did display some distinct differences in synaptology as compared to cholinergic populations described in the published literature. For example, Oda et al. reported a higher incidence of VAChT-labeled axons forming synapses in the AVN (~60% versus 35-36% in the present study). Moreover, both VAChT and ChAT-labeled axons have been reported to synapse onto cell bodies in this region (Hallanger et al 1990; Oda et al 2003), which we did not observe. In the VTA, the frequency of synapses reported here is better matched to previous estimates (~ 50% versus the present 47%) (Garzon et al 1999; Omelchenko & Sesack 2006). Nevertheless, we again did not observe any CHT-containing axosomatic synapses in the VTA, despite prior reports of these synapses using other markers of cholinergic axons (Garzon et al 1999; Omelchenko & Sesack 2006).

The reasons for these discrepancies are not immediately clear, although differences in the sampling strategies used across studies are likely to contribute. For example, studies focused on identifying the post-synaptic targets of cholinergic axons may have been biased towards varicosities that were in direct apposition to other neuronal elements and therefore more likely to be observed making synapses (Oda et al 2003). Our sample included all axonal profiles that contained synaptic vesicles and CHT immunoreactivity in excess of our inclusion threshold, leading us to examine both synapsing and non-synapsing varicosities. Alternatively, both the lower synaptic frequency of CHT-positive profiles in the AVN observed in our study and our failure to detect axosomatic synapses in both regions could indicate that CHT-labeled boutons constitute a subset of all cholinergic varicosities in the AVN and VTA. Additional studies using dual immunolabeling methods for CHT and VAChT are required to address this possibility.

Interestingly, the extrapolated synaptic incidence of cholinergic boutons in the AVN in this study (35%) is similar to that that observed in other thalamic nuclei receiving PPT/LDT cholinergic projections, including the reticular nucleus of the thalamus (33%) and the dorsolateral geniculate nucleus (39%), but stands in contrast to the cholinergic innervation of the parafascicular nucleus of the thalamus, where the incidence is reportedly 100% (Parent & Descarries 2008). As noted by those authors, this contrast suggests that the formation of synapses may be determined by the functional role(s) played by acetylcholine in each distinct region.

2.4.3 Differences between AVN and VTA CHT-labeled profiles

Variable rates of ACh turnover have been reported between the striatum and cerebral cortex (Wecker & Dettbarn 1979), indicating a lack of uniformity in functional measures across

different cholinergic cell groups in the CNS. Whether this functional variability in ACh transmission reflects structural differences in these axons or their content of CHT remains to be addressed. Still, it is tempting to speculate that the differences we observed in morphology, synaptology, and CHT distribution between cholinergic axons in the AVN and VTA have functional correlates. According to a general scaling principle (Pierce & Lewin 1994), axon terminal size is positively correlated with activity. It is important to note that this principle has been demonstrated only for amino acid transmitter-containing axons (Lisman & Harris 1993; Pierce & Lewin 1994) and has not yet been investigated for cholinergic systems. Still, CHT-positive varicosities in the VTA might be more active and release greater amounts of ACh based on their larger size and higher apparent rate of synapse formation. Alternatively, the higher total content and greater membrane distribution of CHT in AVN profiles suggests an overall higher demand for ACh synthesis that necessitates steady replenishment of choline. It is difficult to reconcile these seemingly paradoxical observations, and neurochemical studies are needed to specifically test for differences in ACh transmission between the thalamus and midbrain.

In addition to possible differences in overall activity level, it could be that the pattern of ACh release also differs between these areas and that this results in distinct demands for choline uptake. Different activity patterns have been recorded for presumed cholinergic neurons in the mesopontine tegmentum, including cells whose firing varies across sleep-wake states, as well as neurons with state-independent activity (Koyama et al 1994; Datta & Siwek 2002). If cells with phasic patterns of ACh release innervate the VTA, then their axonal stores of transmitter could be replenished during quiescent periods using a relatively small number of membrane-associated transporters. Conversely, AVN cholinergic axons might be subjected to tonic activity patterns that require greater continuous reuptake of choline and therefore a higher level of membrane

CHT. In this regard, it is interesting to note that increased membrane CHT has been reported in the cerebral cortex during sustained attention tasks that require tonically accelerated ACh transmission (Apparsundaram et al 2005).

The fact that many CHT-labeled boutons in both the thalamus and midbrain failed to display evident synaptic specializations suggests that ACh released from brainstem cholinergic cells may be acting on extrasynaptic targets through volume transmission, as already suggested for forebrain cholinergic systems (Descarries et al 1997). The lower apparent rate of synapse formation in the AVN as compared to the VTA further suggests that volume transmission may play a more important role in the former structure. Nevertheless, there is evidence consistent with extrasynaptic ACh transmission in both regions. For example, the AVN is likely to be the source of ACh for the adjacent anterodorsal thalamic nucleus that expresses cholinergic receptors (Sikes & Vogt 1987; Vogt et al 1992) but lacks direct cholinergic input (Levey et al 1987; Oda et al 2003). For the VTA, diffuse ACh transmission has been suggested based on the localization of α7 nicotinic receptors on glutamate axon terminals (Jones & Wonnacott 2004) and the absence of axo-axonic synapses in this region.

Finally, the higher dense-cored vesicle content observed for VTA versus AVN cholinergic boutons suggests that peptide co-transmission may play a larger role in the modulation of VTA neurons. Cholinergic cells in the mesopontine tegmentum have been demonstrated to synthesize and release substance P (Vincent et al 1983; Sutin & Jacobowitz 1990) and these neurons may utilize other peptide co-transmitters as well (Crawley et al 1985; Standaert et al 1986).

2.4.4 Functional significance

It is interesting to note that, while the AVN and VTA have no direct connections between them (Beckstead et al 1979; Simon et al 1979), and even project to distinctly separate cortical and subcortical regions (Bentivoglio et al 1993), both nuclei have been implicated in cue-driven behavior (Gabriel et al 1980; Pan & Hyland 2005). The AVN is best recognized for its contribution to spatial memory (Warburton & Aggleton 1999) but also partially mediates conditioned avoidance responses (Gabriel et al 1980; Sparenborg & Gabriel 1992). In contrast, the VTA plays a crucial role in conveying reward prediction to forebrain circuits that determine behavioral output (Schultz 2007; Redgrave et al 2008). The cholinergic input to the VTA is especially necessary for both novel and conditioned cue-driven responses of VTA dopamine neurons (Ikemoto & Panskepp 1996; Pan & Hyland 2005). Hence, it seems likely that both the AVN and VTA must receive information about external cues that can guide behavior. This information might be transmitted by cholinergic neurons in the PPT and LDT, as these neurons are responsive to sensory input (Grant & Highfield 1991; Pan & Hyland 2005). It is therefore tempting to speculate that environmental stimuli could influence divergent parts of the limbic system through collateral projections from the cholinergic brainstem. Collateralized projections of cholinergic neurons to thalamic nuclei and other regions have been documented (Jourdain et al 1989; Semba et al 1990; Bolton et al 1993; Oakman et al 1999), although to date the possible existence of such projections to the VTA and AVN has not been explored. Alternatively, such information may be relayed by the non-cholinergic neurons in these regions, or through separate populations of cells.

If the projections to the AVN and VTA are ultimately shown to arise from a common brainstem cell population, then the regional differences observed here in CHT-labeled axons

would argue for local factors being the main determinants of bouton morphology and CHT distribution. This supposition is supported by recent evidence that the cholinergic innervation of several thalamic nuclei displays striking differences in synaptic incidence, even when this innervation arises from similar sources (Parent & Descarries 2008). In regard to differences in CHT distribution, CHT localization and function can be influenced by intracellular signaling events triggered by the activity of neurotransmitter receptors on the surface of cholinergic axons (Breer & Knipper 1990). Increases in high-affinity choline transport can be achieved through activation of protein kinase A or C, and corresponding decreases can be effected by phosphatase 1/2A (Breer & Knipper 1990; Gates et al 2004). It is therefore plausible that the heterogeneity of CHT labeling observed in this study reflects differences in the extracellular milieu in the AVN versus the VTA. Our finding of a significant interaction effect of region and total gold density on the membrane gold density of CHT-labeled axonal profiles is consistent with some as yet unidentified factor that is differentially active in these regions. One possibility is that the presence of extracellular dopamine released from somatodendritic compartments in the VTA might decrease the membrane density of CHT in this region. This possibility is supported by *in vivo* data showing that elevated extracellular dopamine levels in the striatum are associated with reductions in high-affinity choline transport, consistent with decreased membrane levels of CHT (Parikh et al 2006).

Alternatively, the differential expression of the choline-sensitive α7 nicotinic acetylcholine receptor (nAChR) may contribute to the differences in membrane CHT content reported here. In the VTA, activation of presynaptic α7 nAChRs results in the potentiation of glutamate release from excitatory afferents (Schilström et al 2000; Jones & Wonnacott 2004), but all forms of cholinergic transmission in the AVN are mediated through non-α7 nAChRs

(Guseva et al 2006; Rasmussen & Perry 2006) or through muscarinic receptors. The α7 nAChR is desensitized by extracellular choline (Alkondon et al 1997; Mike et al 2000; Uteshev et al 2003; Alkondon & Albuquerque 2006). Hence, the membrane content of CHT might be inversely correlated with the availability of α7-mediated modes of cholinergic transmission. In this case, the lower membrane content of CHT in the VTA might be driven by a need to keep extracellular choline levels high, thereby restricting the activation of α7 nAChRs and preventing excessive glutamate excitation.

Although differential regulation of choline transport could be accomplished at a local level, the collective morphological differences observed between the CHT-immunolabeled axons in the AVN and VTA are most easily explained by cholinergic innervations arising from separate populations of neurons in the mesopontine tegmentum. Alternatively, the parent populations of AVN and VTA cholinergic inputs could be partially overlapping subsets of PPT/LDT cholinergic cells. This mixed afferent population could produce a range of axon characteristics that favor smaller varicosities with more dense CHT content in the AVN and the converse characteristics in the VTA. This idea is supported by tract-tracing studies showing input from both PPT and LDT populations to the VTA (Satoh & Fibiger 1986; Oakman et al 1995; Omelchenko & Sesack 2005), but a heavier input from the LDT to the AVN (Shibata 1992). Tract-tracing studies will be essential for clarifying the nature of these circuits and facilitating a systems-level interpretation of the present findings.

3.0 DUAL IMMUNOFLUORESCENCE FOR VAChT AND CHT: COMPARISON OF COLOCALIZATION OF CHOLINERGIC PROTEINS IN THE AVN AND VTA

3.1 INTRODUCTION

The neurotransmitter acetylcholine (ACh) is synthesized through the reaction of acetyl coenzyme A, a molecule produced in mitochondria during cellular respiration, and choline, an essential nutrient that must be obtained from dietary sources (Cooper et al 2003; Löffelholz & Klein 2006). This reaction is catalyzed in cholinergic neurons by the enzyme choline acetyltransferase (ChAT), and newly synthesized ACh is packaged into synaptic vesicle for future release by the vesicular acetylcholine transporter (VAChT) (Erickson et al 1994). The choline used as a substrate for ACh synthesis is transported into these neurons through the action of the high-affinity choline transporter (CHT) (Yamamura & Snyder 1972; 1973; Simon et al 1976). Availability of choline is rate-limiting for ACh synthesis, making the functional high-affinity choline uptake crucial to maintaining normal cholinergic signaling (Mulder et al 1974). Accordingly, CHT expression levels are typically increased by the same regulatory factors that increase levels of VAChT and ChAT (Lips et al 2003; Lecomte et al 2005), the two other proteins whose expression defines the cholinergic phenotype (Erickson et al 1994; Ichikawa et al 1997).

In the central nervous system, CHT is expressed exclusively in cholinergic neurons (Misawa et al 2001; Ferguson et al 2003; Kus et al 2003). However, CHT-*ir* is notably absent from at least one subset of cholinergic terminals within the brain (Misawa et al 2001), reflecting the fact that CHT expression can be regulated independently from that of the vesicular acetylcholine transporter (VAChT) or choline acetyltransferase (ChAT) under some conditions (Lecomte et al 2005). Further evidence that transcription and translation of CHT protein can be dissociated from that of the other cholinergic proteins comes from reports of CHT expression by non-cholinergic cells (Masland & Mills 1980; Haberberger et al 2002). Within axons, CHT is predominantly localized to small synaptic vesicles that provide a mechanism for its trafficking to the plasma membrane. Although not all cholinergic synaptic vesicles contain CHT, virtually all CHT-containing vesicles contain VAChT (Ferguson et al 2003), indicating that the localization of the two proteins are closely linked. Still, the trafficking of CHT and VAChT protein from the cell body appears to occur through separate pathways (Misawa et al 2008), allowing the possibility that CHT may be concentrated at some sites of ACh release, yet absent from others.

Within the brain, there is robust colocalization of CHT with VAChT or ChAT in cholinergic cell bodies (Ferguson et al 2003; Kus et al 2003), but quantitative analysis of CHT and VAChT colocalization in axonal profiles has not been reported for any region within the CNS. Furthermore, differences in high-affinity choline uptake and subsequent rates of acetylcholine synthesis have been reported for different cholinergic systems in the rat brain (Wecker & Dettbarn 1979; Stanton & Johnson 1987). Finally, CHT and VAChT dual labeling in the ventral horn of the spinal cord suggest a population of VAChT-*ir* puncta without detectable levels of CHT-*ir* (Ferguson et al 2003), indicating that the degree of colocalization of VAChT and CHT may vary between different cholinergic systems, and even between cells of the same

cholinergic group. Thus, even if VAChT and CHT are highly colocalized in some cholinergic axon terminals, this is not necessarily generalizable to the brainstem tegmental cholinergic projections, a system in which the expression and regulation of CHT is less well-characterized than in the basal forebrain cholinergic system or in striatal cholinergic cells.

Our recent investigation of CHT subcellular localization in the axon terminals of the anteroventral thalamus (AVN) and the ventral tegmental area (VTA) revealed that CHT-immunoreactive varicosities in the VTA were larger and less heavily labeled for CHT than their counterparts in the AVN (Holmstrand et al 2010). VTA CHT-ir axons also more frequently contained dense-cored vesicles, indicating a larger role for peptide co-transmission in these projections. Finally, CHT-ir profiles in the VTA were more frequently observed to form synaptic contacts than those in the AVN, suggesting that the projections to the VTA may operate via point-to-point synaptic transmission to a greater degree than in the AVN (Agnati et al 1995). Although these brain regions are both innervated by cholinergic neurons in the brainstem pedunculopontine and laterodorsal tegmental nuclei (PPT and LDT, respectively), the collective differences we observed in these axonal populations indicate that cholinergic transmission may have distinctive characteristics specific to each brain region.

In Chapter 2, we also noted that none of the synapses we observed were formed with somal postsynaptic targets. This contradicted previous reports, in which a small percentage of cholinergic terminals, identified by immunohistochemistry for VAChT or ChAT, formed synapses on cell bodies in the AVN and VTA (Hallanger et al 1990; Oda et al 2003; Omelchenko & Sesack 2006). While we cannot wholly exclude a possible unconscious bias in our sampling, the large number of terminals that we examined in serial ultrathin sections made it unlikely that we simply overlooked this subset of CHT-immunoreactive terminals.

Alternatively, some cholinergic boutons may express such low levels of CHT that they were excluded from our sample. It is also possible that CHT may be localized to some axonal compartments distinct from those containing the majority of colocalized VAChT and CHT. If either of these latter scenarios is true, this should be reflected by incomplete colocalization of the two markers in these regions. Furthermore, axons in the VTA express lower levels of CHT than those in the AVN (Holmstrand et al 2010), so we expect that the frequency of detectable colocalization of VAChT and CHT to be lower in the VTA than in the AVN.

Due to the rate-limiting effect of high-affinity choline uptake on ACh synthesis, the ability to sustain high neuronal firing rates appears to depend on adequate expression of CHT. During periods of elevated ACh release, a reserve of transporters can be accessed and delivered to the plasma membrane through the exocytosis of CHT-containing synaptic vesicles, resulting in increased high-affinity choline uptake that supports rapid refilling of the vesicular pool of ACh. The refilling of vesicles is also dependent on the actions of VAChT (Van der Kloot et al 2000; Van der Kloot et al 2002). Therefore, it is expected that the levels of VAChT protein within a cholinergic terminal may reflect the size of the vesicular pool of ACh, with higher levels of VAChT being expressed in terminals that can release greater amounts of ACh upon stimulation (de Castro et al 2009; Lima et al 2010). While it seems likely that CHT and VAChT expression would be linked to the relative activity of a given neurons, experimental manipulations can increase CHT expression without affecting VAChT levels (Erb et al 2001; de Castro et al 2009). Whether CHT expression is related to the level of VAChT expression under baseline conditions is unknown.

We chose to examine the colocalization of CHT and VAChT in AVN and VTA axons using state-of-the-art spinning disk confocal immunofluorescence microscopy, to determine if 1)

CHT and VAChT are always colocalized within the axon varicosities of the brainstem tegmental cholinergic neurons; and 2) if the rate of observed colocalization in the AVN is higher than that observed in the VTA. Additionally, we compared quantitative immunofluorescence levels for CHT and VAChT across regions to determine if variation in the levels of CHT or VAChT exists between two populations of axon terminals that arise from the same tegmental cholinergic system. We further assessed whether CHT expression is related to VAChT protein levels, and therefore would be likely to reflect the relative activity of afferents to the AVN and the VTA, by examining the relative levels of CHT to VAChT within individual colocalized boutons in these regions.

3.2 MATERIALS & METHODS

3.2.1 Antibodies and Reagents

All chemicals were purchased from Sigma unless otherwise noted. The monoclonal antibody against CHT (MAB5514, Millipore, Billerica, MA) was raised in mouse against a GST-fusion protein containing an 80 amino acid portion of the C-terminal tail of human CHT (Ferguson et al 2003). Evidence for the specificity this antibody includes Western blot staining of the predicted size of CHT (65 kDa) from PC-12 cells transfected with hCHT but not from untransfected controls (Ferguson et al 2003), and absence of staining in CHT knockout mice (Ferguson et al 2004). The polyclonal antibody against VAChT was raised in rabbit against an 11 amino acid sequence from the carboxyl tail of the transporter, and was a generous gift from

Dr. Yongjian Liu at the University of Pittsburgh. This antibody labels VAChT but not the vesicular monoamine transporter (VMAT) in transfected PC-12 cells (Liu & Edwards 1997). In addition, the pattern of immunostaining that we observed with either of these antibodies matched the known distribution of cholinergic cells and axon terminals in the rat brain.

3.2.2 Tissue Preparation

Five adult male Sprague-Dawley rats were anesthetized with sodium pentobarbital (Nembutal, 100 mg/kg i.p.) and perfused transcardially with 50 mL heparin saline (1000 U/mL) followed by 500 mL PLP fixative (4% paraformaldehyde, 1.4% lysine acetate, 0.1 % sodium meta-periodate in 0.1 M phosphate buffer (PB); (Mclean & Nakane 1974)). The brain was removed from the skull, cut into blocks containing the AVN or VTA, and post-fixed in the same fixative overnight at 4^0C. Tissue was sectioned to 30 µms using a Vibratome, treated for 30 minutes with 1% sodium borohydride in PB, then rinsed extensively in PB.

3.2.3 Immunohistochemistry

From each rat, a one in six series of sections through each region was used for dual fluorescence immunohistochemistry. Briefly, sections were rinsed several times in 0.01 M phosphate buffered saline (PBS), and then incubated for 3 hours at room temperature in a blocking solution containing 0.1% L-lysine, 0.1% glycine, 0.3% Triton X-100 and 5% nonfat dry milk in PBS. Sections were then transferred to vials containing the primary antibodies diluted in blocking solution: polyclonal rabbit anti-VAChT (1:20,000) and monoclonal mouse anti-CHT

(1:100,000). Incubation in primary antibodies proceeded for 48 hours at 4^0C with agitation. Sections were then rinsed several times in PBS and incubated in fluorophore-conjugated secondary antibodies, diluted in blocking solution: Alexa 488 donkey anti-mouse and Alexa 568 donkey anti –rabbit (1:500, Invitrogen, Carlsbad, CA). Sections were incubated in secondary antibodies for 24 hours at 4^0C with agitation, and protected from light during this time.

All sections were rinsed extensively in PBS, mounted on glass slides and allowed to air dry while protected from ambient light. Slides were coverslipped the same day with Fluoromount G (Southern Biotech, Birmingham, AL).

3.2.4 Microscopy

All sections were photographed at low magnification (4X) in the 488 channel on an Olympus BX51 microscope (Olympus, Center Valley, PA) equipped with Xenon/Argon illumination source with very brief exposure times, so as to limit photobleaching of this fluorophore. These low power images were used to delineate the borders of the AVN and the VTA and to select regions for high-magnification (60X) imaging by confocal microscopy. A numbered sampling grid was overlaid on these low-magnification images, and the sections and grid squares to be sampled were selected using a random number generator in Microsoft Excel.

High magnification images were collected on an Olympus BX51W1 microscope equipped with a spinning disc confocal unit (Olympus), and a motorized stage (Bioprecision stage with MAC 6000 controller, Ludl Electronics Products, Ltd., Hawthorne, NY) with XYZ-axis encoding (Heidenhain, Schaumburg, IL). Sections were illuminated with a metal arc lamp (Prior Lumen 200, Prior Scientific, Rockland, MA) and excitation and emission fluorescence were filtered to appropriate wavelengths with matched filter sets (89000 Sedat Quad Filter Set,

Chroma Technology Corp, Bellows Falls, VT). Images were captured at 60X magnification (PlanApo Objective, 1.42 N.A., Olympus) with a CCD camera (Orca R2, Hamamatsu, Bridgewater, NJ) and SlideBook software (version 5.0, Intelligent Imaging Innovations, Inc., Denver, CO). Paired images were obtained from the 488 and 568 channels at 0.25 µm intervals along the Z-axis, starting 1-2 µm from the surface of the bottom of the section and continuing through to a plane 1-2 µm below the surface of the top of the section.

Due to the large difference in the number of immunofluorescent puncta between the AVN and the VTA, overall fluorescence intensity was much higher in image stacks obtained from the AVN. It was therefore necessary to use different capture parameters in order to optimize detection of immunofluorescent objects without saturating the camera. For AVN stacks, the 488 channel was collected with a gain of 0 and exposure time of 1700 ms, and the 568 channel was collected with a gain of 0 and exposure time of 1500 ms. In the VTA, images from the 488 channel were collected with a gain of 50 and exposure time of 2500 ms, and 568 channel images were collected with a gain of 0 and exposure of time 2300 ms. In order to compare the fluorescence intensity values (FI) of our sample puncta, we applied a correction to the AVN data that was determined empirically from calibration with reference fluorescent polystyrene beads (Inspeck Green beads and Inspeck Orange beads, 6 µm, 0.3% intensity, Invitrogen, Carlsbad, CA). This correction, detailed below in Section 3.2.6.2 Exposure and Gain Corrections, scaled the AVN data to the same quantitative range as our VTA data points, making quantitative comparison of the two regions possible.

3.2.5 Image Analysis

Image stacks were corrected for photobleaching and deconvolved using a constrained iterative approach and a calculated point spread function. The deconvolved images were background subtracted using the mode FI value in each channel as "background." A masking procedure (Figure 10) identified immunofluorescent objects using a simple threshold segmentation of the 488 (CHT) or 568 (VAChT) channels. The fluorescence channel used to define an object (e.g. 488-CHT for CHT-*ir* objects) was designated the primary channel for that object. The threshold value applied to each stack was equal to 2x the background intensity (i.e. mode value) of the original deconvolved image stack. This value was then applied to the background subtracted image, making the effective intensity criterion for each voxel 3x the background fluorescence. A size criterion of 3 voxels was applied to the resulting objects, to reduce the number of false positive objects included in the sample. After defining objects in each mask (CHT-*ir* and VAChT-*ir* objects, respectively), colocalization of the two markers within the same objects was assessed using the overlap of the primary VAChT or CHT masks. Each VAChT-*ir* or CHT-*ir* object was thus assigned to a colocalized or non-colocalized group.

The mean 488 and 568 fluorescence intensities of both VAChT-*ir* and CHT-*ir* objects were recorded. These means were calculated over the set of voxels defined for each object within a selection mask, including those voxels that had subthreshold intensity values in the secondary (i.e. non-selection) channel (see Figure 11). Paired mean fluorescence intensities were exported to Microsoft Excel, along with the volume, x-, y-, and z-axis center co-ordinates, and colocalization status of each VAChT-*ir* and CHT-*ir* object.

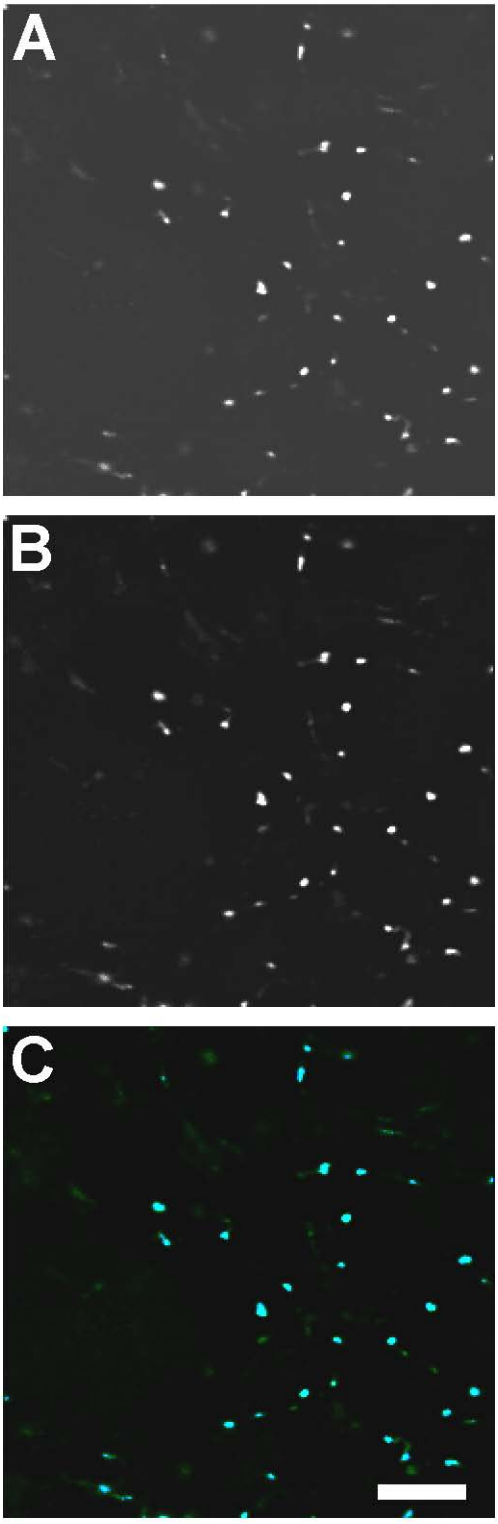

Figure 10 Segmentation masking of fluorescent objects.

The procedure for masking objects began with single channel deconvolved image data. Original images (**A**) were background subtracted using the mode intensity value of the corresponding channel (**B**). A simple threshold of 2x the mode value of the original image was applied to the background subtracted image. The automated analysis identified the edges of objects as voxels that met or exceeded the threshold, and treated all voxels contained within this border as a single immunofluorescent object. The resulting mask is shown in **C**. Scale bar in **C** represents 10 µm and applies to all panels.

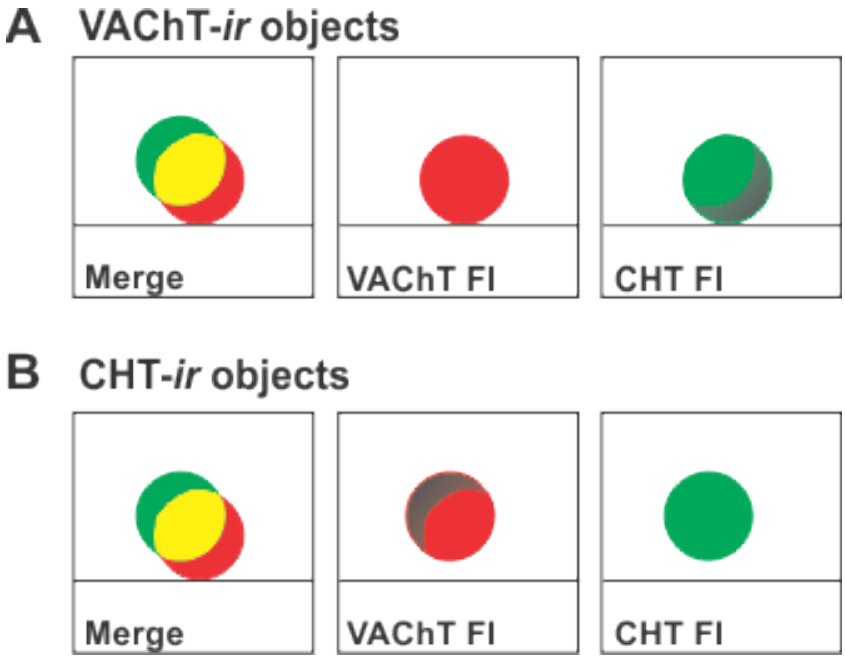

Figure 11 Component voxels used to calculate mean fluorescence intensities in VAChT-*ir* and CHT-*ir* objects.

VAChT-*ir* (**A**) and CHT-*ir* (**B**) objects were defined by the set of voxels that had fluorescence intensities (FI) greater than the stack-specific threshold value in the corresponding channel (e.g. 568-VAChT channel for VAChT-*ir* objects). A colocalized object (left panels, **A** and **B**), identified by overlapping VAChT-masked and CHT-masked objects, has both VAChT-*ir* and CHT-*ir* component objects. The mean VAChT and CHT FI values could be calculated for each VAChT-*ir* or CHT-*ir* object, by averaging over the set of voxels that comprised the VAChT-*ir* or the CHT-*ir* objects. This approach resulted in the inclusion of voxels that had above threshold values in the selection channel but that could have subthreshold values in the secondary channel (darkened pixels in the CHT FI panel in **A**; in the VAChT FI panel in **B**). The horizontal line is shown to indicate which puncta from the merged panel is used for calculating mean FI. For non-colocalized puncta, the mean FI of each channel was still calculated, even though the voxels in the secondary channel were below threshold.

A guard zone was applied to these data, removing any objects that lay within the first or last 20 pixels in the x and y dimensions, or if objects were located outside of the central 6 µm of the Z-stack. Microsoft Excel was used to filter data in preparation for statistical analysis and to prepare summary tables and graphs.

3.2.6 Statistical Analysis

3.2.6.1 Odds Ratios

To compare the rate of colocalization observed in the AVN versus the VTA, we calculated the odds ratio (OR) of colocalization for the AVN in reference to the VTA. The odds ratio (OR), defined as $OR = \frac{\hat{p}_{AVN}}{\hat{p}_{VTA}}$, where $\hat{p}_{AVN}$ is the odds of colocalization for VAChT-*ir* or for CHT-*ir* puncta in the AVN, $\hat{p}_{VTA}$ is the odds of colocalization for VAChT-*ir* or CHT-*ir* puncta in the VTA. These parameter estimates were obtained using the following definitions:

$$\hat{p} = \frac{p_{coloc}}{(1-p_{coloc})}, \qquad p_{coloc} = \frac{\#\ colocalized\ puncta}{\#\ total\ puncta} \quad .$$

Point estimates and 95% confidence intervals of the odds ratio of colocalization with the secondary immunofluorescent marker were calculated for both the VAChT-*ir* and CHT-*ir* populations using Microsoft Excel.

3.2.6.2 Exposure and Gain Corrections

To compare mean FI values across regions, we first applied a correction to the AVN data to compensate for the lower exposure time and lower gain setting used to collect data in this region. We determined that the effects of varying exposure time (ms) or gain on mean 488 FI

were linear by imaging reference fluorescent beads with varying exposure and gain settings (see Appendix B, Figure 25). For the 488-corrections, Green beads of 0.3% intensity were imaged to create calibration curves over the range of exposure times and gain settings used to collect images from immunolabeled tissue. For the 568-corrections, Orange beads of 0.3% intensity were imaged to calibrate FI over the range of exposure times only. These image stacks were deconvolved and background subtracted in the same manner as the data obtained from tissue sections. Linear regression of the mean FI values obtained from these calibration stacks revealed a significant dependence of FI on both the exposure and gain used for capture in the 488 channel, and a significant effect of exposure on the mean FI of 568 labeled beads (see Appendix B, Figure 26). For mean 488 FI, the calibration data were fit to the following regression line: $y = 0.237(\text{exposure (ms)}) + 11.570\ (\text{gain})$, $R^2 = 0.991$. For mean 568 FI the regression line was defined as: $y = 1.243(\text{exposure})$, $R^2 = 0.980$ (Appendix B, Figure B-3). Therefore, we transformed our AVN CHT mean FI values by the addition of ((0.237*800 ms) + (11.570*50)) = 768.1. Similarly, we scaled the AVN VAChT mean FI values by adding ((1.243)(800 ms)) = 994.4 to all AVN 568 FI mean intensities.

3.2.6.3 Mixed Model Analysis of Mean CHT and Mean VAChT FI

To test for differences in the mean FI of CHT immunoreactivity and VAChT immunoreactivity between the AVN and VTA populations, a linear mixed model was used. The model tested for a fixed effect of brain region (AVN versus VTA) and included the random effects of animal and section within animal to control for variability in the data due to repeated sampling from the same rats and the same tissue sections. For these analyses, we compared the

mean FI of immunofluorescence for the primary channel used to define the object (e.g. mean CHT FI in CHT-*ir* objects).

In colocalized objects, we examined the relationship between CHT immunofluorescence intensity and VAChT immunofluorescence intensity within individual boutons by calculating the Pearson's correlation coefficients for the log(mean FI) for CHT and VAChT within colocalized objects.

Finally, we compared the ratio of mean FI in the secondary channel to mean FI in the primary channel to determine if the relative levels of CHT and VAChT within colocalized objects (i.e. likely cholinergic boutons) differed systematically between the AVN and VTA populations. A linear mixed model with the same fixed and random effect structure described above was used to test for regional differences in the ratio of $\frac{\log(mean\ CHT\ FI)}{\log(mean\ VAChT\ FI)}$ in objects defined by VAChT immunofluorescence (VAChT-*ir* objects) that also displayed above threshold CHT fluorescence, thus meeting criterion for colocalization. For the CHT-*ir* objects, the ratio compared across regions was $\frac{\log(mean\ VAChT\ FI)}{\log(mean\ CHT\ FI)}$. All statistical tests were performed with PASW 18 (SPSS Inc, Chicago, IL) with a significance level set at $p = 0.05$.

3.3 RESULTS

3.3.1 Extent of Colocalization of VAChT and CHT

Representative 60x dual fluorescence images from the AVN and the VTA are shown in Figure 12. Qualitatively, it appeared that most puncta in both regions displayed colocalized

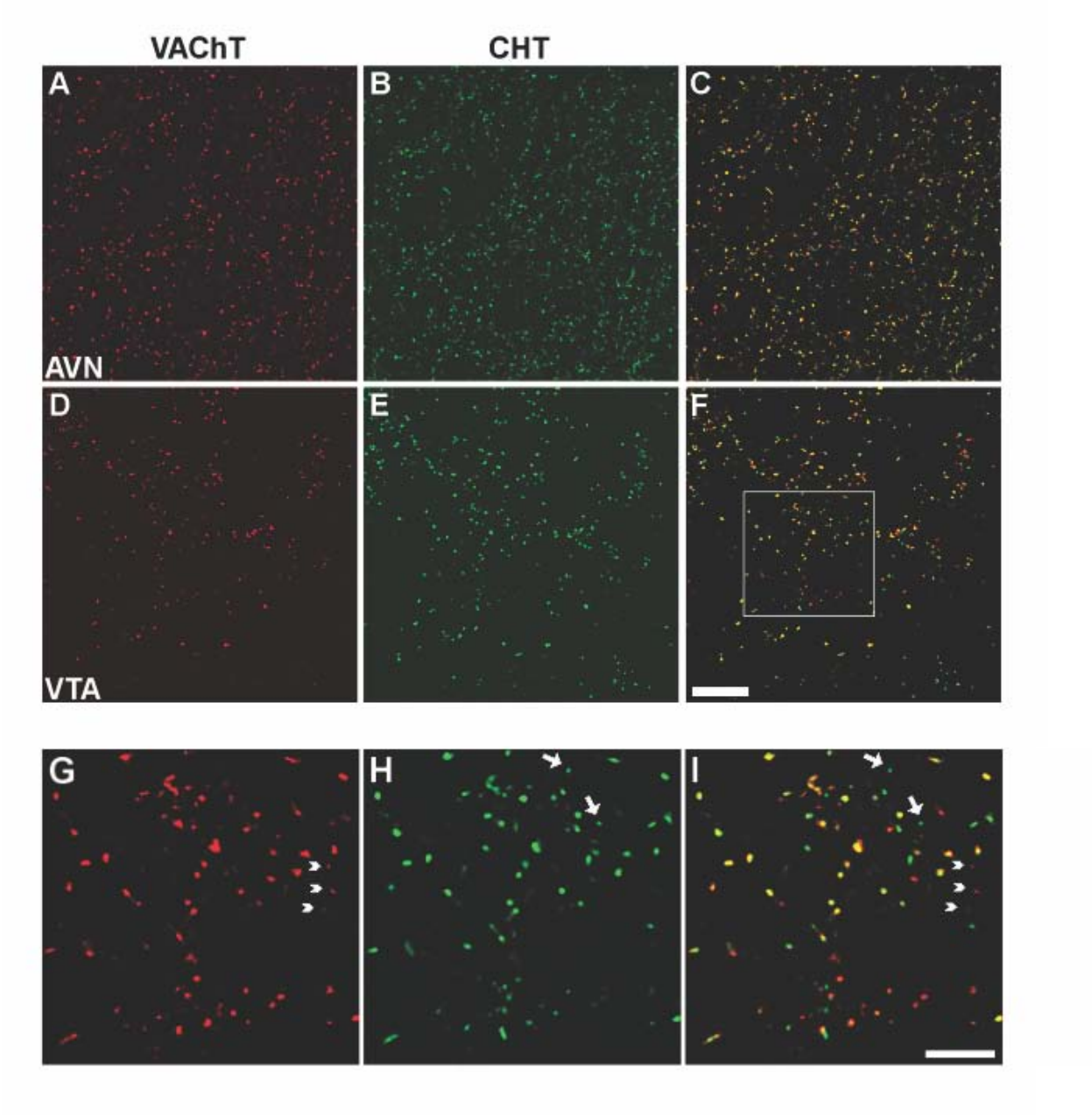

Figure 12 Dual immunofluorescence for VAChT and CHT in the AVN and the VTA.

Paired Z-stack projection images depicting Alexa-568-VAChT immunoreactivity (**A,D,G**) and Alexa 488-CHT immunoreactivity (**B,E,H**) were merged to display colocalization of the two proteins (**C,F,I**). In both the AVN (**A-C**) and the VTA (**D-F**), prominent colocalization was observed in structures resembling axon terminals. Closer examination of the region indicated in panel **F** (**G-I**) revealed puncta singly labeled for VAChT (arrowheads) or CHT (arrows) in these regions. Scale bar in **F** represents 10 µm and applies to **A-F**, scale bar in **I** applies to **G-I** and represents 5 µm.

immunofluorescence for VAChT and CHT, but singly labeled puncta could also be identified. Hence, both regions contained a mix of colocalized and non-colocalized immunofluorescent puncta.

The total number of VAChT-*ir* and CHT-*ir* objects sampled from each animal, and the number and percentage of these that were colocalized is shown in Table 2. Overall, it appeared that immunofluorescent objects in the VTA were less likely to display both CHT and VAChT immunoreactivity compared to similar objects in the AVN (63% versus 75% for VAChT-*ir* objects and 55% versus 75% for CHT-*ir* objects in the VTA versus the AVN, respectively). Nevertheless, in both regions the majority of objects showed labeling above threshold for both proteins. In order to determine if the rate of colocalization differed on a regional basis, we calculated the odds ratio of colocalization in the AVN versus the VTA from the VAChT-*ir* and the CHT-*ir* samples. For VAChT-*ir* objects, the odds ratio for colocalization in the AVN population with reference to the VTA population was 1.4, with a 95% confidence interval of 1.2 – 1.7. As the lower bound of this confidence interval was >1, colocalization was more likely to be observed in the AVN population than in puncta imaged from the VTA. For objects identified on the basis of CHT-*ir*, the odds ratio for colocalization of VAChT in the AVN versus the VTA populations was 2.8, with a 95% confidence interval of 2.2 – 3.4, again suggesting a regional difference in the extent of colocalization of the two proteins.

Puncta immunoreactive for VAChT and/or CHT displayed a similar distribution of volumes, shown in Figure 13A. The frequency distributions of both VAChT immunoreactive objects and CHT immunoreactive objects were heavily skewed toward small volumes, with 70-80% of each dataset having calculated volumes below 0.3 μm^3. Furthermore, there were clear size-dependent differences in the rate of colocalization of VAChT and CHT immunoreactivity

Table 2 Colocalization of VAChT and CHT immunoreactivity in the AVN and VTA

A. AVN

VAChT-*ir* objects

Animal	Colocalized VAChT objects	Total VAChT objects	% colocalized
1	1261	2009	63%
2	809	1165	69%
3	1627	1998	81%
4	1425	1965	73%
5	1905	2196	87%
		Average	**75%**

CHT-*ir* objects

Animal	Colocalized CHT objects	Total CHT objects	% colocalized
1	1320	1564	84%
2	749	1085	69%
3	1127	1632	69%
4	1599	2025	79%
5	1938	2588	75%
		Average	**75%**

B. VTA

VAChT-*ir* objects

Animal	Colocalized VAChT objects	Total VAChT objects	% colocalized
1	206	298	69%
2	223	377	59%
3	210	303	69%
4	381	709	54%
5	309	497	62%
		Average	**63%**

CHT-*ir* objects

Animal	Colocalized CHT objects	Total CHT objects	% colocalized
1	203	274	74%
2	215	527	41%
3	204	444	46%
4	374	722	52%
5	323	530	61%
		Average	**55%**

A

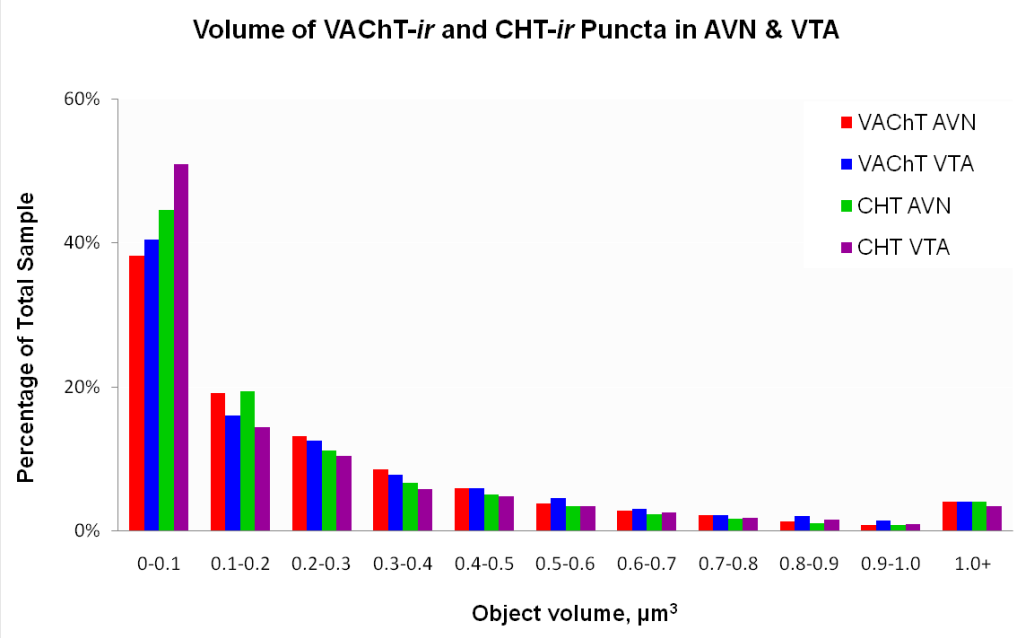

B

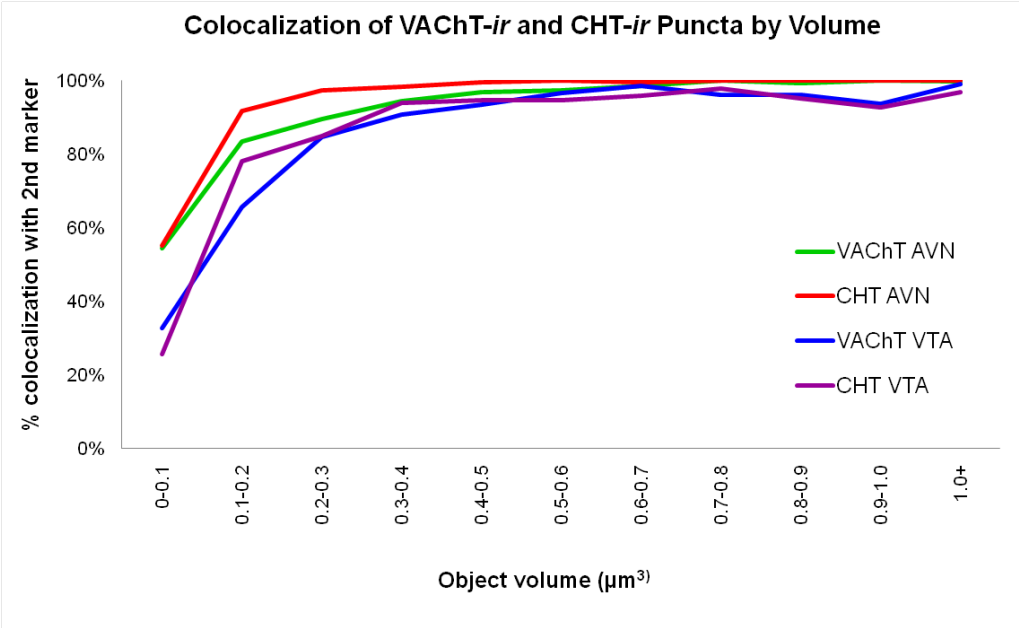

Figure 13 Frequency distribution of object volumes and colocalization rates of object volumes in the AVN and VTA.

A The volumes of CHT-immunoreactive and VAChT-immunoreactive puncta in both brain regions were strikingly similar, with most of the sample population having a volume < 0.3 µm^3. **B** The rate of colocalization observed in the smaller profiles (< 0.3 µm^3) was lower than in larger immunofluorescent objects. Above this volume, colocalization with the second marker was observed in over 90% of profiles.

across the range of volumes, such that only the smallest objects showed a substantial tendency toward non-colocalization (Figure 13B). In puncta with a volume greater than 0.3 μm^3, colocalization was detected in >90% of both VAChT- and CHT-immunoreactive objects from either brain region.

An obvious technical concern for colocalization studies is whether the antibodies used to detect the two proteins penetrated the tissue sections equally. However, we observed roughly equal numbers of CHT- and VAChT-*ir* objects throughout the Z-axis of the stack (Figure 14), indicating that single labeled puncta were not contained within a zone of suboptimal labeling in the secondary immunofluorescence channel**.** The visual inspection of image stacks similarly led to the qualitative impression on our part that non-colocalized objects were distributed throughout the same three-dimensional space as colocalized ones.

3.3.2 Quantitative Immunofluorescence Assessment of VAChT and CHT Levels Within Individual Puncta

Object colocalization was formally determined on the basis of immunofluorescence intensity above a stack-specific threshold in each channel (see Methods). Therefore, the lower incidence of colocalization in VAChT-*ir* objects and CHT-*ir* objects from the VTA compared to the AVN could result from lower overall expression of these proteins within the VTA. The simple threshold used (effectively >3x background fluorescence, see Methods) would presumably exclude more immunoreactive puncta in the VTA if, overall, CHT expression is lower in axon terminals innervating this region. To ascertain if VAChT or CHT FI differed systematically by region, a linear mixed model analysis was used to evaluate mean FI of the

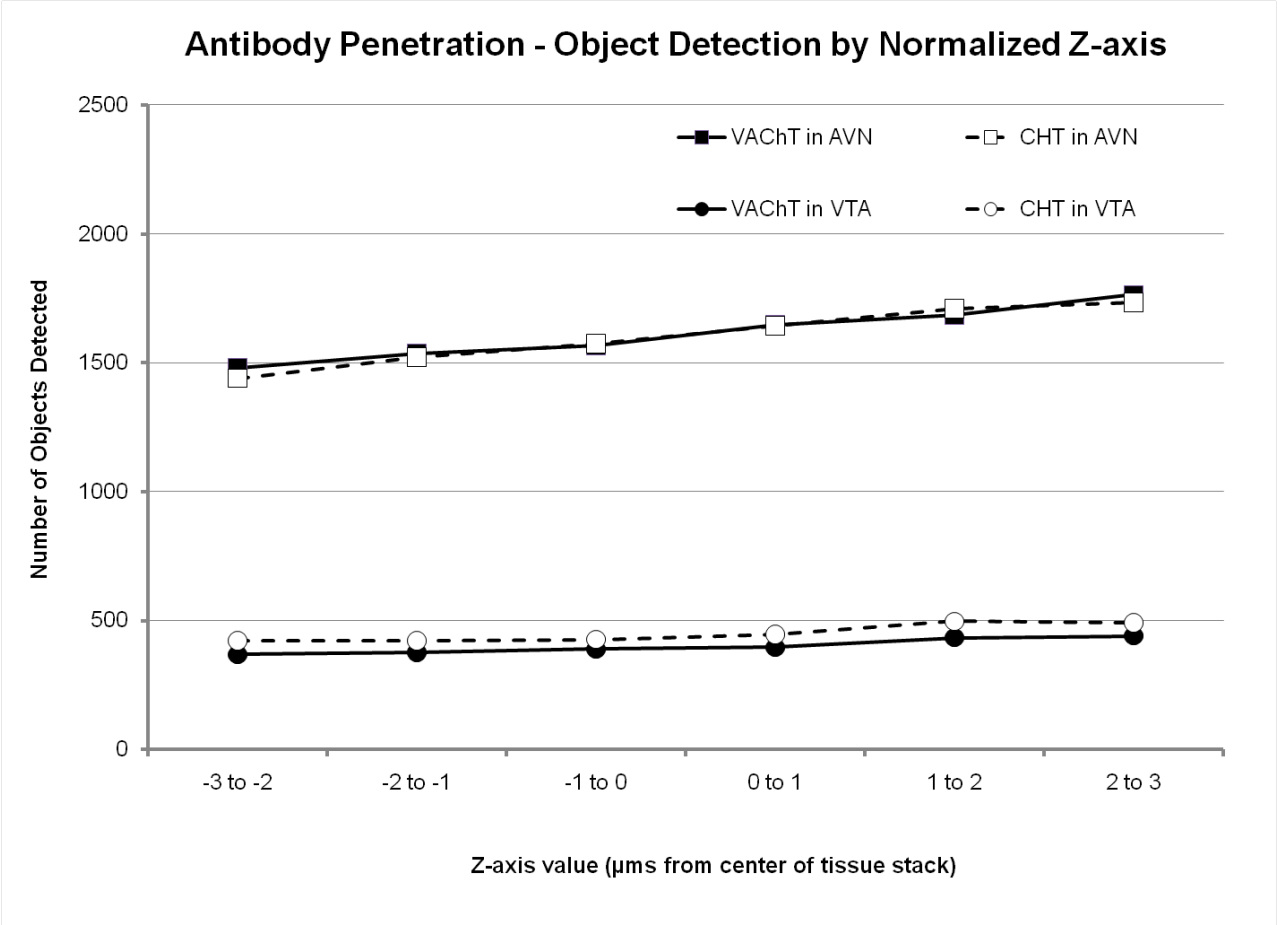

Figure 14 Detection of CHT-*ir* and VAChT-*ir* objects throughout the sample tissue sections.

anti-CHT and anti-VAChT antibodies appeared to penetrate the tissue sections equally well, as similar numbers of immunofluorescent objects for each marker throughout the tissue thickness. Although there was an increase in objects towards the top of the section in the AVN (top lines, squares), this was equivalent for both CHT and VAChT-*ir* puncta. The equal penetration of antibodies against both proteins argues against artifactual explanations for the lack of complete colocalization of CHT and VAChT.

primary mask marker used to define objects, without regard to colocalization status (e.g. mean CHT FI of all CHT-*ir* objects; see Figure 11). Analysis of the exposure- and gain-corrected mean CHT fluorescence intensities observed within CHT-*ir* objects (shown in Appendix B, Figure 27, *top panel)* revealed a significant effect of region ($F_{(1, 47.94)} = 42.52$, $p < 0.001$). The estimated means of CHT FI indicated that AVN puncta contained greater immunoreactivity for CHT than VTA puncta (AVN = 1493, VTA = 1029, diff = 464). Similar differences in VAChT FI within VAChT-masked objects were detected between the two regions ($F_{(1, 45.38)} = 45.267$, $p < 0.001$; estimated means: AVN = 2088, VTA = 1318, diff = 770; distribution of sample values is shown in Figure 27, *bottom panel*).

To assess whether the level of CHT expression might be correlated with the level of VAChT expression in individual cholinergic boutons, we examined the relationship between VAChT and CHT immunofluorescence intensities within individual puncta in the AVN and VTA. We restricted this analysis to those CHT-*ir* and VAChT-*ir* objects that met criteria for colocalization in order to focus on likely sites of ACh release. We plotted the log-transformed mean CHT and VAChT FI for each these object in both the AVN and VTA populations (Figure 15). Pearson's correlation coefficients indicated a significant but surprisingly weak positive association of CHT and VAChT FI in both VAChT-*ir* and CHT-*ir* populations sampled from the VTA and the AVN. Although there was a general trend for objects with more intense fluorescence in the primary channel (*x*-axis) to also show higher mean FI in the secondary channel, there was substantial dispersion in the data that most likely contributed to the low Pearson's *r* values obtained for both regional populations.

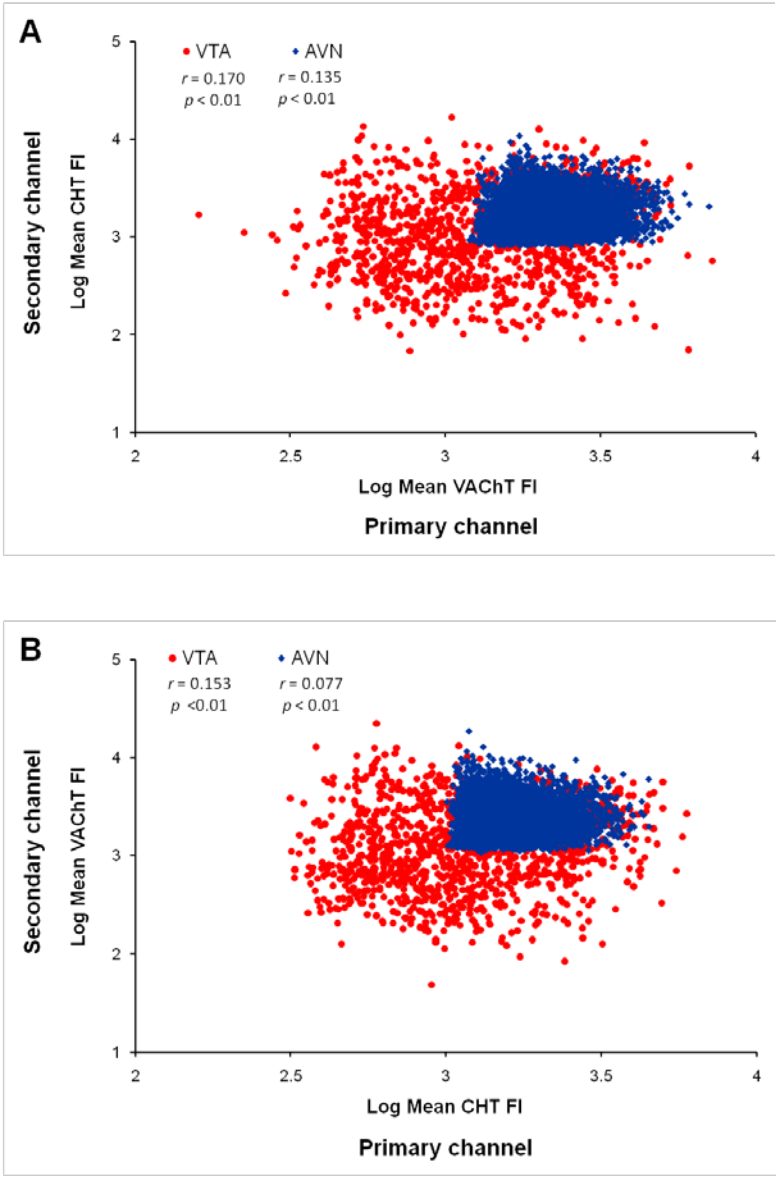

Figure 15 Relative mean fluorescence intensities of CHT and VAChT in colocalized puncta in the AVN and VTA.

The relationship between the mean CHT and VAChT intensity within CHT-*ir* puncta (A) and VAChT-*ir* puncta (B) that met colocalization criteria is plotted to demonstrate the correlation of intensity values. In both graphs, the intensity of the protein used to define objects (e.g. CHT for CHT-*ir* puncta in A) is plotted on the *x-axis*, while the intensity of the 2nd marker is on the *y-axis*.

Finally, we evaluated the ratio of CHT immunofluorescence intensity relative to VAChT intensity in individual colocalized VAChT-masked puncta across brain regions, using a linear mixed model analysis. For VAChT-masked objects, there was no significant difference in the ratio of log(mean CHT FI) / log(mean VAChT FI) ($F_{(1, 45.12)} = 0.436$, $p = 0.512$) . The estimated mean ratios for each region indicated that CHT immunoreactivity, relative to VAChT immunoreactivity, is remarkably similar between the two regions (AVN mean ratio: 0.950, VTA mean ratio: 0.964).

Similarly, in colocalized objects defined in the CHT mask, mixed model analysis of the ratio of log(mean VAChT FI) / log(mean CHT FI) revealed no significant difference across brain region ($F_{(1, 44.71)} = 1.370$, $p = 0.248$; AVN mean ratio: 1.055, VTA mean ratio: 1.027).

3.4 DISCUSSION

This study represents the first examination of CHT and VAChT colocalization, and the first quantitative analysis of CHT and VAChT immunofluorescence, within individual terminals of tegmental brainstem cholinergic axons. Our results indicate that CHT and VAChT colocalization is prevalent but not complete in cholinergic axon boutons. The rate of colocalization also varied between varicosities innervating the AVN and those innervating the VTA. In addition, we were able to evaluate immunofluorescence intensities for these two cholinergic proteins within individual puncta. The intensities of CHT and VAChT immunofluorescence were positively correlated within varicosities that contained detectable levels of both proteins. However, despite regional differences in the mean intensities of CHT and VAChT immunofluorescence within CHT-*ir* and VAChT-*ir* puncta, respectively, the relative

levels of CHT and VAChT within dually-labeled boutons did not differ across brain regions. The methodological caveats and functional interpretations of these findings are discussed below.

3.4.1 Methodological Considerations

The primary antibodies used in this study have been previously characterized and shown to label their target proteins with a high degree of specificity (see Materials & Methods), and both VAChT and CHT are localized primarily at sites of vesicular ACh release (i.e. axon terminals) (Arvidsson et al 1997; Misawa et al 2001; Ferguson et al 2003). Immunofluorescent labeling for VAChT and CHT was punctate in appearance, consistent with the localization of both proteins in axon varicosities. Furthermore, the range of object volumes observed is consistent with the volumes estimated from ultrastructural studies of cholinergic terminals in these regions. The minimum value of 0.01 μm^3 observed in the present sample populations corresponds to a sphere with a diameter of approximately 0.26 µm. Objects of this approximate size were observed in our previous sample of immunogold-silver labeled CHT-*ir* axon varicosities, although they comprised less than 20% of those profiles (*unpublished observations from that dataset*). Of course, cholinergic boutons are not necessarily spherical in shape, and the immunofluorescent labeling used for volume calculations in the present study probably does not accurately depict the full morphological dimensions of these boutons. Therefore, comparison between these two studies is useful only for confirming that immunofluorescent objects detected here are roughly consistent in size with the dimensions of cholinergic axon terminals in the AVN and the VTA, and that our size exclusion criterion was not inappropriate.

The detection of non-colocalized puncta raised concerns that a failure of one or the other primary antibody to adequately penetrate the brain tissue resulted in false-negatives. Limited antibody penetration prevents dual-labeling of these proteins in material for electron microscopic examination (Sesack et al 2006), particularly because the use of detergents to improve antibody penetration is detrimental to the preservation of tissue morphology needed for ultrastructural analysis. By using a light-microscopic approach, we were able to gain better antibody penetration through the generous use of Triton X-100 and long (48 hours) antibody incubation steps, facilitating access to the subcellular compartments containing the target proteins. We did not observe any differences in the distribution of CHT versus VAChT immunofluorescent objects detected throughout the depth of the tissue section, suggesting that the antibodies penetrated the sections equally well. Qualitatively, puncta singly labeled for CHT or VAChT were interspersed with other profiles that showed strong colocalization. Finally, it seems unlikely that experimental factors contributing to false negative staining would have differential effects on tissue sections from the AVN versus the VTA. The difference in the rate of colocalization between brain regions is most easily explained by the assertion that the singly labeled objects in our study are true examples of non-colocalization, and not false negative data.

However, we must stress that lack of colocalization in objects from our sample does not necessarily indicate that these puncta do not express any of the second protein, only that the levels of protein were low in comparison to objects that met criteria for colocalization. Nevertheless, such variability in the levels of CHT and VAChT immunoreactivity within probable cholinergic terminals are still expected to have functional significance for ACh levels in the brain.

3.4.2 Functional Significance of Incomplete Colocalization of VAChT and CHT in Axons

Consistent with the view that CHT is an integral component of cholinergic function, a majority of cholinergic axon varicosities displayed significant immunoreactivity for both VAChT and CHT protein. The co-expression of CHT and VAChT in the AVN and VTA verify the colocalization of these proteins for the brainstem tegmental cholinergic neurons, just as shown for most other cholinergic systems examined to date (Misawa et al 2001; Lips et al 2002; Ferguson et al 2003; Kus et al 2003; Nakata et al 2004). Colocalized puncta probably represent ACh release sites, where CHT and VAChT reside on the same synaptic vesicles and these vesicles are densely packed within the axon terminal. This supposition, however, require explicit testing by ultrastructural analysis that is not technically feasible at this time.

We also detected some VAChT-*ir* terminals that did not contain significant levels of CHT immunoreactivity in both the AVN and the VTA. Furthermore, VAChT-*ir* objects from the AVN were more likely to colocalize suprathreshold levels of CHT immunoreactivity than their counterparts in the VTA, as shown by the odds ratio estimate. This probably reflects the higher overall levels of CHT contained within cholinergic axons in the AVN, a finding previously reported from immunogold-silver ultrastructural analysis of AVN and VTA axon varicosities (Holmstrand et al 2010).

Surprisingly, we also found evidence of CHT-*ir* puncta that were not colocalized with VAChT immunoreactivity. Similar to singly labeled VAChT-*ir* puncta, this population of non-colocalized CHT-*ir* puncta accounted for a larger percentage of the total CHT-*ir* population in the VTA than in the AVN. It is not clear what these sites of single CHT labeling represent. If they are cholinergic terminals with subthreshold levels of VAChT, then high levels of CHT should not be necessary, given that the vesicular pool of ACh would be expected to be small

(Oosawa et al 1999). It is possible for choline transported through CHT to be utilized for other choline-dependent cellular processes, such as membrane lipid synthesis (Farber et al 1996; Cooper et al 2003), even though cholinergic cells also express low-affinity choline transporters that usually suffice to provide choline for this purpose. The larger axon profiles we observed in Chapter 2 might require higher levels of choline for phospholipid generation, simply in order to maintain their larger surface area. CHT could be used to help meet this demand if it exceeded the capacity of low-affinity uptake mechanisms. However, the predominantly vesicular (versus plasmalemmal) localization of CHT immunoreactivity reported in all prior studies makes this proposed secondary function of CHT unlikely, as the transporter must be situated in the plasma membrane in order to transport choline.

Alternatively, these small, singly labeled puncta might result from the clustering of non-vesicular CHT within varicosities or intervaricose segments. Indeed, the restriction of most non-colocalized puncta to the smallest object volumes observed in this study suggests that the lack of colocalization could result from the concentration of the two proteins within different subcellular compartments. For example, the non-colocalized CHT-*ir* puncta could result from antibody binding to clusters of transporters within the plasma membrane of axons, perhaps in the intervaricose segments, or a pool of CHT that has been recently retrieved from the plasmalemma via endocytosis, and is located on early endosomes that do not contain VAChT. A third alternative is that these small non-colocalized puncta represent CHT or VAChT that is in transit from the cell body to axonal varicosities. While the resolution limits of fluorescence microscopy (in this study, the minimum displacement for two-point resolution in the xy dimensions is estimated at 220 nm for the 488-channel and 255 nm for the 568-channel; in the z plane, these distances are 777 nm and 903 nm, respectively) would most likely prevent the detection of

separate CHT containing and VAChT containing vesicular pools within a single terminal, concentration of CHT within intervaricose segments of the axonal plasma membrane might be discriminable.

In experiments using CHT-transfected cultured cells, the transporter is rapidly endocytosed through vesicle recycling pathways, making clustering of transporters at the plasma membrane unlikely (Ivy et al 2001; Ribeiro et al 2003; Ribeiro et al 2005; Ribeiro et al 2006). However, the promotion of internalization of CHT by phosphorylation of the transporter (Gates et al 2004) suggests that the retention of CHT in the plasma membrane can be varied by the relative activation of protein kinases and phosphatases, as well as by a number of interacting proteins (Ribeiro et al 2007b; Wang et al 2007; Misawa et al 2008). To date, protein kinase C has been shown to increase CHT internalization, and PKC-dependent modulation of choline transport can be induced through the activation of certain G-protein coupled receptors (Breer & Knipper 1990; Gates et al 2004). The activation of heteroreceptors on cholinergic axons could therefore potentially alter the phosphorylation of CHT, leading to greater retention of functional transporters in the plasma membrane of the VTA. Finally, recent evidence that reactive oxygen species can alter CHT membrane trafficking (Pinthong et al 2008) may have special relevance for the regulation of choline uptake in these brainstem cholinergic pathways, as PPT/LDT ACh neurons also release nitric oxide as a co-transmitter (Williams et al 1997).

Future work aimed at identifying intracellular pathways that influence high-affinity choline uptake by altering the levels of membrane CHT might provide insight into how the specific extracellular milieu impacts cholinergic function. Such work could also reveal unique expression patterns of heteroreceptors on cholinergic axons that would differentially impact high-affinity choline uptake in the AVN versus the VTA.

We previously reported that CHT immunogold particles were more concentrated in the plasma membrane of AVN axon terminals, contradicting the aforementioned speculation. However, we excluded labeled profiles that did not contain synaptic vesicles in that study; therefore, we may have overlooked evidence of CHT clustered in intervaricose segments of axons. Further examination of CHT ultrastructural localization will be necessary to determine if the singly labeled CHT-*ir* puncta in the present study might result from this hypothesized sub-cellular distribution of CHT.

Of course, we cannot summarily dismiss the possibility that some of these small, non-colocalized objects are artifactual, resulting from the selection masking process. For example, if CHT- or VAChT-immunofluorescence does not follow a spherical gradient within puncta (i.e. highly concentrated in the center of the object, uniformly decreasing as distance from the center increases), then the threshold segmentation mask used here could incorrectly split a single CHT-*ir* or VAChT-*ir* puncta into multiple fluorescent objects, with the central object displaying colocalization, but peripheral artifactual objects being more likely to fail to colocalize the second immunofluorescent marker. While our qualitative impression of the masking threshold used to define objects in each channel was that the masks accurately captured all voxels within single puncta, further experimentation is needed to determine if the non-colocalized objects described here are truly examples of differential localization of CHT and VAChT.

Additionally, the larger size of VTA axon terminals observed by electron microscopy might allow greater separation of CHT and VAChT proteins within a single profile. This confound could have affected our estimates of colocalization across the two regions. However, the majority of CHT and VAChT protein is contained within the same synaptic vesicles; the small size of these structures would prevent optical resolution of such a small physical

separation. CHT or VAChT contained within other cellular compartments (e.g. trafficking or recycling endosomes) might be physically separated by greater distances in the larger VTA varicosities, leading to greater numbers of non-colocalized puncta in the present study. Although the estimated size of VTA cholinergic axon terminals is still likely to prevent discrimination of separate vesicle populations, any results concerning these singly labeled puncta should be interpreted with these caveats in mind.

3.4.3 Relative Levels of CHT and VAChT Immunoreactivity in Colocalized Puncta

CHT and VAChT immunofluorescence intensities were significantly correlated in colocalized puncta from either primary mask, indicating that CHT expression is likely to be higher in more active cholinergic axons. VAChT packages newly synthesized ACh into synaptic vesicles; therefore, it is expected that all mature, ACh-containing synaptic vesicles would be immunoreactive for this transporter, and that protein levels of VAChT reflect the relative size of the vesicular ACh supply (Erickson et al 1994; Oosawa et al 1999). It is plausible that cholinergic neurons that release ACh at higher rates, or that have distinctive firing patterns such as bursting behavior, would require a larger functional pool of vesicles that could be recruited during periods of elevated neuronal activity, and therefore would contain more VAChT protein. In parallel, higher rates of ACh synthesis would also be expected to require greater uptake of choline to supply the enzymatic reaction. A linear relationship between CHT and VAChT immunoreactivity is indicated by the significant correlations of immunofluorescence intensity for these two proteins that we reported here. This finding supports the view that CHT expression is primarily driven by the requirements of ACh synthesis in all cholinergic neurons. However, the associations between CHT and VAChT intensities were remarkably weak, suggesting significant

variability in the relative levels of these proteins, even across cholinergic boutons innervating a single brain region.

However, formal testing of the ratio of CHT to VAChT immunofluorescence intensities in VAChT-*ir* objects revealed that there is no significant regional difference in the relative levels of these proteins within individual puncta. Similarly, the ratio of VAChT to CHT immunofluorescence intensity in CHT-*ir* objects did not differ between the two regions. The strikingly stable relationship of VAChT and CHT immunoreactivity within AVN and VTA boutons provides further support for the view that the expression of these two proteins is similarly influenced by cellular mechanisms of transcriptional regulation, and probably reflects the importance of CHT expression for the maintenance of adequate vesicular pools of ACh.

3.4.4 Functional Implications

The stable relationship of VAChT and CHT immunoreactivity levels, combined with the higher overall levels of both VAChT and CHT immunofluorescence in the AVN population suggests that these axons have a greater overall demand for ACh synthesis. While the higher synthetic load in these terminals might reflect higher rates of release, an alternative explanation is that the morphological characteristics of AVN cholinergic boutons contribute to the need for high levels of ACh synthesis. Cholinergic terminals in this region are smaller than their counterparts in the VTA (Hallanger et al 1990; Omelchenko & Sesack 2006; Holmstrand et al 2010), and presumably contain fewer synaptic vesicles packed into this smaller space. If the total number of vesicles in AVN terminals is lower than in similar terminals in the VTA, the rate of recycling for synaptic vesicles would have to be quicker in this region to support similar levels

of ACh release. Consequently, these vesicles might contain multiple copies of VAChT and be more likely to contain CHT as well, a hypothesis that is consistent with the present finding that both VAChT and CHT-immunofluorescence levels are higher in AVN boutons. Quantification and comparison of the number of synaptic vesicles within AVN versus VTA cholinergic axon terminals could help distinguish between these possibilities.

Alternatively, differential demand for choline may be driven by unique features of the extracellular microenvironment in this thalamic nucleus. The dense cholinergic innervation of the AVN is thought to supply ACh to cholinergic receptors in the adjacent anterodorsal nucleus of the thalamus, as there are no cholinergic projections to this region (Sofroniew et al 1985; Levey et al 1987; Gonzalo-Ruiz et al 1995; Arvidsson et al 1997). Furthermore, there is high cholinesterase activity in the ADN, while in the adjacent AVN such activity displays a gradient distribution (Paxinos & Watson 1986; Darvesh & Hopkins 2003; Alelú-Paz & Gimenéz-Amaya 2007). High levels of cholinesterases are found in the ventrolateral portion of the AVN, but enzymatic staining methods reveal diminished activity of these enzymes in the dorsomedial division that lies between the ventrolateral AVN and the dorsally situated ADN (Figure 16). The more medially situated anteromedial nucleus (AM) also displays only moderate cholinesterase activity and has a relatively light cholinergic innervation. Light or absent cholinergic innervation would result in lower concentrations of ACh in these regions, and the high cholinesterase levels in the AD would further reduce extracellular levels of ACh, creating a steep concentration gradient through which ACh, released from axons in the AVN, could diffuse. Diffusion to neighboring regions would lower the extracellular levels of ACh in the dorsomedial AVN (AVDM), blunting the elevations of choline that would be expected to result from local hydrolysis of ACh in the immediate vicinity of the axon terminal.

A

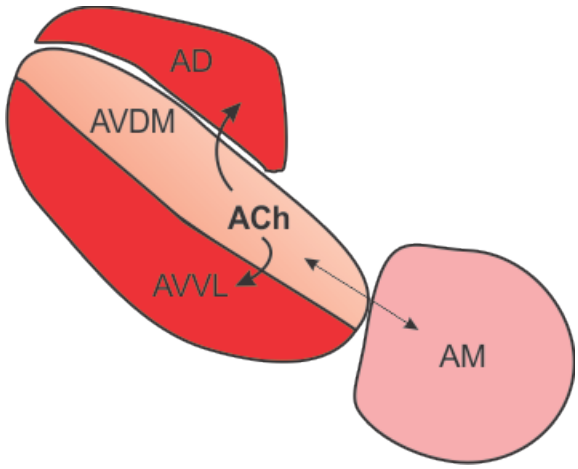

B

	ACh innervation	Cholinesterase Activity	Predicted ACh levels	Predicted Choline levels
AD	none	high	low	moderate
AVDM	high	moderate to low	low	low
AVVL	high	high	low	high
AM	low	low	low	low to moderate

Figure 16 Cholinergic microenvironment in the anterior nuclei of the thalamus.

A Illustration of cholinesterase activity in the anterior nuclei of the thalamus. The anterodorsal nucleus (AD) displays high levels of cholinesterase activity, despite having no innervation by cholinergic fibers. In the anteroventral nucleus, a gradient of cholinesterase is seen, higher levels of enzyme activity in the ventrolateral division (AVVL) and lower activity in the dorsomedial division (AVDM). The anteromedial nucleus (AM) displays a low level of cholinesterase activity and a low cholinergic innervation (Paxinos & Watson 1986; Groenewegen & Witter 2004). ACh released in the AVDM could theoretically diffuse toward the other nuclei (*arrows*) and would preferentially diffuse to the AD and AVVL where ACh concentrations would be lower due to hydrolysis by cholinesterases. **B** Summary characteristic ACh innervation and cholinesterase activity in the anterior thalamic nuclei, with predicted relative extracellular levels of ACh and choline. In the AVDM, choline would be scarce due to the diffusion of ACh out of this nucleus, combined with low cholinesterase activity. In the AD, diffusion of ACh from the AVDM would result in higher ACh concentrations than would otherwise result (as ACh is not released here), but still limited by diffusion and the amount of ACh released in AVDM. High cholinesterase activity would efficiently hydrolyze any ACh in this brain region.

Extracellular choline levels might therefore also be lower, and cholinergic axons in the AVN might show a high level of choline uptake in order to compensate for the reduced availability of substrate.

Additionally, the high density of cholinergic terminals packed into the AVN probably contributes to an environment of intense competition by many transporters for limited substrate molecules, placing further demands on the high-affinity choline uptake system in this region. In this case, the increased VAChT immunoreactivity observed within AVN terminals might not have a functional relevance, but might be the result of increased activity of transcriptional regulatory mechanisms, prompted by the need to increase CHT protein levels, that coincidentally increases the expression of VAChT. Additional experimentation is needed to directly measure the levels of extracellular ACh and choline, and to assess functional high-affinity choline uptake in this region in order to further our understanding of the dynamics of cholinergic signaling in different brain microenvironments.

4.0 PROJECTIONS FROM THE RAT PEDUNCULOPONTINE AND LATERODORSAL TEGMENTAL NUCLEI TO THE ANTEROVENTRAL THALAMUS AND VENTRAL TEGMENTAL AREA ARISE FROM LARGELY SEPARATE POPULATIONS OF NEURONS

Having found differences in the expression and localization of CHT between cholinergic axons innervating the AVN and the VTA, we hypothesized that these differences might reflect the innervation of these regions by separate sub-populations of PPT/LDT afferents. However, brainstem cholinergic neurons frequently send axon collaterals to thalamic and non-thalamic targets, allowing for the possibility that differential regulation of CHT trafficking in axons could produce the regional differences in CHT immunoreactivity that we observed. Dual tract-tracing from the AVN and the VTA was combined with VAChT immunohistochemistry in order to elucidate the nature of PPT/LDT afferents to the AVN and the VTA.

4.1 INTRODUCTION

The brainstem pedunculopontine (PPT) and laterodorsal tegmental (LDT) nuclei contain cholinergic neurons noted for their wide-reaching projections to diverse brain structures. Cholinergic neurons in these regions provide ascending input to virtually the entire thalamus (Hallanger et al 1987; Jones & Webster 1988; Heckers et al 1992), the midbrain dopaminergic

cell groups in the substantia nigra pars compacta (SNc) and ventral tegmental area (VTA) (Beninato & Spencer 1987; Oakman et al 1995), the basal forebrain (Woolf & Butcher 1986; Hallanger & Wainer 1988), the hypothalamus (Satoh & Fibiger 1986; Woolf & Butcher 1986; Cornwall et al 1990), and, in a more limited manner, the cerebral cortex (Crawley et al 1985; Satoh & Fibiger 1986). Furthermore, several studies indicate that these brainstem cholinergic neurons can innervate both thalamic and extrathalamic target structures through divergent axonal branches (Woolf & Butcher 1986; Cornwall & Phillipson 1989; Jourdain et al 1989; Bolton et al 1993; Losier & Semba 1993).

The ascending cholinergic projections play an important role in the regulation of behavioral state and the detection of salient environmental stimuli (Inglis & Winn 1995; Reese et al 1995b; Yeomans 1995; Kobayashi & Isa 2002; Pan & Hyland 2005). Interestingly, these cholinergic groups innervate many brain structures associated with limbic circuitry (Mesulam et al 1983; Mesulam 1995a). This is particularly true of the LDT, whose cholinergic neurons send projections to the anterior, parafascicular, mediodorsal and intralaminar thalamic nuclei, and even provide a minor input to the medial prefrontal cortex (Satoh & Fibiger 1986; Woolf & Butcher 1986; Cornwall et al 1990). Additionally, cholinergic LDT neurons innervate other ascending neuromodulatory systems important for limbic functions, such as serotonin neurons in the raphé nuclei and dopamine neurons in the VTA (Satoh & Fibiger 1986; Cornwall et al 1990; Omelchenko & Sesack 2006; Mena-Segovia et al 2008).

Although collateral projections from single LDT neurons have been described for the VTA and the intralaminar/midline thalamic groups (Bolton et al 1993), the possibility of collateralized projections to the VTA and anterior thalamus (AVN) has yet to be examined. We previously examined the expression of the high-affinity choline transporter (CHT) in two limbic

areas that receive afferent cholinergic innervation exclusively from the brainstem tegmental nuclei: the VTA and the AVN (Holmstrand et al 2010). We found that axons in the AVN displayed higher total levels of CHT immunoreactivity and greater plasma membrane density of CHT immunogold particles. Cholinergic terminals in the VTA were larger, more frequently formed synaptic junctions, and were more likely to contain dense-cored vesicles, an indication of neuropeptide co-transmission. Given these differences, we hypothesized that the cholinergic afferents to the AVN and the VTA would originate from separate populations of PPT/LDT cells.

The existence of separate projections to the AVN and VTA is supported by the known distribution of related afferents to these regions. The AVN innervation arises predominantly from the LDT (Shibata 1992), while afferents to the VTA appear to more equally derive from the PPT and LDT (Oakman et al 1995; Holmstrand & Sesack 2004; Mena-Segovia et al 2008). With regard to forebrain connections of the AVN and VTA, these nuclei are interconnected with cortical and subcortical limbic regions that are largely exclusive of each other. For example, the mesocortical dopamine innervation heavily targets medial prefrontal cortex and the anterior cingulate cortex (Beckstead et al 1979; Loughlin & Fallon 1984), whereas AVN neurons project only to the posterior cingulate cortex (Shibata 1993), at least in the rat (Barbas et al 1991). Another significant target of VTA dopamine neurons is the nucleus accumbens, yet the AVN does not send a substantial projection to this region (Giménez-Amaya et al 1995; Erro et al 1999; Smith et al 2009). Such segregated circuitry suggests that these systems may receive specific cholinergic modulation from distinct subpopulations of PPT/LDT neurons.

We tested this hypothesis by performing dual retrograde tract-tracing using the beta subunit of cholera toxin (CTxβ) and fluorescent latex microspheres (Retrobeads™) as discriminable tracing agents from the AVN and VTA, respectively. We combined tracing with

immunofluorescence histochemistry for VAChT to determine whether the ascending input to these target regions arises from separate groups of brainstem cholinergic and non-cholinergic neurons or results from the collateralization of ascending axons.

4.2 MATERIALS AND METHODS

All procedures were conducted in accordance with protocols approved by the Institutional Animal Care and Use Committee (IACUC) at the University of Pittsburgh. All chemicals were purchased from Sigma (St. Louis, MO) unless otherwise noted.

4.2.1 Surgical Procedures

Male Sprague-Dawley rats (Hilltop, 250-300g) were anesthetized with a mixture of ketamine, xylazine and acepromazine (35 mg/kg, 6 mg/kg, 1.2 mg/kg respectively, i.m.), and placed in a stereotaxic apparatus. Throughout the surgical procedure, body temperature was maintained at 37°C with a heating pad. Supplement al anesthetic was administered when necessary to maintain suppression of the limb withdrawal reflex throughout the surgical procedure. Unilateral injections of CTxβ (1% solution, List Laboratories, Campbell, CA) were made in the AVN by pressure or iontophoresis at the following co-ordinates, referenced to Bregma: AP: -1.8 mm, ML: 1.8 mm, DV: 5.0 – 5.2 mm ventral to the surface of the brain. Iontophoretic injections were made using a Midgard constant current source (Stoelting, Wood Dale, IL) set to deliver a pulsed 5 µA current (8 sec ON, 8 sec OFF). These injections proceeded for 5-8 minutes. Unilateral injections of green fluorescent latex microspheres (Retrobeads™,

Lumafluor Inc., Naples, FL, referred to hereafter as Rbeads) were made by pressure into the ipsilateral VTA at the following co-ordinates, with reference to Bregma, and at an angle of 5° from vertical in the mediolateral plane: AP: -5.3 - -5.8 mm, ML: 1.6 – 1.8 mm, DV: 7.6 – 7.8 mm from the surface of the brain. A total of ~100 nL of the Rbeads was injected into the VTA. The scalp wound was treated with a topical antibiotic ointment and local anesthetic (Xylocaine 2% jelly) and subsequently closed with surgical staples. Rats were administered additional analgesic (ketoprofen, 2 mg/kg, i.m.) and had access to oral acetaminophen solution (3.25 mg/mL) in their food and water during the post-operative recovery period (5-7 days).

4.2.2 Tissue Preparation

Rats were deeply anesthetized with sodium pentobarbital (Nembutal, 100 mg/kg, i.p.), and perfused transcardially with ~ 50 mL of heparin saline (1000 U/mL), followed by 500 mL of 4% paraformaldehyde containing L-lysine acetate and sodium meta-periodate (PLP fixative, (Mclean & Nakane 1974)). The brain was removed, cut in the coronal plane into blocks 4-5 mm thick, and post-fixed for 24 hours at 4°C.

Blocks through the thalamus, midbrain, and mesopontine tegmentum were rinsed in 0.1 M phosphate buffer (PB) and sectioned to 50 μm. All sections were then treated for 30 minutes with sodium borohydride (1% in PB) and rinsed extensively in PB.

4.2.3 Visualization of Injection Sites

CTxß injections were examined with immunoperoxidase staining for proper placement in the AVN and adequate deposit of tracer. Briefly, sections were rinsed in 0.1 M Trizma buffered saline (TBS) and then treated for 30 minutes in a blocking solution containing 1% bovine serum albumin (BSA; Spectrum Chemical Corp.) and 0.2% Triton X-100. Sections were then incubated overnight in blocking solution containing primary antibody (goat anti-CTxß, 1:20,000, List Laboratories). After rinsing several times in TBS, sections were incubated for 30 minutes in secondary antibody (biotinylated rabbit anti-goat IgG, 1:500, Jackson ImmunoResearch, West Grove, PA). Sections were rinsed again in TBS, and processed for peroxidase staining using the ABC Elite kit (Vector, Burlingame, CA). Peroxidase staining was developed for 3-5 minutes in 0.022% diaminobenzidine and 0.003% hydrogen peroxide. Finished sections were rinsed several times in TBS and 0.01 M phosphate buffered saline (PBS) before mounting on glass slides (Superfrost, Fisher, Pittsburgh, PA). Slides were dried, dehydrated through a series of increasing ethanol concentrations, soaked in three changes of xylene, and coverslipped with Cytoseal-60 (Richard-Allan Scientific, Kalamazoo, MI).

Due to their intrinsic fluorescence, Rbead injections could be visualized without any histochemical processing. Accordingly, sections through the VTA were rinsed in PBS and mounted directly onto glass slides. Long xylene exposures are detrimental to the fluorescence of the Rbeads (per the manufacturer's instructions); therefore these slides were coverslipped immediately with a water-based fluorescence-compatible mounting medium (Fluoromount-G, Southern Biotech, Birmingham, AL).

4.2.4 Dual Immunohistochemistry of Brainstem Sections

In order to identify AVN-projecting, VTA-projecting, and cholinergic neuronal populations in the tegmentum, sections through the PPT/LDT of successful cases were processed to reveal CTxß and VAChT immunofluorescence, and examined for each of these markers, as well as for the presence of intrinsically fluorescent Rbeads. A one in six series of sections was used for quantification of these neuronal populations. During all immunohistochemical steps, sections were protected from light exposure to minimize fading of the Rbeads. Briefly, sections were rinsed several times in PBS, and treated for 3 hours with a blocking solution containing 5% nonfat dry milk, 0.3% Triton X-100, 0.1% L-lysine acetate and 0.1% glycine. Sections were then incubated in primary antibodies diluted in the same blocking solution for 48 hours at 4°C: goat anti- CTxß (1:10,000) and rabbit anti-VAChT (1:5000, gift from Dr. Yongjian Liu, University of Pittsburgh). Sections were rinsed extensively in PBS, and incubated overnight at 4˚C in fluorescent-tagged secondary antibodies, diluted in blocking solution: Alexa 568 donkey anti-goat IgG and Alexa 647 chicken anti-rabbit IgG (1:500 each, Invitrogen Corp., Carlsbad, CA). All sections were rinsed extensively in PBS, mounted on glass slides, and coverslipped with Fluoromount-G. Slides were protected from light exposure while drying and prior to microscopic examination.

4.2.5 Identification of Labeled Neurons

Sections were examined on an Olympus BX51 microscope (Olympus, Center Valley, PA) equipped with a xenon/argon illumination source, a CCD camera (Hamamatsu, Sewickley, PA), and image acquisition software (SimplePCi, Hamamatsu). Sections were first

photographed at 4x magnification under illumination for Alexa 647/VAChT. This allowed the visualization of the cholinergic cell populations in the brainstem and appropriate selection of regions for further examination at high magnification using triple immunofluorescence. Fields adjacent to the PPT/LDT that contained no VAChT-labeled cells were excluded.

Three channel fluorescence images were then acquired at 20x magnification, using the following filter sets (Chroma Technology Corp., Bellows Falls, VT): 1) Red channel: Alexa 568 (CTxß labeled, AVN-projecting neurons), excitation (ex): 555/28 nm and emission (em): 617/73 nm; 2) Green channel: Rbeads (VTA-projecting neurons), ex: 490/20 nm and em: 528/38 nm; 3) Blue channel: Alexa 647 (VAChT-immunoreactive neurons, VAChT-*ir*), ex: 635/20 nm and em: 685/40 nm. Exposure and gain settings were adjusted in the blue channel to maximize signal without saturation; subsequently, the other channels were adjusted to yield equivalent minimum fluorescence values (e.g. equivalent background fluorescence). Three channel RGB images were saved as TIF files. Finally, for each XY location on a section, images were collected from all focal planes that contained unique instances of labeled cells.

All TIF files were examined in Adobe Photoshop (Adobe, San Jose, CA). For each image, the total number of labeled neurons in each channel was recorded. In addition to using specific fluorescence channels to identify labeled neurons, the texture of cellular staining was helpful in identifying true labeling and excluding the possibility of cross-channel excitation. Furthermore, neurons labeled in more than one channel were classified as belonging to one of the following groups: 1) collateralized, cholinergic ($CTx\beta^{+}$ $Rbead^{+}$ $VAChT^{+}$); 2) collateralized, non-cholinergic ($CTx\beta^{+}$ $Rbead^{+}$ $VAChT^{-}$); 3) cholinergic, AVN-projecting only ($CTx\beta^{+}$ $Rbead^{-}$ $VAChT^{+}$); or 4) cholinergic, VTA-projecting only ($CTx\beta^{-}$ $Rbead^{+}$ $VAChT^{+}$). Tallies of these cell populations were made using Microsoft Excel (Microsoft, Redmond, WA). For locations

with multiple focal planes, great care was taken to avoid counting any labeled neuron more than once.

Tables were prepared using Microsoft Excel. Figures were prepared using Photoshop to adjust brightness and contrast and to add figure labels.

4.3 RESULTS

4.3.1 Injection Sites

Seven cases resulted in acceptable injections for both the AVN and VTA targets. An additional case (Case 35) was examined to contrast the afferents to the paratenial nucleus (PT) with those of the more lateral AVN.

Figure 17 shows representative injections of both CTxβ (A) and Rbeads (B) from Case 34. Immunoperoxidase for CTxβ typically filled the anterodorsal (AD) and anteroventral nuclei, with additional reaction product evident in the anteromedial (AM) nucleus and intralaminar paracentral nucleus (PC). Much of the reaction product in the PC was contained within retrogradely labeled cells, and punctate processes having the appearance of axon terminals suggested a degree of anterograde transport from the injection site as well (Figure 17A inset). Anterogradely transported CTxβ was also present in the contralateral AVN. These observations may be explained by inclusion of the anteromedial most portion of the reticular thalamic nucleus in the injection site (Gonzalo-Ruiz & Lieberman 1995; Kolmac & Mitrofanis 1998). It is possible that the CTxβ itself spread to the ipsilateral AM, given that diffuse reaction product was

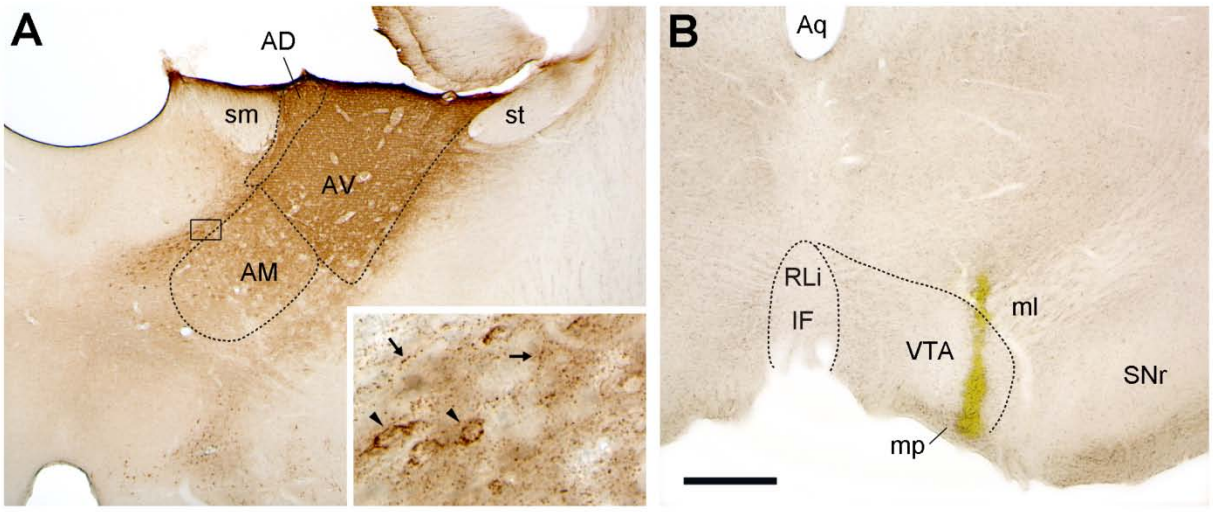

Figure 17 Representative examples of tracer injections in the AVN and VTA.

Immunoperoxidase staining for CTxβ in the AVN from case 34 shows that the tracer diffused from the center of the injection to fill the AVN. Additional tracer spread was evident in the adjacent AD and AM. Peroxidase product was also observed in midline and intralaminar nuclei (insert; the black box in **A** indicates the region shown at higher magnification). The punctate appearance of this labeling (small arrows) suggests that it represents anterograde transport. Retrograde labeling of cell soma (arrowheads) was also visible in these areas. The Rbead deposit involved primarily the lateral VTA near the edge of the medial lemniscus (ml) and just above the mammillary peduncle (mp). Abbreviations: AD, anterodorsal nucleus; AM, anteromedial nucleus; IF, interfascicular nucleus; RLi, rostral linear nucleus; sm, stria medullaris; SNr, substantia nigra pars reticulata; st, stria terminalis. Scale bar represents 500 µm in panels **A** and **B**, 50 µm in insert.

also apparent in the neuropil, similar to what is visible within the AVN at the core of the injection site.

The relative size and placement of CTxβ and Rbead injection sites for all cases are illustrated in Figures 18 and 19. For ease of display, we grouped these cases by the extent of CTxβ spread to thalamic structures medial to the anterior nuclei. As shown in Figure 18, Cases 25, 27, and 34 had injections of CTxβ that were predominantly restricted to the AVN, AD, and AM. The remaining cases had large AVN injections (Figure 19) that typically filled both the AVN and AM, with additional spread of CTxβ laterally in some cases to the ventral nuclei and medially in other cases to midline/intralaminar nuclei: paracentral (PC), centrolateral (CL), or lateral division of the mediodorsal (MD). One additional case (Case 35; Figure. 18) was included as a control, as the CTxβ injection was centered on the PT nucleus and spread to the anterior most portions of the MD and PC thalamic nuclei. In addition to serving as a control, the PT injection allowed comparison as a limbic thalamic division whose projections overlap those of the VTA DA system (e.g. projections to the nucleus accumbens) (Beckstead et al 1979; Kelley & Stinus 1984; Giménez-Amaya et al 1995; Erro et al 1999; Vertes & Hoover 2008).

4.3.2 Retrograde Transport

Within the PPT and LDT, we observed many neurons that were singly labeled for one retrograde tracer or dually labeled for one tracer and for VAChT. Figure 20 shows singly and dually labeled cells intermingled in the same photographic field. Less often, we observed neurons retrogradely labeled from both regions, such as the example shown in Figure 21, that were not immunoreactive for VAChT (non- VAChT-*ir*). Likewise, triply labeled neurons, i.e.

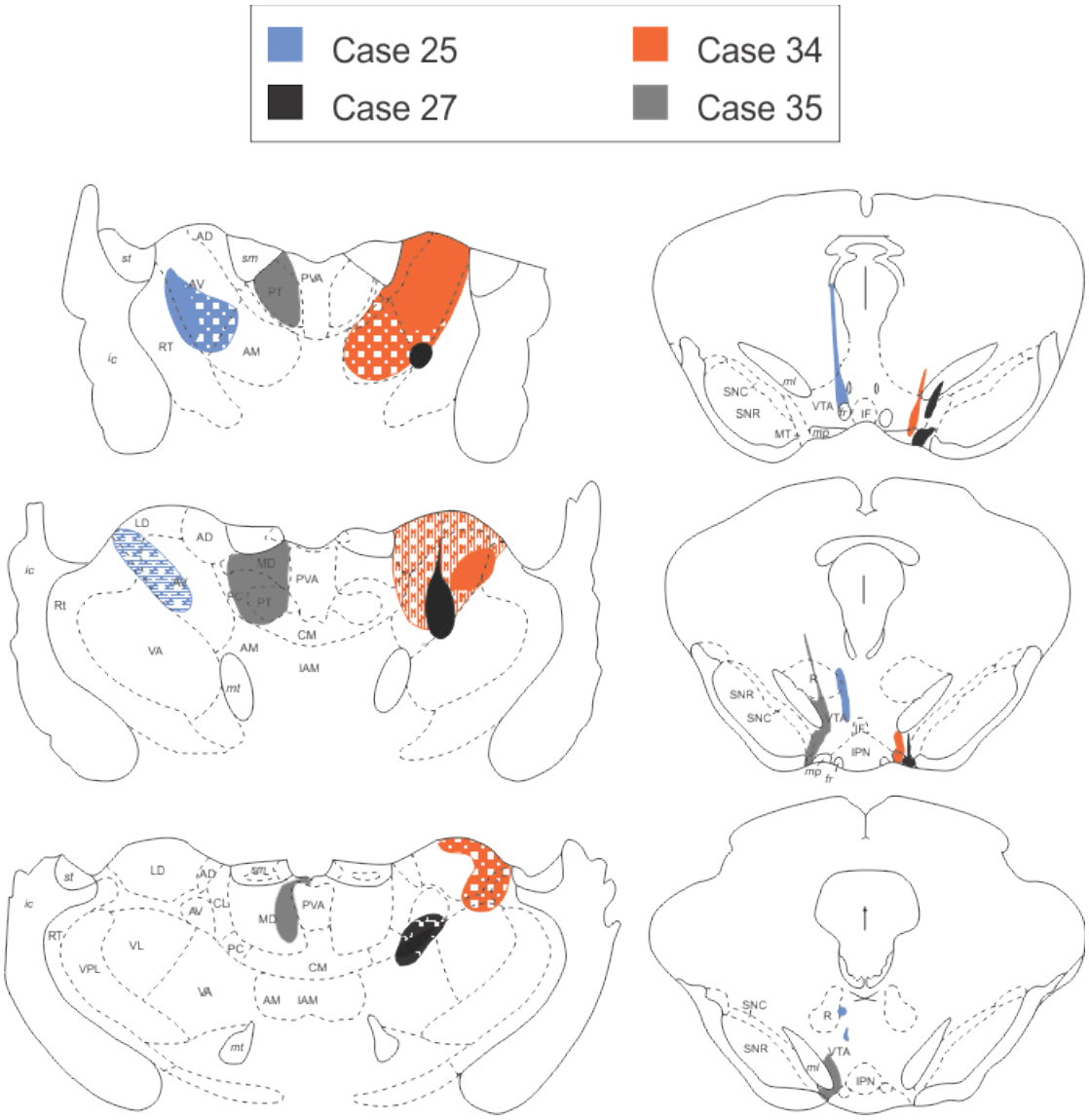

Figure 18 CTxβ and Retrobead tracer deposits in selected cases with small thalamic injections.

Illustration of the extent of CTxβ injections in the AVN (left panels) and Rbead injections in the VTA (right panels) for three cases in which the thalamic injections were well restricted within the anterior thalamic group (AD, AV, AM and LD), with minimal spread to the midline and intralaminar nuclei (PC, PT, MD, CL, CM). The solid areas show the core of the injections, where CTxβ immunoreactivity was most . Hatched regions demarcate the extent of diffusion of CTxβ observed in adjacent regions. An additional control (Case 35) is shown in which the thalamic injection centered on the paratenial nucleus (PT) and did not spread laterally into the AV.

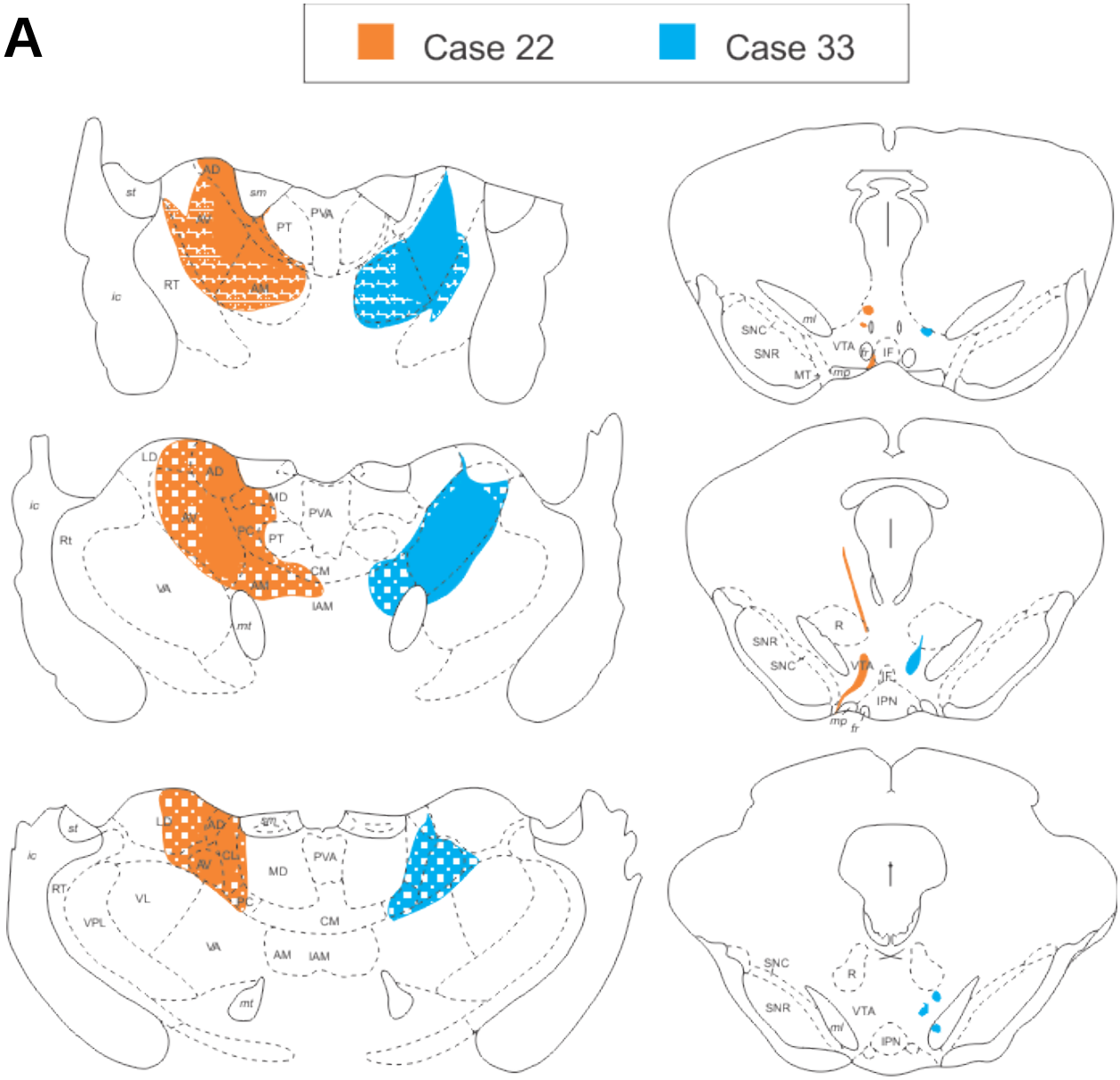

Figure 19 Tracer deposits in the AVN and VTA from tract-tracing cases with large thalamic injections.

Illustrations of CTxβ injections in the AVN (left panels) and Rbead injections in the VTA (right panels) for cases 22 and 33 (**A**) and cases 36 and 37 (**B**). As in Figure 4- 2, the hatched regions show diffusion spread of tracer from the center of the injection represented by the solid regions. Tracer spread was more extensive in these cases, resulting in significant involvement of the intralaminar nuclei medial to the AVN.

B

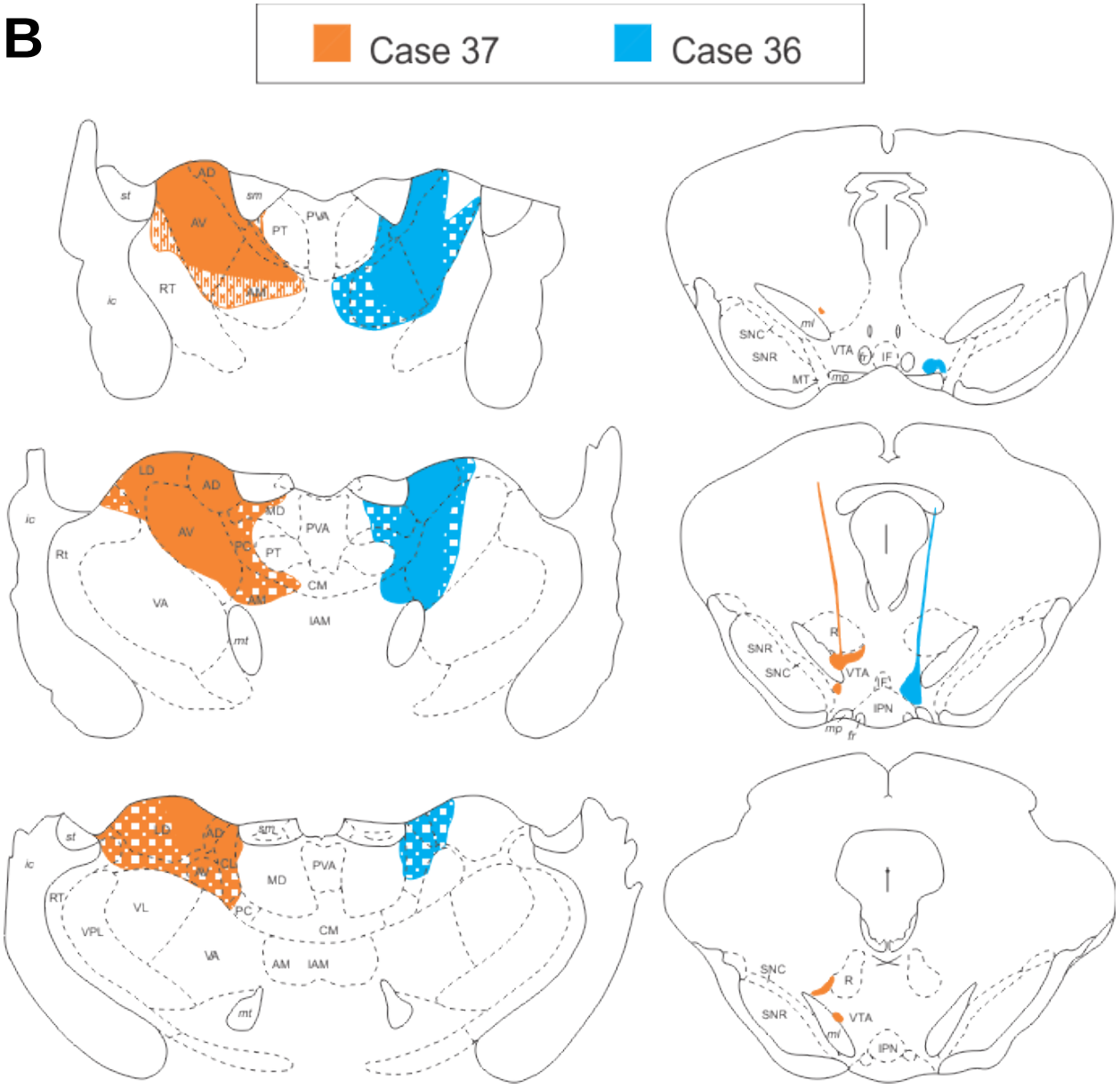
Case 37
Case 36
AD
st
sm
AV
PT
PVA
RT
ic
SNC
ml
SNR
VTA
IF
MT
mp
LD
MD
Rt
PC
CM
VA
IAM
mt
R
IPN
fr
VL
VPL
AM
CL

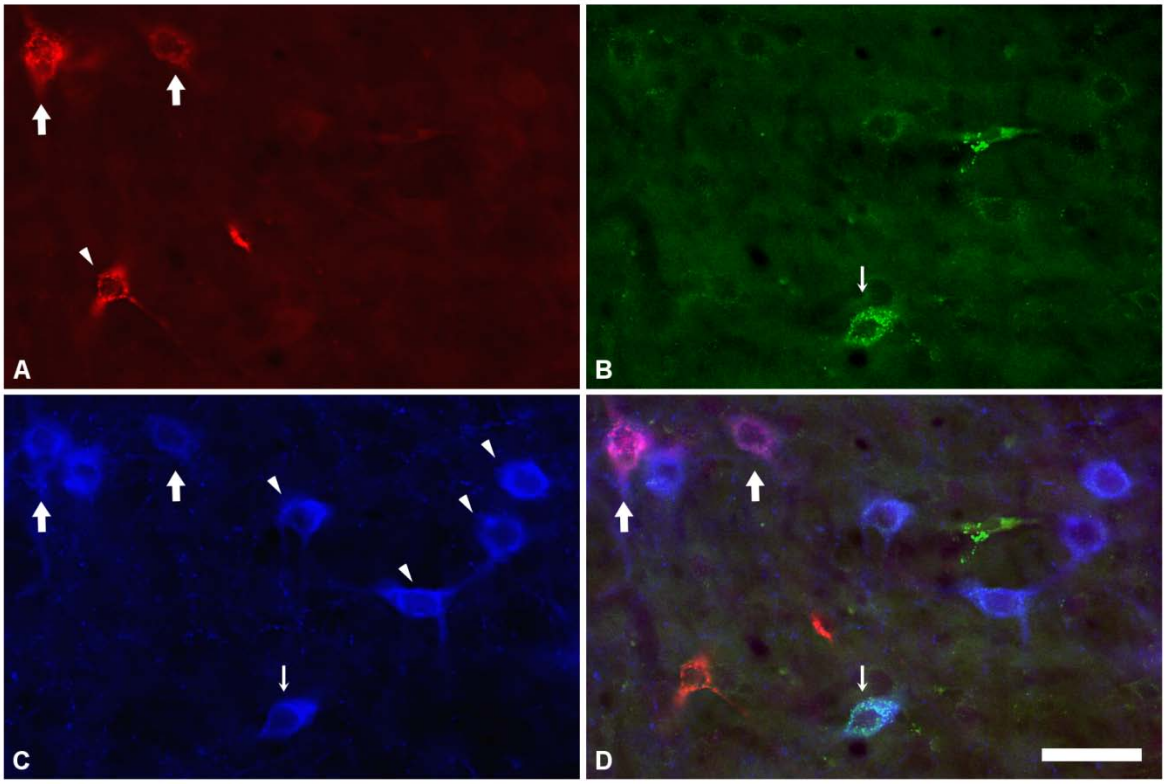

Figure 20 PPT neurons retrogradely labeled from the AVN and VTA singly labeled for tracer or dually labeled for tracer and VAChT.

Examination of single channel immunofluorescence identified neurons containing: (**A**) CTxβ retrogradely transported from the AVN; (**B**) Retrobeads transported from the VTA; and/or (**C**) immunoreactivity for the vesicular acetylcholine transporter (VAChT). (**D**) The three channels were merged to show colocalization of tracers and VAChT. In this field from the lateral PPT, both VAChT-ir (thick arrows) and non-VAChT-ir neurons (arrowhead in **A**) are labeled from the thalamus. A dual Retrobead- and VAChT labeled neuron lies nearby (thin arrows in **B**-**D**). In addition, several neurons singly labeled for VAChT are visible (arrowheads in **C**). Scale bar represents 50 µm in all panels.

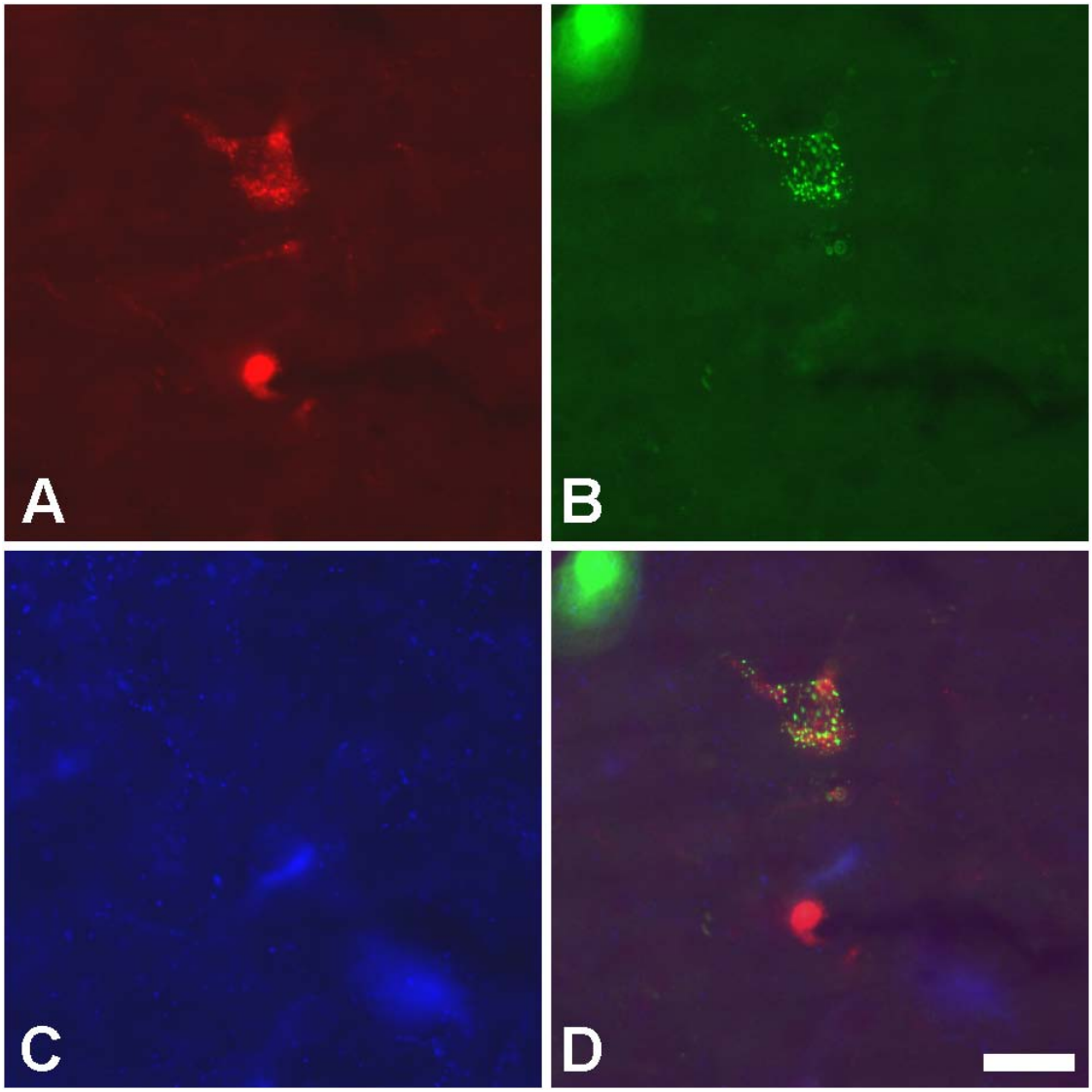

Figure 21 A dual tracer-labeled cell in the LDT does not contain VAChT immunoreactivity.

Triple immunofluorescence image of the LDT revealing a non-cholinergic dual-tracer labeled neuron. CTxβ immunoreactivity (**A**) and Rbeads (**B**) are both present in a single neuron. VAChT immunoreactivity is present in nearby cells (**C**), but absent from the dual-tracer labeled neuron. **D** Merger of the single fluorescence channels demonstrates colocalization of CTxβ-*ir* and Rbeads. Scale bar in **D** represents 20 µm in all panels.

containing both tracers and immunoreactivity for VAChT (Figure 22) were infrequently detected. The total neuronal counts obtained for each immunolabeling category are shown in Table 3. In general, smaller thalamic injections produced fewer CTxβ immunopositive cells, whereas the number of Rbead labeled neurons was more consistent across cases, most likely due to the similar small size of Rbead injections.

The spatial distribution of retrogradely labeled neurons following injections in the AVN and VTA, shown in Table 4, was in agreement with previous studies (Shibata 1992; Gonzalo-Ruiz et al 1995; Oakman et al 1995; Geisler & Zahm 2005). The percentage of each afferent population (CTxβ-labeled or Rbead-labeled) that was observed in each subdivision of the mesopontine tegmentum across hemispheres (i.e. ipsilateral PPT, etc.) is shown for each case. AVN injections resulted in preferential labeling of ipsilateral neurons, and in most cases the majority of CTxβ-labeled cells were found in the LDT. Neurons labeled from VTA Rbead injections were also more likely to be found on the ipsilateral side and were slightly more commonly observed in the LDT. In contrast, cells labeled with CTxβ following injections in the PT nucleus were more evenly distributed across hemispheres and subregions. VAChT-*ir* neurons were also evenly distributed to the ipsilateral and contralateral sides (53% versus 47%, respectively, *data not shown*). These observations suggest that the laterality observed for retrograde transport from the AVN and VTA was not due to uneven or biased sampling of hemispheres.

The percentage of retrogradely labeled neurons that were VAChT-*ir*, shown in Table 5, was also consistent with previous tract-tracing studies (Gonzalo-Ruiz et al 1995; Holmstrand & Sesack 2004). Nearly all injections involving the AVN labeled more VAChT-*ir* than

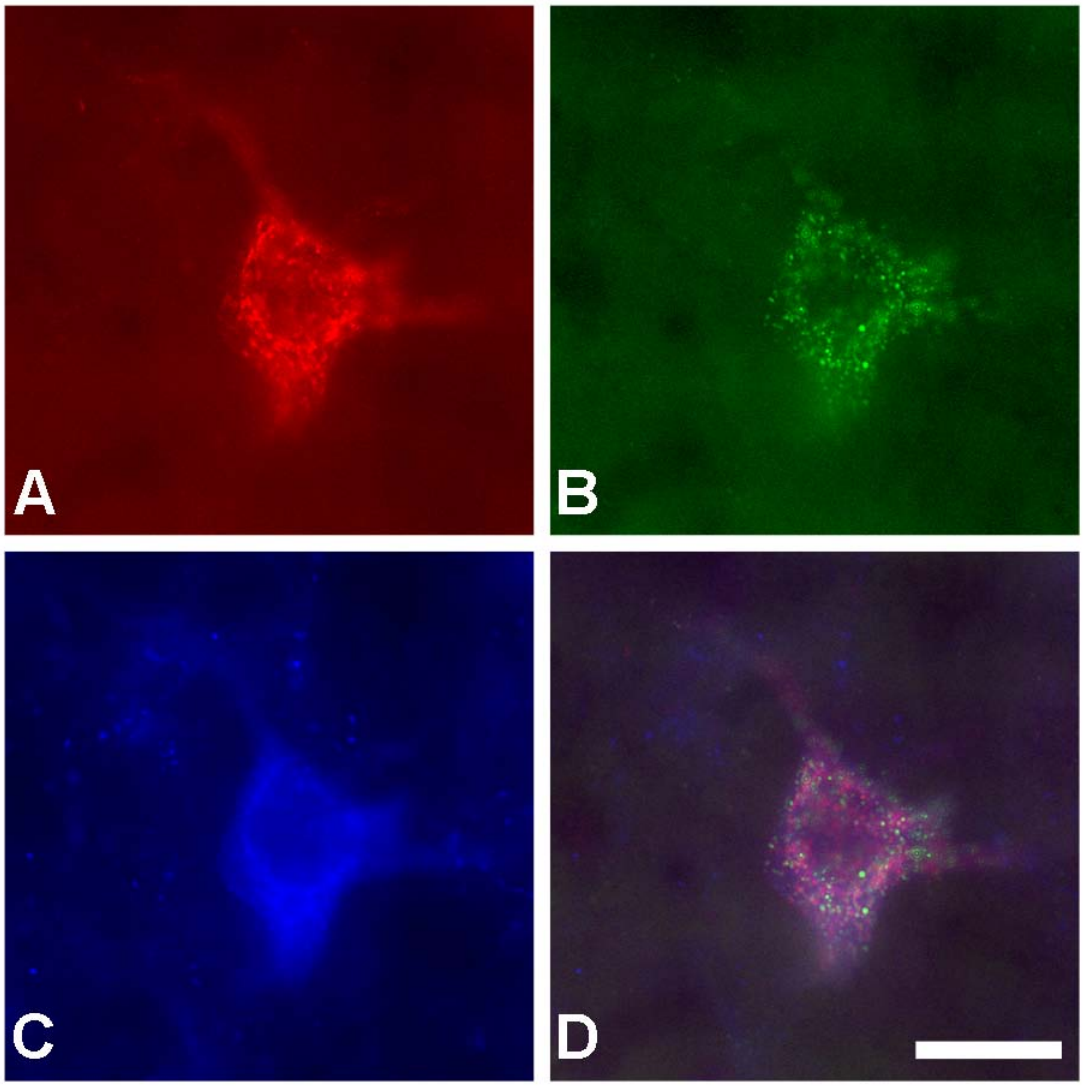

Figure 22 Three channel immunofluorescence for CTxβ, Retrobeads, and VAChT

A triply labeled neuron in the caudal lateral PPT contains labeling for CTxβ (**A**), Rbeads (**B**), and VAChT immunoreactivity (**C**). The merged fluorescence channels shown in **D** demonstrate the distinct textures of the three markers used, eliminating the chance of false positive labeling due to cross channel bleed-through. Scale bar equals 20 μm in all panels.

Table 3 Retrograde tracer labeling and VAChT immunoreactivity in rat PPT/LDT neurons

	A. Total Number of Neurons Labeled for:			B. Subsets of Neurons Labeled for:			
Case	**CTxβ**	**Rbeads**	**VAChT**	**CTxβ+ Rbeads+ VAChT-**	**CTxβ+ Rbeads- VAChT+**	**CTxβ- Rbeads+ VAChT+**	**CTxβ+ Rbeads+ VAChT+**
CTxβ in AVN							
22	210 (111)*	161 (77)	1178 (1000)	0	94	79	5
25	46 (6)	156 (62)	1108 (977)	0	37	91	3
27	9 (1)	56 (40)	794 (770)	0	8	16	0
33	261 (61)	163 (86)	1398 (1133)	5	193	70	2
34	260 (107)	201 (155)	1239 (1055)	5	143	36	5
36	179 (75)	111 (63)	836 (688)	1	101	45	2
37	216 (86)	179 (87)	1154 (945)	4	121	83	5
CTxβ in PT							
35	179 (49)	267 (166)	874 (751)	18	40	72	11

* Numbers in parentheses denote the total number of neurons that were labeled for only a single marker

Table 4 Distribution of retrogradely labeled neurons by tegmental subregion and hemisphere

	Cells with CTxβ				Cells with Rbeads			
	PPT		LDT		PPT		LDT	
Case	ipsi	contra	ipsi	contra	ipsi	contra	ipsi	contra
CTxβ in AVN								
22	38%	15%	38%	10%	24%	13%	39%	25%
25	13%	4%	63%	20%	19%	19%	45%	17%
27	11%	0%	78%	11%	34%	2%	55%	9%
33	42%	12%	30%	16%	41%	12%	29%	18%
34	20%	7%	48%	24%	20%	5%	58%	17%
36	28%	8%	45%	19%	27%	16%	33%	23%
37	31%	18%	31%	20%	40%	30%	20%	10%
Average all AVN cases								
	26%	**9%**	**48%**	**17%**	**29%**	**14%**	**40%**	**17%**
CTxβ in PT								
35	**31%**	**27%**	**27%**	**14%**	**45%**	**26%**	**24%**	**6%**

Table 5 Proportion of retrogradely labeled neurons that colocalize VAChT immunoreactivity

Case	CTxβ + VAChT CTxβ	Rbeads + VAChT Rbeads
CTxβ in AVN		
22	47.1%	52.2%
25	87.0%	60.3%
27	88.9%	28.6%
33	74.7%	44.2%
34	56.5%	20.4%
36	57.5%	42.3%
37	58.3%	49.2%
Average all AVN cases		
	67.2%	42.4%
CTxβ in PT		
35	28.5%	31.1%

non-VAChT-*ir* cells in the PPT/LDT. Qualitatively, the smaller, more discrete AVN injections (e.g. Cases 25 and 27) resulted in retrograde transport by predominantly VAChT-*ir* afferents. In contrast, injection of CTxβ into the PT resulted in substantially more labeling of non-VAChT-*ir* neurons, with VAChT-*ir* detected in only 28% of cells retrogradely labeled from the PT.

The contribution of VAChT-*ir* neurons to the mesopontine projection to the VTA was variable and ranged from ~20-60% with an average of about 40% (Table 5). This indication that non-cholinergic neurons contribute substantially to the midbrain innervation is consistent with a prior preliminary estimate from our laboratory (Holmstrand and Sesack, 2004).

Finally, we examined the extent of collateralization (i.e. colocalization of both retrograde tracers) to the AVN and VTA from the brainstem tegmentum. As shown in Table 6, few PPT/LDT neurons (<5%) with projections to either region exhibited evidence of branching to the other target area. This was true for both VAChT-*ir* and non-VAChT-*ir* populations of mesopontine tegmental cells. Conversely, tegmental neurons retrogradely labeled from the PT were more likely to also contain retrograde tracer from the VTA and vice versa (~11-16%). Again, this greater degree of dual labeling was similar for both VAChT-*ir* and non-VAChT-*ir* populations, although the percentage of afferents that showed evidence of collateralized projections was somewhat higher for VAChT-*ir* neurons.

Finally, the rates of collateralization of both VAChT-*ir* and non-VAChT-*ir* neurons observed within different subregions of the tegmental brainstem nuclei are shown in Figure 23. Although collateralization to the VTA and the AVN or PT was observed in PPT neurons, a greater percentage of LDT afferents to the midbrain and thalamus were labeled by both injections.

Table 6 Proportion of collateralized neurons in the rat PPT/LDT with and without VAChT-ir

	All Retrogradely Labeled Neurons		Non VAChT-ir		VAChT-ir	
	CTxβ + Rbeads	Rbeads + CTxβ	CTxβ + Rbeads	Rbeads + CTxβ	CTxβ + Rbeads	Rbeads + CTxβ
Case	CTxβ	Rbeads	CTxβ	Rbeads	CTxβ	Rbeads
CTxβ in AVN						
22	2.4%	3.1%	0.0%	0.0%	5.1%	6.0%
25	6.5%	1.9%	0.0%	0.0%	7.5%	3.2%
27	0.0%	0.0%	0.0%	0.0%	0.0%	0.0%
33	2.7%	4.3%	7.6%	5.5%	1.0%	2.8%
34	4.0%	5.3%	4.5%	3.1%	3.4%	12.2%
36	1.7%	2.7%	1.3%	1.6%	1.9%	4.3%
37	4.2%	5.0%	4.4%	4.4%	4.0%	5.7%
Average all AVN cases						
	3.1%	**3.2%**	**2.5%**	**2.1%**	**3.3%**	**4.9%**
CTxβ in PT						
35	**16.2%**	**10.9%**	**14.1%**	**9.8%**	**21.6%**	**13.3%**

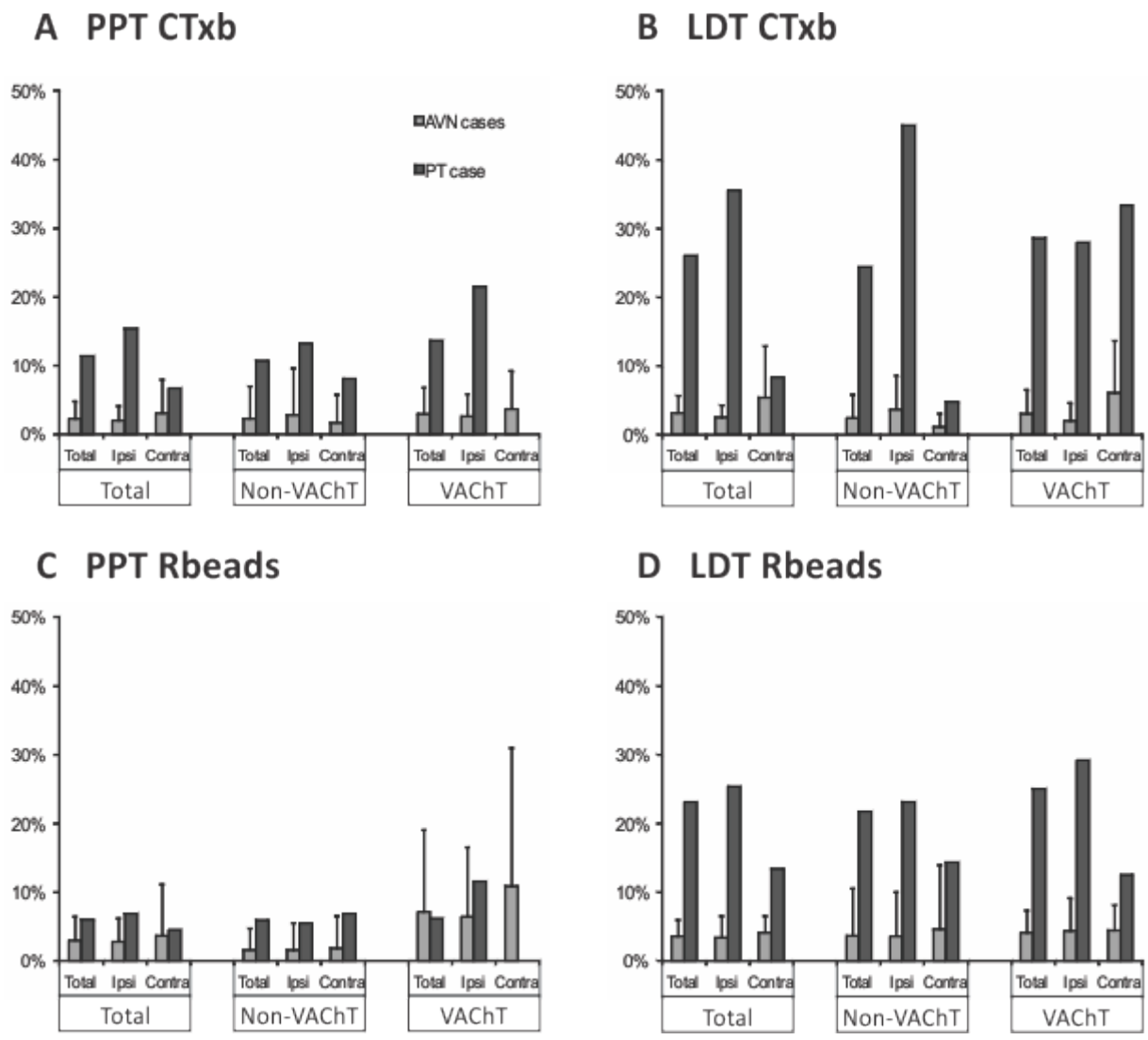

Figure 23 Collateralized afferents to the midbrain VTA and AVN or PT in subregions of the PPT/LDT.

The percentage of all thalamic (**CTxβ, A & B**) and VTA (**Rbeads, C & D**) afferents that were also labeled from the other brain region is shown divided by tegmental subregion and hemisphere (relative to the injected side). Although neurons in the PPT projected to both the thalamus and the VTA, the proportion of LDT afferents that showed such collateralization was markedly higher, especially for the paired PT/VTA case.

4.4 DISCUSSION

Our results indicate that the cholinergic innervation of the AVN and the VTA arises from largely separate populations of PPT/LDT cholinergic neurons. This novel report of the relative infrequency of collateralization in these afferent populations indicates that the brainstem cholinergic system maintains relatively segregated projections to functionally distinct limbic forebrain structures. Furthermore, the greater frequency of collateralization observed following the CTxβ injection that involved the PT nucleus is consistent with a previous report of collateralized PPT/LDT projections to the VTA and midline and intralaminar thalamic nuclei (Bolton et al 1993). Furthermore, this pattern of labeling demonstrates that the low percentage of dual retrograde labeling from the AVN and VTA does not result from a general segregation of thalamic and midbrain projections from the brainstem. From a functional standpoint, collateralized cholinergic input to the VTA and the AVN versus the midline/intralaminar thalamic nuclei suggests that cholinergic modulation is coordinated across different components of an interconnected limbic circuit, while remaining distinct from that impinging on functionally separate circuits.

4.4.1 Methodological Limitations

Neuronal tract-tracing studies are limited by the specificity of the tracer used, and the placement and size of the injection. The first limitation, specificity, refers to intrinsic properties of the tracer that determine whether it can be taken up by non-terminating axons that traverse a region, thereby leading to the labeling of neurons that are not true afferents of the injected brain region. This uptake by fibers of passage is a well-known drawback to the use of CTxβ (Chen &

Aston-Jones 1995), but was not of paramount concern in this study. The cholinergic afferents to the AVN are assumed to terminate in this region, as there is extensive arborization of cholinergic axons present here and these nuclei form the most anterior pole of the thalamus. Since there are no nuclei anterior to the AVN to which axons traversing this region could be directed, we do not believe that our CTxβ-labeled population is unduly affected by the fiber-of-passage problem. CTxβ can also be transported both retrogradely and anterogradely, especially when deposits are made by pressure injection (Luppi et al 1990). Fortunately, anterograde and retrograde labeling are easily distinguished based on the size and appearance of labeled structures (e.g. cell body versus axon terminal), eliminating the need to utilize strictly unidirectional tracers.

In contrast to the AVN, the VTA is traversed by many axons originating in the tegmentum that ultimately target brain regions that lie anterior to the VTA. For this reason, we chose to use Rbeads as the retrograde tracer for this region, as the beads demonstrate little to no uptake by fibers of passage (Katz et al 1984; Cornwall & Phillipson 1988a; Schofield 2001). Unfortunately, the specificity of uptake is gained at the expense of complete labeling of afferents, as the beads do not diffuse far from the injection site. Based on the size of our injections, it is reasonable to conclude that we labeled only a portion of the afferents to the VTA, and therefore our estimates of the collateralization of AVN and VTA afferents should be interpreted with caution as a minimum estimate of the true rate of collateralization. However, our VTA injections did not systematically exclude any particular division of the VTA, and displayed enough topographical variation to inspire confidence that the low rate of tracer co-localization was not simply due to omission of a particular subregion of the VTA which collateralized afferents might target.

We did note that the contribution of VAChT-*ir* neurons to the mesopontine projection to the VTA appears to be higher in the present study (~ 20-60%) than in a previous investigation from our laboratory (~ 25%) (Holmstrand & Sesack 2004), perhaps due to our failure to label the entire population of afferents to the VTA. It should be noted however, that the larger FluoroGold tracer injections in those experiments may have resulted in uptake by fibers-of-passage ((Luppi et al 1990) *and unpublished observations*). Consequently, we felt that underestimating the total population of afferents to the VTA was preferable to spurious labeling from non-specific uptake.

Finally, the higher proportion of collateralization observed following the paratenial thalamic injection demonstrates that the restricted VTA injections did not artificially limit detection of collateralized afferents to the lower proportions found in our other cases. While our results should be interpreted with caution due to these technical limitations, we feel that our findings are still representative of the true organization of PPT/LDT cholinergic forebrain projections.

A final limitation of our methodology concerns the use of antibodies to detect relevant proteins in the PPT/LDT neuronal population. All immunohistochemical studies are limited by the specificity of the antibodies used, by the potential for cross-reaction of secondary antibodies, and by the ability of reagents to penetrate the relevant structures in order to bind to their target epitopes. The use of Rbeads, which do not require immunohistochemical detection, helped to limit possible cross-reactivity and false-colocalization, and facilitated the selection of appropriate antibody complexes to detect the presence of VAChT and/or CTxβ. The goat anti-CTxβ antibody has been characterized previously (Angelucci et al 1996; Pakan et al 2008; Xu et al 2009). Evidence for the specificity of this antibody includes the labeling of a single band of

cholera toxin subunit B by Western blot (Xu et al 2009), labeling in expected brain regions following injection of tracer, and the absence of immunoreactivity in uninjected controls. The rabbit anti-VAChT antibody has been previously shown to specifically label cells transfected with VAChT, but not the vesicular monoamine transporter (Liu & Edwards 1997), and the pattern of immunoreactivity obtained in our experiments was consistent with the known distribution of cholinergic neurons and axon terminals in the rat CNS.

4.4.2 Comparison of Target Connectivity: Diversity in Limbic Structures

Although both the AVN and the VTA are considered to be components of the limbic system, the anatomical connections of these individual nuclei are largely exclusive of each other. The mesocortical dopamine projections arising from the VTA terminate preferentially in the prefrontal and anterior cingulate cortices (Beckstead et al 1979; Berger et al 1991), with innervation of more posterior limbic cortical areas such as the retrosplenial cortex reported as either sparse (Berger et al 1985) or nonexistent (Theirry et al 1973; Thierry et al 1973; Hökfelt et al 1974; Lindvall et al 1974). In contrast, the AVN is reciprocally interconnected with the retrosplenial granular cortex (Domesick 1969; Shibata 1993; Shibata & Naito 2005), and with structures comprising the hippocampal region, but does not send significant projections to the anterior cingulate, prelimbic or infralimbic cortices, or to orbital areas (Vogt et al 1992). Sparse projections to the anterior thalamic nuclei from the limbic prefrontal cortex have been reported, but these mainly target the AM (Xiao et al 2009), which also innervates the anterior cingulate (Shibata & Naito 2005). Similarly, one of the major subcortical targets of VTA dopamine projections is the nucleus accumbens, but this region is not innervated by the AVN. AVN

neurons receive input from the hippocampus and mammillary body, both of which receive only minor, if any, dopamine projections from the VTA in the rat (Oades & Halliday 1987). In contrast, the midline/intralaminar nuclei of the thalamus are connected with cortical and subcortical structures that receive VTA dopamine inputs (Beckstead 1976; Berendse & Groenewegen 1990; 1991; Erro et al 2002; Smith et al 2009), some of which send reciprocal excitatory or inhibitory projections to the VTA. Additionally, the mediodorsal thalamic nucleus (MD) receives direct dopamine innervation in both rats and primates (Beckstead et al 1979; Simon et al 1979; Sanchez-Gonzalez et al 2005), and other midline/intralaminar thalamic nuclei appear to be targets of dopamine input in primates as well (Sanchez-Gonzalez et al 2005). Conversely, the AVN does not appear to be directly influenced by dopaminergic modulation. The paratenial nucleus used as a control thalamic region in our study sends a dense projection to the nucleus accumbens (Erro et al 1999), and is reciprocally connected with prefrontal cortical regions (Krettek & Price 1977; Vertes & Hoover 2008), indicating that it participates in limbic circuitry that is subject to substantial dopaminergic modulation by VTA neurons.

The segregation of anatomical connections of the VTA and the AVN indicate that there are likely to be separate circuits operating within the broader limbic system (Vertes 2006). At least two of these might include: 1) a prefrontal-accumbens-ventral pallidal-intralaminar thalamic circuit that is heavily influenced by dopaminergic projections from the midbrain VTA and SNc; and 2) a circuit involving the AVN, the retrosplenial cortex, hippocampal structures, the mammillary body and other hypothalamic nuclei, that is not a significant target of mesocorticolimbic DA projections. Interestingly, our results indicate that these separate circuits receive specifically targeted cholinergic and non-cholinergic innervation from largely separate neurons in the PPT/LDT. The finding that > 20% of the cholinergic afferents to the PT showed

evidence of sending a collateral projection to the VTA, combined with prior studies demonstrating collateralization of brainstem inputs to the VTA and mediodorsal, parafascicular, and midline thalamic nuclei (Bolton et al 1993), implies that components of the same circuit receive coordinated cholinergic modulation and non-cholinergic input from the brainstem.

The restriction of projections to and from the AVN to distinct cortical and subcortical regions with poor dopamine innervation may be a species-specific phenomenon. In both cats and primates, AVN neurons have an expanded projection field that includes the anterior cingulate cortex (Niimi et al 1978; Barbas et al 1991), and possibly the ventral striatum as well (Giménez-Amaya et al 1995). Furthermore, dopamine innervation of thalamic nuclei is markedly expanded in primates beyond the restricted projections to the mediodorsal nucleus observed in rodents (Melchitzky et al 2006; Garcia-Cabezas et al 2009). Given the specific organization of collateralized PPT/LDT projections to functionally related thalamic and subcortical nuclei, these relationships must be examined in higher mammals as well as in rodent, to determine whether the expansion of overlapping limbic projections is accompanied by increased collateralization of brainstem cholinergic and non-cholinergic afferents.

4.4.3 Sub-Populations of Brainstem Cholinergic Neurons: Functional Implications

Our previous investigation of the cholinergic axons innervating the AVN and the VTA indicated that afferents to the AVN display greater total immunoreactivity for CHT compared to VTA axon terminals, and that the density of transporters associated with the plasma membrane is greater in the AVN as well (Holmstrand et al 2010). We recognized that these differences in CHT membrane density might reflect different properties of distinct subsets of cholinergic cells.

Alternatively, if the two regions were innervated through collateralization of a common afferent population, the unique environment of an innervated region might result in the different axonal properties we observed. The results reported here support the former perspective by indicating that the AVN and VTA receive input from largely segregated cholinergic cell groups. Given that CHT is delivered to the plasma membrane through the fusion of synaptic vesicles during neuronal activity (Ferguson et al 2003), our findings of predominantly discrete PPT/LDT innervation of the AVN and VTA suggest that differences in firing rates between the separate populations of neurons could underlie the differences in levels of membrane-associated CHT immunoreactivity (Holmstrand et al 2010). Variations in the basal activity of PPT and LDT neurons have been reported (Steriade et al 1990a; Pascoe & Kapp 1993; Datta & Siwek 2002); however, direct electrophysiological evidence of differences between the AVN and VTA afferent populations has yet to be reported.

In addition to possible differences in baseline firing rate of these cholinergic sub-populations, the patterns of activity across sleep-wake states of both cholinergic and non-cholinergic afferents to the AVN and VTA might differ, given that some PPT/LDT neurons show variation in the association of their activity with wakefulness, slow-wave sleep, and REM sleep (Steriade et al 1990a; Datta & Siwek 2002). While the characterization of these activity patterns is more complete for the PPT than for the LDT, both regions appear to contain at least three population of cells: 1) neurons that display increased activity during wake and/or REM sleep; 2) neurons that display a progressive increase in activity from wakefulness to slow-wave-sleep to REM, with significantly greater activity during REM sleep than during the other stages; and 3) neurons whose firing rates do not correlate with sleep-wake states.

The possibility that afferents to the AVN versus the VTA might arise from different physiologically-identified populations of PPT/LDT neurons is intriguing in light of the lack of sleep-wake associated variation in VTA dopamine cell firing (Trulson & Preussler 1984; Lee et al 2001). Perhaps the state-independent neurons comprise most of the VTA afferent population. However, it should be noted that despite the absence of changes in firing rate, sleep-wake state correlated changes in dopamine release in forebrain areas suggest that the pattern of VTA DA cell firing can vary across behavioral states (Monti & Monti 2007). These questions will require the careful identification of the projection targets of individual neurons during electrophysiological investigation of PPT/LDT function. Finally, the specific inputs to these sub-populations might reveal further important clues to the organization and function of brainstem modulatory influence over specific limbic circuitry.

Cholinergic neurons in the brainstem have been noted to co-localize immunoreactivity for substance P (Vincent et al 1983; Sutin & Jacobowitz 1990) and other peptide co-transmitters (Crawley et al 1985). Cholinergic axon terminals in the AVN and VTA also contain dense-cored vesicles, a marker of neuropeptide co-transmission, although the more frequent observation of these structures in the VTA suggests that peptide co-transmission may play a larger role in shaping VTA activity (Holmstrand et al 2010). Further work is needed to determine whether cholinergic neurons that utilize peptide co-transmitters preferentially project to the VTA and the midline/intralaminar thalamic groups. Additional experiments will also be required to elucidate the identity of the relevant peptides and to determine whether the separate projections from the PPT/LDT might be identified on this basis. More generally, any biological marker that could delineate these projections would be useful for future investigations of PPT/LDT function.

A clearer understanding of the organization and function of the PPT and LDT may also aid our understanding of human health and disease. Many studies have noted PPT/LDT pathology in tissue from patients with neurodegenerative diseases and over the course of normal aging (Zhang et al 2005). There is cell loss in the PPT in the brains of both Parkinson's disease patients and patients with progressive supranuclear palsy (Halliday et al 1990; Jellinger 1991; Emre 2003), although whether this loss is causative rather than symptomatic is still debated (Xuereb et al 1990). In addition, changes in cell number and cell size have been reported in schizophrenic brains (Karson et al 1991), and the sleep disruptions that are characteristic of a wide range of mental disorders indicate that the role of PPT/LDT in maintaining normal limbic functions may be underappreciated. Further study of the specific connections and phenotypes of these brainstem nuclei may reveal important pathophysiological details and present new targets for therapeutic intervention.

5.0 GENERAL DISCUSSION

These studies represent the first quantitative evaluations of the expression and localization of CHT in the ascending cholinergic projections of the brainstem PPT and LDT. We found subtle but statistically significant differences in the population characteristics of CHT immunoreactive axon terminals in two different limbic targets of the PPT/LDT cholinergic system. Furthermore, boutons in these regions showed morphological differences indicating that the ascending cholinergic innervation of the AVN and the VTA arise from separate sub-groups of PPT/LDT cholinergic neurons, a hypothesis that we confirmed by dual retrograde tract-tracing from these regions. The combined findings suggest that the differences we found with respect to CHT immunoreactivity and localization across these two brain regions result from this specific and segregated pattern of innervation. These findings support our original hypothesis that levels of CHT expression, and therefore high-affinity choline uptake, can vary among innervation targets of the ascending projections from the cholinergic brainstem. While the initial aim of these studies was to detect such differences, taken in total, our results strongly indicate that the mechanisms regulating high-affinity choline uptake are remarkably robust across different groups of cholinergic terminals arising from the PPT/LDT.

The major findings are discussed below in relation to general principles regarding regulation of CHT expression and subcellular trafficking, and about the brainstem tegmental cholinergic system specifically. Briefly, we will discuss the greater total expression of CHT and

how this is predicted to impact the functional levels of high-affinity choline uptake. The likely mechanisms underlying the difference in total CHT content of these axons will be explored. Finally, the implications of the segregation of ACh projections to these regions are treated. Throughout these treatments, the methodological limitations of these studies, and how these limitations constrain the conclusions that can be drawn from of our results are carefully considered.

5.1 CHOLINERGIC TERMINALS IN THE AVN HAVE MORE CHT THAN SIMILAR BOUTONS IN THE VTA

Our most significant finding was that total levels of CHT immunoreactivity were higher in the AVN terminals than in the VTA. This was independently determined in two experiments, using electron microscopy to examine immunogold-silver staining for CHT at the ultrastructural level (Chapter 2), and confirmed in the immunofluorescence study of VAChT and CHT (Chapter 3). The size of this difference in total immunolabeling for CHT was also large enough to have clear biological relevance.

The differential fluorescence imaging settings applied to AVN versus VTA tissue sections might cast doubt on the validity of this regional difference, but quantification of immunogold-silver labeling for CHT demonstrated that the mean density of CHT immunoreactivity within AVN axon terminals was nearly twice as high as that seen for the VTA population. By immunofluorescence, the relative difference in labeling intensity was smaller, with the mean CHT FI of AVN CHT-*ir* profiles approximately 45% higher than the mean CHT

FI of VTA profiles. This discrepancy is most likely due to differences in the methods of sampling used between the two studies. Furthermore, intrinsic differences in the labeling methods complicate direct comparison of the effect size between the studies. Suffice it to say, that the relationship between AVN CHT levels and VTA CHT levels was shown to be qualitatively similar across two independent immunohistochemical methods. The complementary findings of these two studies refute concerns that methodological limitations contributed significantly to the observed regional differences in CHT immunoreactivity.

Furthermore, we observed colocalization of CHT and VAChT immunofluorescence within axon terminals imaged from the AVN more frequently than in VTA immunofluorescent puncta. The simple threshold criteria used to identify CHT-*ir* and VAChT-*ir* puncta precludes the interpretation that singly labeled terminals contain no molecules of the sub-threshold protein, but the presence of these singly immuolabeled profiles does indicate that levels of protein expression can vary at different sites of ACh release.

5.1.1 Immunoreactivity as a Measure of Protein Concentration: Methodological Considerations

Although a subset of labeled terminals in the AVN and VTA were examined in serial ultra-thin sections for morphological characterization, gold particle density was quantified from a single section through each profile (Table 1). In contrast, fluorescence intensity data was obtained throughout the entirety of the immuolabeled volume, and quantitative comparisons were carried out on the mean intensity of all component voxels. This produced a more complete assessment of total CHT immunoreactivity than the immunogold-silver analysis, as CHT is

present throughout the three dimensional volume of axon varicosities. Furthermore, the size differences between AVN and VTA cholinergic axon varicosities indicate that a single ultrathin section through the VTA varicosities would represent a lower proportion of the total volume of these profiles compared to the AVN; therefore, the number of gold particles detected would be a smaller percentage of the total number of particles distributed throughout the terminal. In the AVN, the smaller size of CHT-*ir* profiles would result in a single section capturing a greater proportion of all gold particles contained within the labeled axon, as profiles would be divided into fewer ultrathin sections. In contrast, imaging throughout the entire volume of CHT-*ir* puncta by immunofluorescence removes this sampling limitation.

Although we did not apply systematic random sampling in these studies, it was nevertheless assumed that the single section examined for immunogold silver density was randomly selected, even for the profiles for which serial section data were available, as we chose to quantify immunogold labeling in the micrograph that was produced from the first visual identification of each labeled profile. When serial micrographs were collected, we generally photographed at least 2 ultrathin sections that were more superficial than the first section, and 2 sections that were deeper from the tissue surface than the first section as well. Sometimes, the labeled profile disappeared from the photographic field in one of these directions, and expanded in the opposite direction, indicating that the 1st section in which the profile was encountered was not taken through the center of that profile (*personal qualitative observations*). Thus, we did not necessarily obtain our measurements of total gold density from those sections with the heaviest labeling, but sampled pseudo-randomly from all possible sections through a given labeled profile. When combined with the smaller proportion of total terminal volume that a single section would represent in VTA profiles versus AVN profiles (due to the regional size

differences in CHT-*ir* structures), this sampling strategy may have resulted in unequal underestimation of the total amount of CHT immunoreactivity within VTA versus AVN terminals, and may have contributed to the larger difference in CHT immunoreactivity observed by immunogold-silver staining.

The independent confirmation of greater immunoreactivity for CHT in AVN terminals by fluorescence microscopy provided assurance that the immunogold-silver results were not purely an artifact of this sampling strategy. However, it is important to note that both of these methods effectively measure the concentration of CHT within labeled profiles, since fluorescence intensity will be dependent on the concentration of fluorophores within a discrete volume. The larger size of VTA axon varicosities would be expected to produce less intense labeling even if the same total number of transporters were present in these profiles, assuming an even distribution of CHT throughout the axonal compartment. Still, larger terminals are also expected to contain more synaptic vesicles (Lisman & Harris 1993; Pierce & Lewin 1994), and so the relatively lower concentration of CHT immunoreactivity in these larger terminals probably still represents a functional difference in the availability of transporters that can be recruited to the plasma membrane. Unfortunately, we did not count synaptic vesicles in our sample of CHT-*ir* axon varicosities, so cannot independently confirm that this is true. Although we are comparing concentrations of CHT and not absolute numbers of transporters, these measurements are of sufficient value as to inform some functional predictions based on our results.

The different immunohistochemical procedures used for these studies may also have contributed to the mismatched effect size observed between methods. Immunogold silver labeling has lower sensitivity than other immunohistochemical methods, such as immunofluorescence (Sesack et al 2006). This characteristic stems from the relatively poor

penetration of antibodies into tissue treated for electron microscopy. Good ultrastructural images require the morphological preservation of lipid membranes in order to accurately identify the spatial limits of discrete neuronal elements. Detergent additives that increase the permeability of cell membranes to antibodies, thereby increasing access to intracellular protein epitopes and improving the sensitivity of immunohistochemical detection, physically degrade the plasma membrane. The use of detergents must therefore be restricted in ultrastructural studies if discrimination of distinct structures is to be obtained. However, the low levels of detergent used for ultrastructural preservation impede antibody penetration. The penetration of gold-conjugated secondary antibodies is particularly sensitive to this experimental detail, and pre-embedding immunogold-silver labeling is typically only found within the first few microns of the tissue surface. While we drew our sample micrographs only from regions with apparently adequate levels of staining (i.e. within regions of tissue where multiple labeled profiles were visible, typically 1-2 µm from the interface of the tissue and the embedding medium), this determination was subjective, and we cannot unequivocally assert that all of the terminals in our study were exposed to equivalent concentrations of primary or secondary antibodies. Rather, there was likely to be a gradient of antibody penetration, such that terminals from deeper parts of the section would show less labeling than more superficial profiles, even if these contained equivalent amounts of antigen. However, this methodological limitation would presumably affect labeling in the AVN and VTA tissue equally, so we were still able to compare the relative amounts of CHT immunoreactivity across labeled profiles in the AVN and VTA populations.

In contrast, fluorescence imaging can theoretically detect the photons emitted from a single fluorophore (Wouterlood 2006; Hohlbein et al 2010) and, presumably, such methods detect more of the antibody complexes that are bound to CHT than the less sensitive

immunogold-silver method. The uncertain stoichiometry of antibody binding to transporter prevents the interpretation that some fixed unit of fluorescence intensity above background represents a single transporter, but higher fluorescence intensities can reasonably be assumed to arise from a greater concentration of antigen within the axonal compartment. Furthermore, the generous use of detergents that is possible with light microscopic staining method improves antibody penetration, as evidenced by the relatively stable detection of objects throughout the center of the dual-fluorescence image stacks examined in Chapter 3 (see Figure 14). This undoubtedly improved the detection of antigens compared to the EM study, yet did not change the general finding that CHT immunoreactivity is higher per terminal in the AVN compared to the VTA.

5.1.2 Implications of Increased CHT expression in AVN versus VTA Cholinergic Boutons

The robust difference in total immunoreactivity for CHT that we observed between these populations of cholinergic boutons suggests that the transcription and translation of CHT mRNA is elevated in neurons innervating the AVN. This indicates that cholinergic inputs to the AVN and VTA are likely to arise from different PPT/LDT neurons, and that the intracellular mechanisms which regulate the transcription and/or sub-cellular trafficking of CHT are differentially activated between these afferent populations. The pattern of retrograde labeling observed following injection of tract-tracing agents into these two brain regions confirms that the axonal populations used to compare CHT immunoreactivity originate from distinct cells within the cholinergic brainstem tegmental complex. Furthermore, the morphological differences in the relative size, synaptic incidence, and frequency of dense-cored vesicle presence reported in

Chapter 2 all support the conclusion that the AVN and VTA are modulated by different cholinergic brainstem neurons. Similar to other studies on the functional anatomical connections of the PPT and LDT (Woolf & Butcher 1986; Hallanger et al 1987; Gould et al 1989), we found that the segregation of these afferents is not complete, as a mix of cholinergic afferents from the PPT and LDT were labeled from either site, and a few cholinergic neurons could be retrogradely labeled from both innervation targets. However, the majority of ACh input to these regions appears to be specifically targeted to the recipient brain structures, as evidenced by the low rate of collateralization reported in Chapter 4.

Importantly, the observed measurements of CHT immunoreactivity indicated that the two bouton populations have overlapping distributions of CHT levels, but that a greater proportion of profiles in the AVN display intense immunostaining for the transporter. The similar scale of CHT immunoreactivity in AVN and VTA cholinergic boutons suggests that the characteristics of PPT/LDT neurons that determine the level of CHT expression are not widely variable, but rather differ only in subtle ways. Although cholinergic neurons in the PPT/LDT show considerable variability in their anatomical connections and peptidergic co-expression, as a population their physiology is relatively uniform. Most of these neurons show tonic firing rates that increase during behavioral states associated with an "activated" thalamocortical system (W and REM-sleep) (Steriade et al 1990a; Datta & Siwek 2002; Boucetta & Jones 2009). A minority of these cells may be capable of firing bursts of action potentials from a highly depolarized state (Wilcox et al 1989), but the majority of PPT/LDT cholinergic neurons are thought to be fire only in the tonic mode. Still, sensory stimulation can dramatically increase their tonic firing rate (Kang et al 1990; Leonard & Llinás 1990; Boucetta & Jones 2009), presumably leading to increased release of ACh in the regions innervated by these cells. The

relatively homogenous population responses of PPT/LDT cholinergic cells might account for the considerable overlap in our population measurements. Slight variability in spontaneous firing rates might be reflected by differential expression of CHT, thereby providing a functional correlation to the differences in relative expression of CHT observed in Chapters 2 and 3.

5.2 TOTAL CHT EXPRESSION IS LIKELY TO BE DRIVEN BY THE FUNCTIONAL DEMANDS FOR HIGH-AFFINITY CHOLINE UPTAKE WITHIN AXON TERMINALS

The hypothesis that overall levels of CHT expression (i.e. total number of transporters) reflects the relative demand for choline uptake, and thus may be an indicator of ACh turnover in cholinergic axons, is supported by considerable experimental evidence. The relatively exclusive expression of CHT by neurons that also express VAChT and ChAT proteins (Apparsundaram et al 2000; Okuda et al 2000; Misawa et al 2001; Kus et al 2003; Geyer et al 2008) reflects the importance of this protein for proper cholinergic function. Functional high-affinity choline uptake limits the synthesis of ACh (Yamamura & Snyder 1972; 1973; Mulder et al 1974; Simon et al 1976; Wecker & Dettbarn 1979) and the ability of cholinergic neurons to sustain high rates of ACh release (Guyenet et al 1973; Van der Kloot et al 2002; Ferguson et al 2004; Matthies et al 2006). The coupling of CHT membrane trafficking to neuronal activity, and the stable estimates of the relative distribution of CHT to the plasma membrane versus cytoplasmic vesicular pool further suggests that nerve terminals with greater numbers of transporters probably have a greater capacity for high-affinity choline uptake (Ivy et al 2001; Ferguson et al

2003; Grailhe et al 2009). Higher macroscopic choline uptake is generally associated with increased rates of ACh synthesis (Guyenet et al 1973; Köppen et al 1997) that can more rapidly refill the vesicular pool of ACh (Van der Kloot et al 2000). Increased capacity of HACU, mediated by greater numbers of transporters contained within the axon terminal and therefore able to be recruited to the plasma membrane, would be expected in neurons that release ACh at higher rates, presumably due to higher neuronal firing.

Experimental manipulations that decrease the synthesis of ACh, without reducing the frequency of release events, induce upregulations in CHT mRNA and protein expression, presumably through some feedback mechanism that is activated when ACh synthesis falls below normal levels (Brandon et al 2004; Mellott et al 2007). Furthermore, the depression of vesicular ACh release resulting from activation of muscarinic autoreceptors decreases the total capacity of the high-affinity choline uptake system (Breer & Knipper 1990). Although changes to the rate of endocytosis of CHT can be effected by multiple intracellular processes (Gates et al 2004; Ribeiro et al 2007b; Wang et al 2007; Misawa et al 2008), the activity-dependent mobilization of transporters to the plasma membrane exceeds the rate of endocytosis during periods of increased neuronal activity. This temporary imbalance of the rates of exocytic and endocytic processes results in a net increase of high-affinity choline uptake (Mulder et al 1974; Simon & Kuhar 1975; Murrin & Kuhar 1976).

Our immunohistochemical results fit well within this theoretical framework, and further indicate that the regulation of CHT trafficking in the mesopontine tegmental cholinergic system is tightly controlled, probably by the same cellular mechanisms that operate in other cholinergic systems.

5.2.1 Strict Regulation of CHT Membrane Trafficking in Cholinergic Axons

The pattern of ultrastructural localization we observed in Chapter 2 resembled that found in all cholinergic axons examined thus far. Not only is the majority of CHT immunoreactivity found associated with small clear vesicles contained within axons, but the relative amount of membrane/total CHT immunoreactivity has been previously estimated at 5- 20% (Nakata et al 2004), similar to what we observed in the AVN and VTA (see Appendix A, Figure 24). These results resemble measurements of plasma membrane and vesicular-associated CHT levels measured by Western blot (Ferguson et al 2003). Interestingly, this percentage also corresponds to the estimated size of the readily releasable pool of synaptic vesicles at the neuromuscular junction (Van der Kloot 2003), supporting the assumptions that the immunogold-silver method we used accurately represents the relative distribution of CHT and that our cytoplasmic pool of transporters corresponds to the "reserve" pool of synaptic vesicles. The strict agreement of our observations with the characteristics of CHT localization in other cholinergic systems indicates that the cellular processes regulating membrane trafficking of CHT within cholinergic axons are robust and are probably strictly conserved within all cholinergic neurons.

The stable proportional distribution of membrane to cytoplasmic CHT immunoreactivity levels described in all of these studies predicts that under equivalent levels of ACh release, axons with increased numbers of transporters should have increased choline uptake. Using an immunodepletion protocol on isolated synaptic vesicles, Ferguson and colleagues demonstrated the existence of two distinct populations of VAChT containing synaptic vesicles, differentiated by the absence or presence of CHT (Ferguson et al 2003). The presence of more CHT+ synaptic vesicles relative to CHT- vesicles within an axon terminal would increase the overall probability of fusion events resulting in the insertion of "new" transporters into the plasma membrane.

Accordingly, we found evidence that the total gold density of an individual terminal was a significant predictor of that terminal's membrane gold density (Chapter 2), providing further evidence that functional levels of choline uptake can be influenced by the total protein expression of CHT.

5.2.2 CHT is a Possible Indicator of Relative Activity in Cholinergic Terminals

Our results also suggest that the relative rate of ACh release, and the extent to which release can be increased within individual cholinergic terminals, may be reflected by the total expression of CHT. If we make the reasonable assumption that terminals with higher concentration of VAChT protein probably have higher rates of vesicular ACh release (Song et al 1997; Roghani & Carroll 2002), then the significant correlations of VAChT and CHT fluorescence intensities that we reported for both the AVN and VTA bouton populations suggest that CHT expression levels are similarly correlated with neuronal ACh release. Further evidence of a strong association between absolute levels of VAChT and CHT expression was obtained by comparing the ratio of CHT to VAChT immunofluorescence in VAChT-*ir* boutons. We found that this ratio was invariant across different populations of cholinergic terminals that nevertheless showed significant differences in the intensities of both CHT and VAChT immunofluorescence labeling (Chapter 3). This result implies that the relative levels of these proteins are stable in cholinergic boutons even when CHT and VAChT expression are both upregulated. The most parsimonious explanation for this is that the expression of these genes is upregulated by similar transcription factors. Although the expression of CHT can be differentially driven in some circumstances (Sherman & Friedman 1990; Lecomte et al 2005), previous studies have

confirmed that many of the experimental manipulations that increase VAChT or ChAT expression have similar qualitative effects on CHT expression (Oosawa et al 1999; Berse et al 2005; Madziar et al 2008).

An important caveat to this interpretation of our data is that little direct evidence of a linear relationship between VAChT expression levels and activity in cholinergic neurons is available. Certainly the loss of functional VAChT expression abolishes synchronized vesicular release of ACh (de Castro et al 2009; Lima et al 2010), and overexpression of this protein does increase both spontaneous and evoked ACh release (Oosawa et al 1999). However, recent evidence indicates that this is due to changes in the quantal size of each ACh-containing vesicle, and not necessarily due to an increase in the number of vesicles available for release (Van der Kloot et al 2000; Van der Kloot 2003). Although it seems reasonable to assume that all synaptic vesicles within a cholinergic terminal would contain this protein, the membrane trafficking of both VAChT and CHT is probably superimposed on more general membrane recycling pathways (Ferguson & Blakely 2004; Ribeiro et al 2006). Still, if VAChT is inserted into synaptic vesicles at some stable rate, it follows that increasing the concentration of VAChT protein in the axonal compartment would result in an increased proportion of synaptic vesicles that contain VAChT and can package ACh, and that this increase would be proportional to the increase in VAChT protein. A larger pool of synaptic vesicles is further assumed to indicate that a given axon terminal can mobilize more synaptic vesicles from the reserve to the readily releasable pool; therefore, the assumption that neurons with greater VAChT immunoreactivity are capable of firing at higher frequencies than neurons with lower expression of VAChT (i.e. fewer ACh-containing synaptic vesicles) appears at this time to be sound. Even if greater expression of VAChT is not associated with a larger number of vesicles, elevated levels of the vesicular

protein support faster refilling of the recycling pool of synaptic vesicles, allowing ACh neurons to continue signaling for longer periods of time without depleting vesicular ACh stores.

Although our results support the interpretation that CHT expression may be a useful indicator of the physiologically relevant firing capabilities of a given neuron, direct investigation of this claim is necessary. Finally, it should be noted that many of the regional differences found between CHT-*ir* profiles within the AVN and VTA, though statistically significant, were small. The biological relevance of such a small difference in, for example, the relationship between total CHT immunoreactivity and CHT membrane density in these varicosities, as evidenced by the significant effect of region on the interaction of total gold density and membrane gold density (Chapter 2), is not clear. As we suggested in that chapter, it is possible that differences in signaling molecules in the local environment that could impact the rate of endocytosis of CHT within cholinergic terminals might lead to such subtle regional differences. However, the small size of such differences indicate that the rate of delivery of CHT to the plasma membrane is balanced by the rate of endocytosis of this protein under the conditions of our experiments, which only revealed the resting state of PPT/LDT cholinergic projections.

5.2.3 Limitations of Immunohistochemical Methods: Reduced Activity in the PPT/LDT System

One concern with the use of immunohistochemical methods for examining the localization of CHT in PPT/LDT axons arises from the effects of anesthesia on neuronal activity in this system. In order to obtain well-fixed brain tissue for ultrastructural analysis, it is necessary to perfuse the brain mechanically with strong aldehydes. This procedure requires that

animals be fully anesthetized prior to transcardial perfusion. The elapsed time between administration of anesthesia and the fixation of the tissue (~ 15 mins) could be sufficient for endocytosis of CHT to significantly reduce the number of membrane transporters. Due to the reduced activity of PPT/LDT neurons under barbiturate anesthesia (Pape & Eysel 1988), the rate of delivery of CHT to the membrane is expected to decline, and may have impacted our measurement of membrane CHT. However, the agreement of our findings with biochemical studies of CHT membrane trafficking, suggests that this experimental factor is not wholly responsible for the low levels of membrane associated CHT that we reported in Chapter 2. Still, further experimentation to examine the effects of elevated neuronal firing on the ultrastructural localization of CHT within the axon terminal might reveal an altered membrane versus cytoplasmic distribution of transporters. Such differences have been detected by homogenization and gradient fractionation of membranous components (e.g. synaptic vesicles versus plasma membrane) following depolarization of synaptosomes (Simon & Kuhar 1975; Breer & Knipper 1990; Ferguson et al 2003) and *in vivo* following the performance of an attentionally demanding behavioral task (Apparsundaram et al 2005), but the pattern of subcellular immunohistochemical labeling following neuronal stimulation has not been examined by electron microscopy. Furthermore, the effects of increasing ACh release on high-affinity choline uptake have not yet been in examined in the projections of the brainstem tegmental cholinergic neurons. Although we did not address this issue, our characterization of immunolabeling establishes that the baseline pattern of CHT localization in axon terminals arising from PPT/LDT neurons is similar to that of other cholinergic systems. Furthermore, by comparing these populations, we were able to demonstrate that CHT expression is variable across individual cells of the same anatomical group, and to establish a relationship between total CHT content and probable high-affinity

choline uptake within individual boutons. Finally, the similarity of our results to all existing observations of the subcellular distribution of CHT suggests that the regulation of high-affinity choline uptake is both robust and ubiquitous in cholinergic neurons.

5.2.4 Activity-dependent Upregulation of CHT – Implications for REM sleep

The pattern of immunogold-silver labeling for CHT reported in Chapter 2 suggests a low level of activity in these axons prior to fixation. Separate from any effects of anesthesia, this pattern might also reflect the behavioral state of the animals prior to fixation, as perfusions were performed during the light phase of the circadian cycle during which rats usually sleep. If the PPT/LDT were activated experimentally, greater differences in the membrane CHT levels of AVN and VTA cholinergic axons might be revealed.

PPT/LDT cholinergic neurons show elevated firing rates during REM sleep periods (Steriade et al 1990a; Datta & Siwek 2002; Boucetta & Jones 2009); therefore, activity-dependent upregulation of membrane CHT during REM sleep might also be examined to across behavioral state, and to further the understanding of the cellular environment in targets of PPT/LDT cholinergic projections across behavioral state. The short duration of REM sleep epochs in the rat (Williams et al 1994; Datta & Siwek 2002) poses considerable technical challenges to studying PPT/LDT axon terminals across stages of the sleep-wake cycle; however, many psychotropic drugs have side effects that change sleep architecture (Wilson & Argyropoulos 2005; Doerr et al 2010). Such agents could be used to increase REM experimentally and facilitate studies of CHT trafficking and function during different sleep-wake stages.

Interestingly, disturbances in sleep architecture are also observed in unmedicated patients with depression and schizophrenia (Hinton 1963; Tandon et al 1991; Göder et al 2004; Argyropoulos & Wilson 2005), emphasizing the need to understand the role of PPT/LDT cholinergic neurons in regulating behavioral state. Although increased acetylcholine release has been detected in the thalamus during waking states and in REM sleep (Williams et al 1994), the assumption that similar increases occur in the PPT/LDT cholinergic projections to the ventral midbrain have not been directly tested. Immunogold-silver localization of CHT might be used to indirectly measure changes in cholinergic activity due to experimental manipulations, facilitating the study of these less tractable pathways. In addition, a single nucleotide polymorphism for CHT has been implicated in major depressive disorder (Hahn et al 2008) and is associated with altered corticolimbic reactivity during an behavioral task that requires inhibition of inappropriate responses (Neumann et al 2006), presumably due to altered function of CHT within the projections of the basal forebrain cholinergic neurons. Transgenic models that incorporate this allele could be used to examine the effects of this polymorphism on cholinergic signaling in the innervation targets of the ascending projections of PPT/LDT neurons.

5.2.5 Restricted Membrane Expression of CHT – Functional Implications

Why should choline transport be so limited under resting conditions? High-affinity choline uptake is the rate limiting step in acetylcholine synthesis and it seems counterintuitive that transmitter synthesis should be restricted in this manner. However, CHT membrane content may be tightly regulated in order to limit secondary effects of high-affinity choline uptake on general cellular processes in the vicinity of cholinergic terminals. To our knowledge, no detrimental action of elevated extracellular choline levels has been demonstrated, yet the

transport of this molecule across the blood brain barrier is carefully balanced with choline efflux from the brain, indicating that free choline levels in the brain are controlled by multiple regulatory mechanisms (Klein et al 1992).

In addition to its role as a precursor to ACh, choline is incorporated into membrane lipids as phosphatidylcholine and sphingeomyelin (Löffelholz et al 1993; Cooper et al 2003), so its monopolization by ACh synthesizing compartments could adversely affect non-cholinergic cells in the vicinity of ACh terminals. In some brain regions, synaptic plasticity produces drastic changes in the morphology of spiny neurons (Robinson & Kolb 2004; Hofer & Bonhoeffer 2010; Russo et al 2010), indicating a need for increased production of phospholipid membranes. Furthermore, turnover of membrane components requires the constitutive generation of phospholipids to replace membranes that are degraded (Klein et al 1993b; Löffelholz et al 1993; Michel et al 2006). The total demand for choline for these cellular processes is high, and is met by low-affinity transport mechanisms with low affinity for choline, but faster kinetics than seen for CHT (Michel et al 2006). Although the capacity of low-affinity uptake mechanisms is greater than that of CHT, the difference in affinities of CHT and other choline transporters is sufficiently great that high-affinity choline uptake following neuronal stimulation is estimated to account for up to 60% of total choline uptake in the vicinity of cholinergic terminals (Farber et al 1996). CHT transports extracellular choline with a K_m = 1-5 µM, and so is predicted to be saturated by the typical concentrations of choline in the brain (10-15 µM; (Klein et al 1993a; Cooper et al 2003)). Less restricted expression of membrane CHT would increase the total capacity of the transport system, and might decrease available extracellular choline for use by non-cholinergic cells in the immediate vicinity of cholinergic axons.

5.2.6 Alternative Explanations for the Regional Differences in CHT Expression – Role of the Specific Microenvironment of Innervated Regions

High rates of ACh synthesis would only be required to rapidly refill synaptic vesicles during, or in the wake of, elevated ACh release. Therefore, the tight coupling of the increase in CHT membrane levels to evoked release of ACh represents an elegant implementation of this specific choline uptake mechanism only when functionally necessary. At resting levels of activity, limited membrane transporters exert little effect on extracellular choline levels. During periods of high ACh release, increased high-affinity choline transport could temporarily act as a "sink" of extracellular choline, particularly if cholinergic terminals are dense in the microenvironment, and/or if many terminals were simultaneously activated. However, the rapid endocytosis of CHT would reduce the impact of high-affinity choline transport once activity in cholinergic neurons returned to basal levels.

The consideration of the extracellular environment with respect to choline concentrations raises an interesting possibility that the unique neurochemical architecture of the anterior thalamus might contribute to the higher CHT expression in that region. The cholinergic innervation of the AVN is extremely dense relative to most other thalamic nuclei, and appears to consist of highly ramified axonal arborizations (Woolf & Butcher 1986; Woolf 1991). These structural characteristics suggest that high-affinity choline uptake is likely to be increased in many cholinergic varicosities as a result of the activation of a single cholinergic afferent to the AVN. Furthermore, the distinctive pattern of cholinesterase staining in the anterior thalamic nuclei (including the anterodorsal and anteromedial nuclei) suggests that extracellular choline may be relatively scarce within portions of the AVN (see Figure 16).

As discussed in Chapter 3, the particular elements of the local environment could theoretically influence both the expression and membrane trafficking of CHT. Although the mechanisms that could signal the need for greater CHT expression to the cell body have yet to be identified, both CHT and VAChT mRNA are upregulated by exposure to nerve growth factor (NGF) (Berse et al 2005), indicating that retrograde signaling from axon terminals can influence the expression of these proteins. This regulation appears to depend on intracellular Akt signaling (Madziar et al 2008). The NGF pathway is not likely to operate in the projections that we studied, as the brainstem tegmental ACh neurons do not express receptors for this growth factor (Heckers et al 1992), nor does the AVN or the VTA display immunoreactivity for this receptor (Yan & Johnson Jr. 1989). However, the existence of this regulatory mechanism serves as a proof-of-principle that receptor mediated events occurring at the axon terminal can influence transcriptional processes within the cell body. Undoubtedly, there are other intracellular pathways that could link the relative demand for ACh synthesis to the expression of necessary cholinergic proteins in PPT/LDT cells.

5.2.7 Little Evidence that CHT is Differentially Regulated in Regions with Choline Sensitive nAChRs

Although we had speculated that CHT might be differentially regulated in areas with functionally significant expression of choline-sensitive α7 nAChRs (i.e. VTA compared to AVN), we found little evidence to specifically support this claim. The finding of a significant interaction of brain region and total immunogold density on the density of membrane gold in the same terminals (Chapter 2) could be interpreted as evidence that the specific microenvironment

of an innervated brain region can exert modulatory influence over CHT trafficking; however, a more conservative explanation for this finding lies in the segregation of afferents to these brain regions to separate sets of cholinergic brainstem tegmental neurons. It is possible that our population comparison could not adequately capture differences in the localization of CHT that might indicate a role for the transporter in regulating the excitability of this receptor. Within both the AVN and VTA populations we saw a range of patterns to the immunogold-silver staining, with between 0 - 100% of gold particles being associated with the plasma membrane (See Appendix A, Figure 24). If the relative membrane expression of CHT plays any regulatory role in restricting or facilitating α7 nAChR availability through the regulation of extracellular choline levels in the vicinity of these receptors, this might affect the distribution of CHT immunoreactivity in only a few axonal profiles at any one time, and would be further obscured by the reduced activity in the PPT/LDT neurons resulting from anesthesia. Such hypothesized profiles would be unlikely to significantly skew the regional population statistics that we examined in Chapter 2. In the absence of any additional information linking CHT function to α7 nAChRs, we must conclude that the expression and regulation of CHT is directed solely toward maintaining adequate supplies of vesicular ACh.

However, α7 nAChRs are not particularly dense in the VTA (Whiteaker et al 1999; Tribollet et al 2004), so the relative weakness of any effect that their presence may have on CHT regulation in PPT/LDT axons may have contributed to our difficulty in detecting gross differences in the distribution of CHT. Comparison of cholinergic terminals in the AVN to a region with a heavier reliance on this mode of signaling might be more fruitful in determining if CHT function is altered in regions with choline-sensitive nicotinic receptors. The thalamic parafascicular nucleus (PF) receives a heavy cholinergic innervation from the PPT/LDT (Levey

et al 1987; Cornwall et al 1990; Bolton et al 1993) and shows a high concentration of α7 nAChRs (Whiteaker et al 1999; Tribollet et al 2004). Examination of this region might reveal a difference in the membrane versus cytoplasmic distribution of CHT. Additionally, the more similar density of cholinergic innervation between the AVN and the PF would eliminate the fluorescence imaging problems that necessitated the use of different capture settings in Chapter 3. Although we applied a correction to our data to facilitate the comparison of CHT and VAChT immunofluorescence, the ability to directly compare fluorescence intensity values across regions would strengthen any conclusions arising from comparison of two different brain regions.

5.3 SURPRISING SPECIFICITY IN THE COLLATERALIZED LIMBIC PROJECTIONS OF CHOLINERGIC BRAINSTEM TEGMENTAL NEURONS

Using dual retrograde tract-tracing from the AVN and the VTA, combined with immunohistochemistry for VAChT, we confirmed that the afferents to these limbic regions come from largely separate groups of ACh neurons in the PPT and LDT. This finding confirmed our supposition that the morphological differences between the AVN and VTA populations of axon terminals, as well as differences in CHT immunoreactivity, are most easily explained by the existence of segregated projections to these brain regions. However, the inclusion of a control case in which retrograde tracers were deposited in the midline/intralaminar paratenial nucleus revealed a sharp contrast of a highly collateralized ascending cholinergic input to the thalamus and the VTA. Moreover, the collateralization observed in this case is consistent with similar findings from other laboratories (Woolf & Butcher 1986; Bolton et al 1993). Importantly,

collateralization of ACh inputs to the thalamus and VTA has previously only been investigated specifically for the midline and intralaminar groups which are functionally related to the VTA. Our novel description of a contrasting lack of collateralization between functionally dissimilar limbic regions indicates that the projections of the PPT/LDT are more highly organized than has been previously appreciated.

5.3.1 Functional Organization of the Ascending Tegmental Cholinergic System

Anterograde tract-tracing studies that examined the ascending projections from these tegmental brainstem nuclei emphasized the diverse subcortical targets of PPT/LDT axons (Satoh & Fibiger 1986; Woolf & Butcher 1986; Hallanger & Wainer 1988; Cornwall et al 1990). The confirmation of these projections by retrograde tract-tracing suggested that there was some functional organization to the PPT versus LDT, in that retrogradely labeled neurons were more likely to arise from the PPT if the tracer injection was placed in regions that had clear sensory or motor-associated functions, such as the dorsal lateral geniculate nucleus of the thalamus, superior colliculus, and substantia nigra (Gould et al 1989). Conversely, LDT neurons were more likely to innervate limbic structures whose function is more difficult to characterize (Woolf & Butcher 1986). Preferential retrograde labeling of LDT cells was also observed following tract-tracing from the monoamine cell groups in the locus coeruleus, ventral tegmental area, and dorsal raphé nuclei that innervate many limbic forebrain structures as well (Woolf & Butcher 1989).

These anatomical observations have led to the appreciation of a functional topographic organization in the brainstem PPT/LDT; still, cholinergic neurons in these nuclei are still generally treated as homogenous and interchangeable units in the ascending cholinergic

brainstem system. This follows from the similar physiological phenotypes of these cells demonstrated in electrophysiological recordings from unanesthetized animals (Steriade et al 1990a; Datta & Siwek 2002). Although most PPT and LDT cholinergic neurons are believed to share similar biophysical characteristics (Kang et al 1990; Leonard & Llinás 1990) and firing patterns (Steriade et al 1990a; Grant & Highfield 1991; Steriade et al 1997), these cells do show some variability in sensory responsiveness (Grant & Highfield 1991; Pan & Hyland 2005). Furthermore, reciprocal connections between the PPT/LDT neurons and their forebrain and midbrain targets indicate that the functional topography that exists in the ascending PPT/LDT projections is paralleled by a functional organization of afferent input the brainstem tegmental nuclei (Satoh & Fibiger 1986; Woolf & Butcher 1986; Cornwall et al 1990; Woolf 1991). The functional organization of PPT/LDT cholinergic neurons into separate sub-groups is further supported by studies on the discriminable behavioral effects of lesions or pharmacological manipulations of specific regions of the PPT (Winn 1998; Ainge et al 2004; Kayalioglu & Balkan 2004; Alderson et al 2008). Although less is known about the intrinsic behavioral relevance of the LDT, it has a clearly demonstrated role in the process of addiction (Laviolette et al 2000; Forster et al 2002; Schmidt et al 2009), and its preferential innervation of limbic regions suggests a general role for this brainstem nucleus in higher cognitive functions.

However, the idea that PPT and LDT cholinergic neurons form sub-groups of functionally related modulatory cells has been contradicted by the extensive collateralization of their axons. Following several studies that examined colocalization of two or more retrograde tracers, transported from different brain regions, many concluded that the projections of these neurons were diffusely spread throughout thalamic and subcortical regions (Wainer & Mesulam 1990; Bolton et al 1993). This property of divergent projections to widespread structures from

through the bifurcation of a single axon has been compared to similarly diffuse projections arising from the monoaminergic NE and 5-HT cells in the brainstem (Mesulam et al 1983; Mesulam 1995a; Mesulam 1995b). Furthermore, collateralization of axons is a characteristic property of many neurons found in the reticular formation, an anatomical structure that includes both the PPT and LDT, but encompasses large portions of the brainstem in which neurons are organized without clear nuclear boundaries (reviewed in Jones, 1995).

The contrasting results of our retrograde tract-tracing from the AVN and the anterior medial/intralaminar thalamus help to resolve these conflicting views of the anatomical specificity of PPT/LDT cholinergic neurons. In light of this finding, it was fortuitous that we initially chose to examine CHT immunoreactivity in the AVN rather than a thalamic nucleus with a clearer functional relationship to limbic dopamine projections. All previous studies that suggested heavy collateralization of the ascending PPT or LDT projections have examined related targets of brainstem tegmental ACh (e.g. visual thalamus and superior colliculus (Billet et al 1999), midline/intralaminar thalamic and VTA (Bolton et al 1993)).

As previously discussed (see General Introduction and Discussion, Chapter 4), there is significant topographical organization to limbic forebrain regions that supports the existence of separate functional circuitry within the umbrella concept of the limbic system (Domesick 1969; Krettek & Price 1977; Berendse & Groenewegen 1991; Bentivoglio et al 1993; Giménez-Amaya et al 1995; Gabbott et al 2005; Morgane et al 2005). As delineated by the thalamic components of these functional systems, it is clear that at least two such circuits exist and are relatively isolated from each other. The AVN has prominent connections with cortical regions that subserve spatial learning and memory, and may play a role in conditioned aversion learning as well (Gabriel et al 1980; Sparenborg & Gabriel 1992; Michel et al 2006). These functions

appear more closely related to the association of behaviorally relevant events with a specific location in space, rather than a specific action on the part of the animal (Gibb et al 2006). In contrast, the midline/intralaminar nuclei in the thalamus innervate distinctly different parts of the cerebral cortex and striatum that have well-defined roles in guiding appetitively motivated behavior, particularly in selecting an appropriate action based on environmental cues (Groenewegen & Witter 2004). This characterization of the functions of these systems is, of course, a great simplification. However, the specific behavioral deficits observed following lateral anterior thalamic lesions versus medial/intralaminar thalamic lesions supports this view of the distinctive roles mediated by these circuits (Morgane et al 2005; Mitchell & Dalrymple-Alford 2006). Our results indicate that the anatomical segregation of this circuitry extends to the specific ascending cholinergic modulation of these regions.

5.3.2 Significance of Functionally Targeted Collateralized Projections of the PPT/LDT Cholinergic System

The functional significance of collateral ACh projections from the PPT/LDT has not, to our knowledge, been determined. The general function of ascending cholinergic modulation from the brainstem tegmental ACh system is to promote the excitability of innervated principal neurons (Paré et al 1990; Wainer & Mesulam 1990; Steriade et al 1997); hence coordinated input would presumably increase activity at several different sites within a specific limbic circuit. However, more specific predictions of the integrated effects of coordinated modulatory ACh input to multiple components of the same forebrain circuitry are currently elusive.

Furthermore, the co-transmission of ACh and neuropeptides invites the supposition that collateralization of cholinergic axons to distinct brain regions may represent distinct neurochemical projection systems, and that peptidergic co-expression might be used as a way to identify PPT/LDT ACh neurons which project to specific forebrain and midbrain targets, but further work delineating peptide phenotype and anatomical connections of brainstem cholinergic neurons is needed.

Finally, future investigations might reveal collateral projections of cholinergic afferents to the AVN that target other, functionally related subcortical regions. Interestingly, anterograde labeling from the LDT indicates a substantial projection to the lateral septum (Satoh & Fibiger 1986), a region that is functionally related to the AVN through its similar anatomical connections. If cholinergic neurons in the PPT and LDT possess a general property of collateralized projections to functionally related targets, then dual tract-tracing from the AVN and the septum would be expected to result in labeling from both regions in the same neurons. Conversely, if AVN- projecting tegmental cholinergic neurons do not innervate other related structures, then the heavy collateralization of PPT and LDT projections to medial thalamic nuclei and the midbrain VTA described here and elsewhere (Woolf & Butcher 1986; Bolton et al 1993) may be relatively specific to this limbic circuitry. Interestingly, collateralization of other inputs to midline/intralaminar thalamic nuclei has been demonstrated (Cornwall & Phillipson 1988b; Cornwall & Phillipson 1989), and thalamic neurons in these regions also have branched projections (Otake & Nakamura 1998) suggesting that medial limbic circuitry might be characterized by extensive co-ordination of inputs. Further experimentation is needed to fully understand the anatomical characteristics of these systems, and to appreciate the functional consequences of these collateralized projections.

APPENDIX A

ULTRASTRUCTURAL LOCALIZATION OF CHT IMMUNOGOLD-SILVER LABELING IN AVN & VTA: RATIO OF MEMBRANE TO CYTOPLASMIC GOLD PARTICLES IN CHT IMMUNOREACTIVE AXON VARICOSITIES

The following figures were not included in the published manuscript presented in Chapter 2, but were generated from the same dataset used for that publication (Table 1, Data Set #3). However, this analysis included an additional 20 terminals (3 from AVN and 17 from VTA) that were later discarded due to low total gold labeling relative to background. The estimation and regional comparison of the proportional membrane gold immunolabeling were presented at the 2008 Society for Neuroscience Annual Meeting in poster form (Holmstrand et al 2008), and are shown here with minimal changes.

A.1.1 Materials and Methods

Details of the immunohistochemical procedures and classification of gold particles can be found in the Methods section in Chapter 2. The proportional membrane gold labeling was calculated by dividing the total number of membrane gold particles by total number of gold

particles for each profile. Mean proportions for each region were calculated by averaging this proportion over all profiles within each region. The regional means were compared using a mixed model ANCOVA with fixed effects of region and profile area. Statistical significance was assessed at the $p = 0.05$ level.

A.1.2 Results

The mean proportion of CHT immunogold particles associated with the plasma membrane of all CHT-*ir* profiles in the VTA (0.19) was apparently lower than the mean proportion observed over all CHT-*ir* AVN profiles (0.25, Figure 24A). The lower mean of the VTA population probably resulted from the fact that more VTA profiles showed membrane/total gold ratios in the low range of this value (Figure 24B). In both regions, we saw profiles with a membrane/total gold ratio ranging from 0 (i.e. no membrane-associated CHT), to 1 (i.e. all CHT immunogold particles were < 20 nm from the plasma membrane). However, when we examined the effect of brain region on this proportion while accounting for variability due to repeated sampling from the same tissue sections and animals, the difference in this mean proportion of membrane/total gold was not statistically significant.

A.1.3 Conclusion

Consistent with previous estimates of the subcellular distribution of CHT in other cholinergic neurons, the proportion of membrane/total gold labeling was stable across different regional populations of CHT immunoreactive axon profiles arising from the PPT/LDT cholinergic neurons. The distribution of CHT to membrane versus cytoplasmic cellular

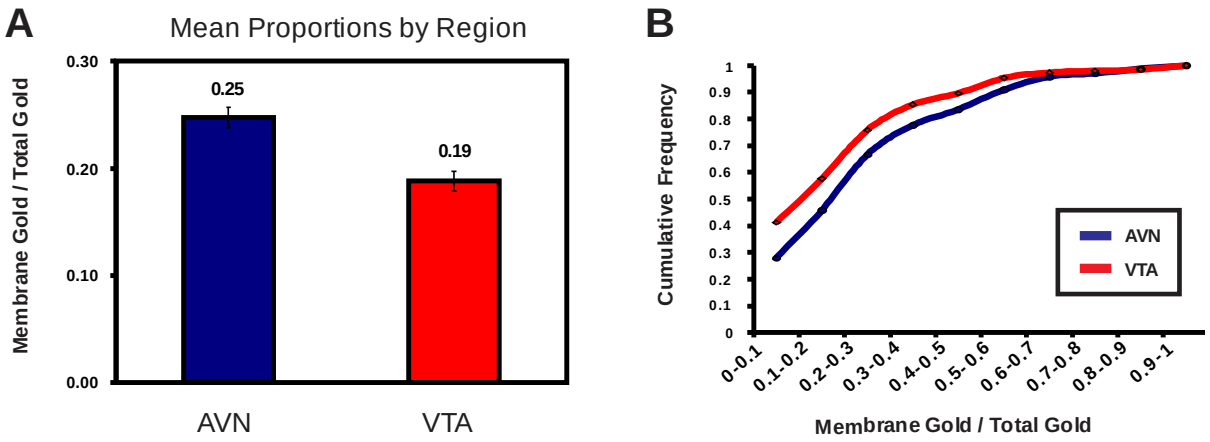

Figure 24 Proportional membrane gold labeling of CHT-*ir* axon varicosities in the AVN and VTA

A Mean values obtained for the proportion of CHT immunogold particles observed within 20 nm of the plasma membrane (# membrane gold particles / # total gold particles). Although the mean for the AVN terminals was apparently higher than that observed in the VTA population, we observed some variability in this relationship across animals. A mixed model ANCOVA was therefore used to analyze the fixed effects of region and profile area on this proportion. The analysis revealed that the effect of region was not significant ($F_{(1, 1064)} = 1.89$; $p = 0.1699$). **B** Cumulative frequency of values observed for the ratio of membrane gold particles / total gold particles in AVN and VTA populations of CHT-*ir* axon varicosities. Although the regional distributions of this ratio were similarly shaped, more VTA varicosities appeared to have low ratios of membrane/total gold labeling for CHT, resulting in the lower (though not statistically significant) apparent mean shown in **A.**

compartments probably reflects the balance of exocytic and endocytic processes. Therefore, the present findings indicate that the equilibrium of these two processes is the same across cholinergic axons innervating the AVN versus the VTA. The stability of this ratio may represent well-conserved cellular processes that control the recycling of CHT under resting conditions. However, the redistribution of CHT to the membrane (e.g. due to prolonged excitation of the parent neurons) may yet reveal regional differences in the functional regulation of high-affinity choline uptake.

APPENDIX B

DUAL IMMUNOFLUORESCENCE FOR CHT AND VAChT: SUPPLEMENTARY TECHNICAL DATA AND ADDITIONAL STATISTICAL ANALYSIS

In the dual immunofluorescence investigation of CHT and VAChT described in Chapter 3 , the higher density of cholinergic terminals in the AVN compared to the VTA resulted in binding of more fluorescent-conjugated secondary antibodies. This concentration of fluorophores resulted in detection of dramatically higher overall fluorescence levels, since each fluorophore theoretically emits a similar number of photons that reach the detector. The non-equivalence of the 488- and 568-fluorescence intensities from the AVN and VTA stacks required the use of different capture settings to avoid unnecessarily low signal to noise ratios in the VTA images, or saturation of the detection system in images captured from the AVN. We used the live-imaging fluorescence intensity histogram to adjust these settings, and aimed to equalize the range of intensity values seen in AVN and VTA image stacks. For the 488 channel, both exposure and gain settings were increased for VTA imaging (exposure = 2500 ms; gain = 50) relative to the settings used for AVN imaging (exposure = 1700 ms; gain = 0). For the 568 channel, only exposure was varied (AVN: exposure = 1500 ms; VTA: exposure = 2300 ms).

In order to compare the quantitative fluorescence intensity data between regions, a correction was applied to the AVN dataset for each channel, based on the fluorescence intensities obtained from imaging

B.1.1 Effects of Varying Exposure Time and Gain on Fluorescence Intensity of Standard Fluorescent Beads

Fluorescent polystyrene calibration beads (InSpeck 0.3% Intensity beads: Green – ex: 505 nm and em: 515 nm; Orange – ex: 540 nm and em: 560 nm; Invitrogen, Carlsbad, CA) were mounted on glass slides, air dried, and coverslipped with Fluoromount-G (Southern Biotech, Birmingham, AL). The beads were then imaged on the same spinning disk confocal system that was used for the dual-immunofluorescence study detailed in Chapter 3.

A range of exposures (1000 – 2500 ms) and gain settings (0 – 50) were used to collect Z-stack images through the entirety of the green beads. Orange beads were imaged in a similar manner, but only the exposure time was varied (1000 – 2300 ms).

Image stacks were corrected photobleaching and deconvolved as in Chapter 3. The mode FI value of the deconvolved image stack was subtracted from the single channel image. The same threshold segmentation approach that was used to identify immunofluorescent puncta in brain tissue was applied to the bead image stacks (threshold value = 2x mode, threshold applied to background subtracted image). The mean FI of each object identified by this threshold masking was exported to Microsoft Excel.

a. Calculation of Exposure and Gain Corrections

Mean 488 nm FI of the calibration beads was plotted against exposure and gain, as shown in Figure 25 A&B. Mean FI was regressed against exposure time and gain using PASW (v18, SPSS, Chicago, IL). The regression was linear and did not include an intercept term. The regression coefficients for exposure and gain (Figure 25C) were used to increase the mean 488-CHT FI of AVN objects to compensate for the higher exposure time (+800 ms) and higher gain (+50) used to image VTA objects.

Similarly, mean 568 nm fluorescence intensities of the orange calibration beads were plotted (Figure 26A) and regressed linearly against exposure times of the calibration data. The resulting linear equation (Figure 26B) was used to transform the mean 568-VAChT FI of AVN objects to compensate for the higher exposure time (+800 ms) used to image the VTA.

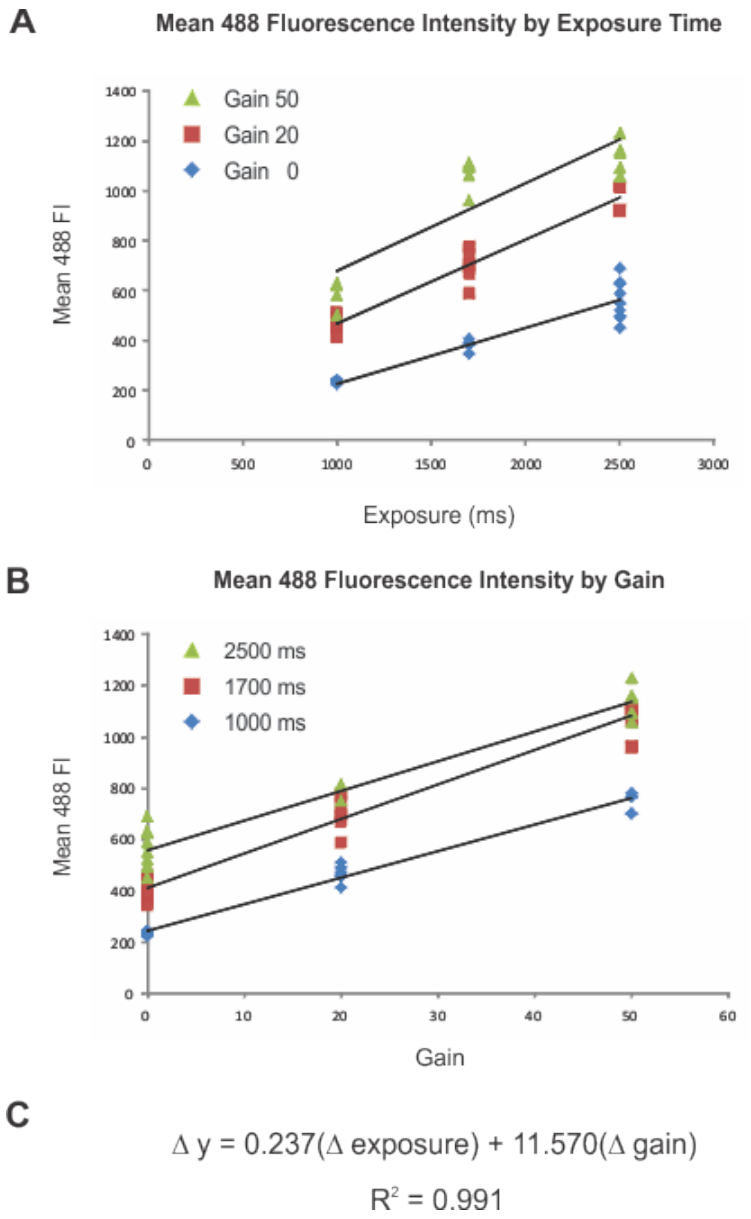

Figure 25 Mean 488 Fluorescence Intensity Calibration Values

Mean fluorescence intensity of green calibration beads plotted against the corresponding (**A**) exposure time or (**B**) gain. Effect of the second variable is shown by series. Lines are shown to for illustrative purposes only. **C** Calibration fluorescence intensity data was regressed simultaneously against exposure and gain. The resulting equation and coefficient of determination (R^2) are shown.

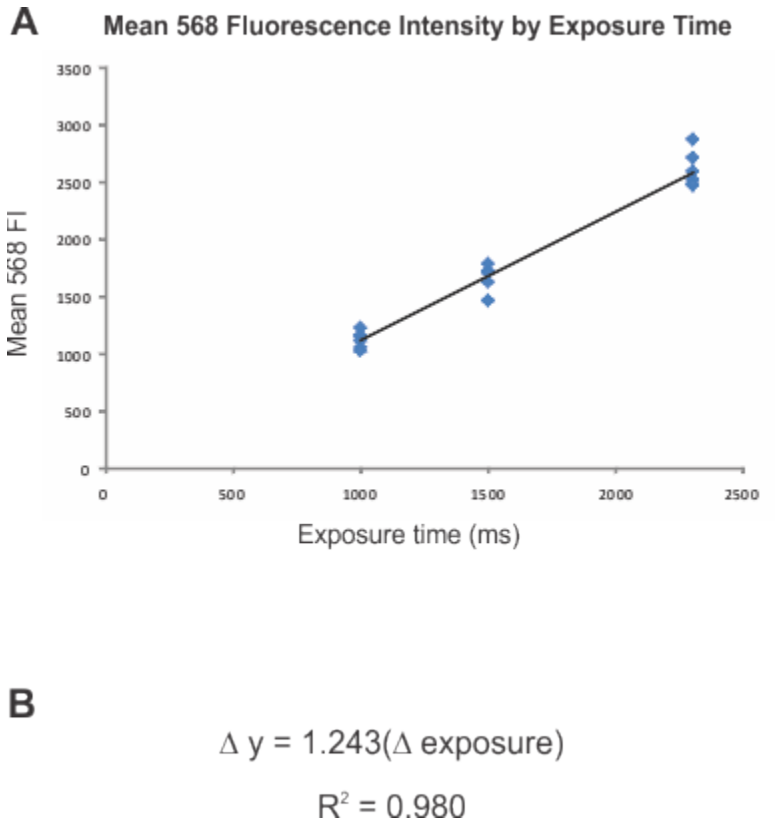

Figure 26 Mean 568 nm Fluorescence Intensity Calibration Values

A Mean fluorescence intensity of orange calibration beads plotted against exposure time. **B** The resulting linear equation used to transform AVN 568-VAChT FI data and coefficient of variation of the regression line.

B.1.2 Revised Statistical Analysis of Dual Immunofluorescence for VAChT and CHT in the AVN and VTA

After consulting with Dr. Alan Sampson, Ph.D., and Josephine Asafu-Adjei in the Department of Statistics at the University of Pittsburgh, some changes were made to the statistical analyses applied to these data. The amended procedures and resulting conclusions are detailed below.

a. Statistical Analysis

Methods of data collection and image analysis remained unchanged from the procedures detailed in Chapter 3. To compare colocalization frequencies observed between the AVN and VTA populations, the percentage of AVN and VTA immunofluorescent puncta that met colocalization criteria were first calculated for each tissue section, these section-specific percentages were then averaged for each animal. The animal specific averages were then transformed by applying the arcsin(sqrt(x)) function. The difference between the arcsin(sqrt(%colocalized)) for the AVN minus the VTA estimates within each rat was calculated, and the distribution of the differences was examined across all rats. These differences were assumed to be normally distributed, as determined by Kolmogorov-Smirnov testing (for VAChT-*ir* objects, $p = 0.200$; for CHT-*ir* objects, $p = 0.160$). The significance of regional differences in the rate of colocalization observed in VAChT-*ir* puncta and CHT-*ir* puncta was determined using a one-sample t-test and significance level of $p \leq 0.05$.

The linear mixed models used to test for regional differences in the fluorescence intensities of VAChT or CHT immunoreactivity outlined in Chapter 3 were deemed appropriate for this study and remain unchanged from their presentation within that chapter.

For comparison of the relative amounts of VAChT and CHT immunoreactivity within each puncta were amended under advisement from Dr. Sampson. Rather than use the ratio of the log mean FIs, the test statistic was changed to the difference of these log values (i.e. [log(mean 2nd marker)] – [log(mean 1st marker)]. The structure of the linear mixed model was not changed, and the random effects of animal and tissue section within animal were retained. Furthermore, although a different permutation of the data was used for the dependent variable, the revised analysis did not change the conclusions presented in Chapter 3.

b. Results

i. Regional comparison of the frequency of colocalization observed for VAChT-ir and CHT-ir immunofluorescent puncta

We recalculated the percentage of immunofluorescent objects that showed colocalization of the second immunofluorescent marker for each animal, resulting in slightly different estimates of this measure for each animal (Table 7). These estimates were different from those initially reported in Chapter 3 because we first estimated the percentages in each tissue sections, then averaged the section-specific estimates for each animal.

Table 7 Percentages of VAChT-*ir* and CHT-*ir* objects that colocalize immunoreactivity for both proteins

A. VAChT-*ir* Objects

Animal	AVN	VTA
1	62%	66%
2	70%	56%
3	77%	67%
4	71%	48%
5	86%	61%

B. CHT-*ir* Objects

Animal	AVN	VTA
1	77%	73%
2	71%	43%
3	75%	45%
4	82%	57%
5	75%	59%

For formal statistical testing, the revised mean colocalization estimates for each animal were transformed by computing the arcsine of the square root of each estimate. For each animal, these transformed values were compared across region by subtracting the value obtained for the VTA population from that obtained for the AVN population. The resulting differences were tested against the null hypothesis that the true difference between the populations was equal to zero, using a Student's one sample *t*-test. For the VAChT-*ir* objects, the null hypothesis was not rejected. The estimated difference of the arcsin(sqrt) values was 0.1486 $\pm$ 0.1272 (mean $\pm$ SD), which corresponds to a difference of less than 0.0007% in the rate of colocalization ($t_{(4)} = 2.613$, $p = 0.059$). This result stood in contrast to the significant difference in colocalization observed between the AVN and VTA populations when the odds ratio was used to construct confidence intervals, as presented in Chapter 3. However, the estimate of the odds ratio did not take into account relatedness of data from the same sections and hence may have underestimated the true variability in the dataset. Given this limitation, and under advisement of the consulting statisticians, we believe that the analysis presented here more accurately captures the true relationship between colocalization of VAChT-*ir* objects in the AVN and VTA. Therefore, we conclude that VAChT-*ir* puncta are just as likely to display colocalization in the AVN as in the VTA.

For CHT-*ir* objects, the same analysis was performed. In this case, one sample *t*-test on the difference in arcsine(sqrt(%colocalized) between the AVN and VTA revealed a significant difference in the percentage of CHT-*ir* puncta between regions ($t_{(4)} = 4.586$, $p = 0.010$). The estimated difference (AVN-VTA) was 0.2225 $\pm$ 0.1085 (mean $\pm$ SD), which corresponds to a difference in percentages of 0.015%. Although statistically significant, the small size of this estimated difference emphasizes that CHT-*ir* objects in both regions were still similar in their

tendency to colocalize VAChT immunoreactivity. The significant difference that we report here most likely arises from a sub-population of CHT-*ir* puncta that are more prominent in the VTA.

ii. Quantitative regional comparison of VAChT and CHT fluorescence intensity

As noted in the methods of this appendix, the comparisons of fluorescence intensities observed in VAChT- or CHT-*ir* objects across regions was not modified from that originally presented in Chapter 3. However, an additional analysis of the fluorescence intensities of the secondary marker in all puncta was performed that was not initially described in that chapter. The distribution of mean object fluorescence intensity of the second marker is shown in Figure 28. Mixed model analysis was used to compare the mean CHT FI of all VAChT-*ir* objects, while accounting for variability due to repeated sampling from the each tissue section and rat. This analysis revealed that AVN objects had higher mean CHT FI than VTA VAChT-*ir* objects ($F_{(1,\ 47.33)} = 7.468$, $p = 0.009$; estimated difference (AVN-VTA) = 424). Similarly, the mean VAChT FI of CHT-*ir* objects in the AVN was also higher than that observed in VTA puncta ($F_{(1,\ 44.35)} = 42.52$, $p < 0.001$; estimated difference (AVN-VTA) = 1019).

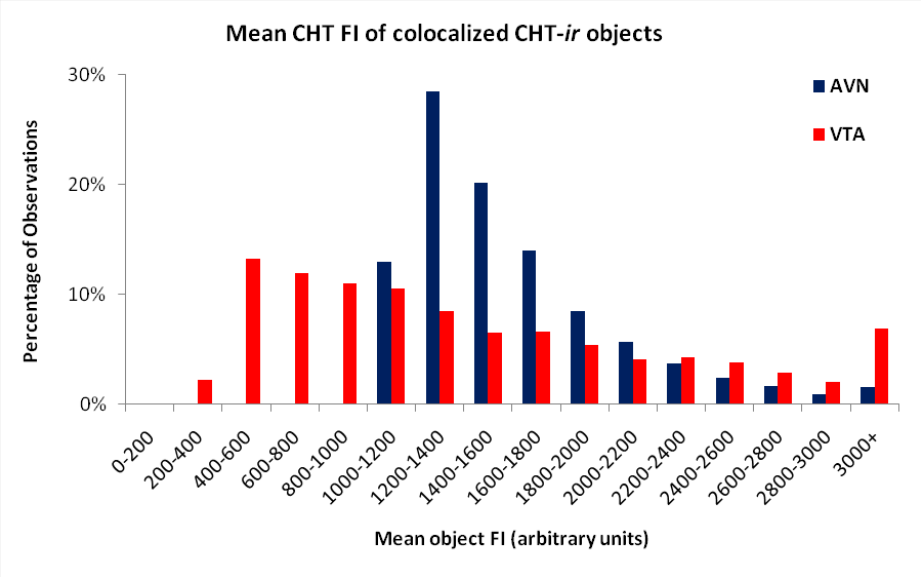

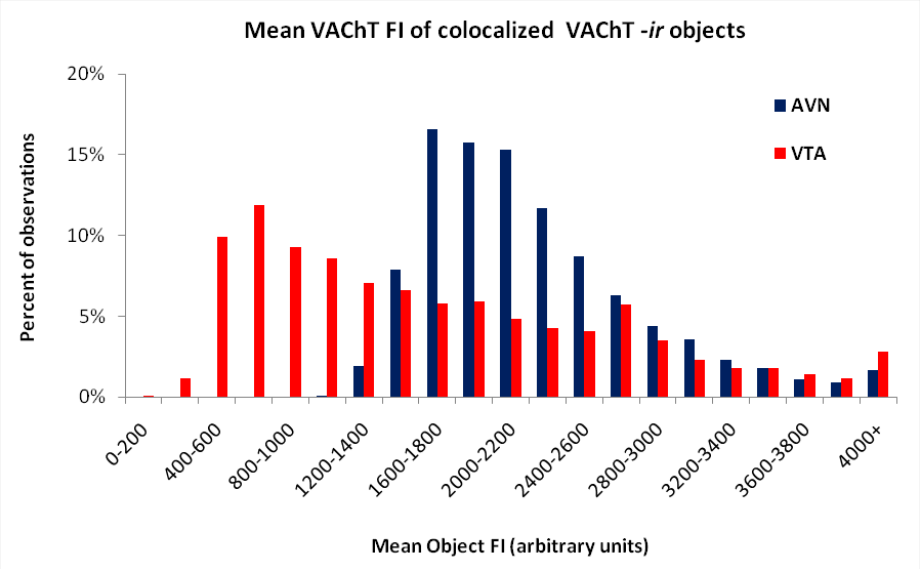

Figure 27 Frequency distributions of mean object fluorescence intensities – primary immunofluorescent marker

Mean CHT FI of CHT-*ir* objects (*top panel*) and mean VAChT FI of VAChT-*ir* objects (*bottom panel*) sampled from the AVN and VTA. Values obtained from the VTA sample had a broader distribution of values, with the lower end of the VTA distribution displaying lower fluorescence intensities than the corresponding distribution of AVN datapoints. However, the VTA distribution extended to similarly high values as that of the AVN.

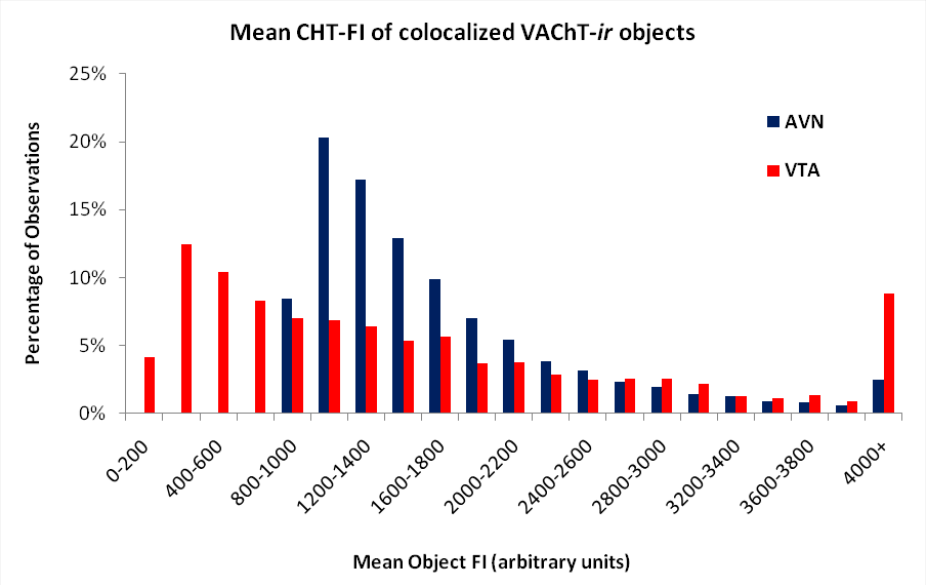

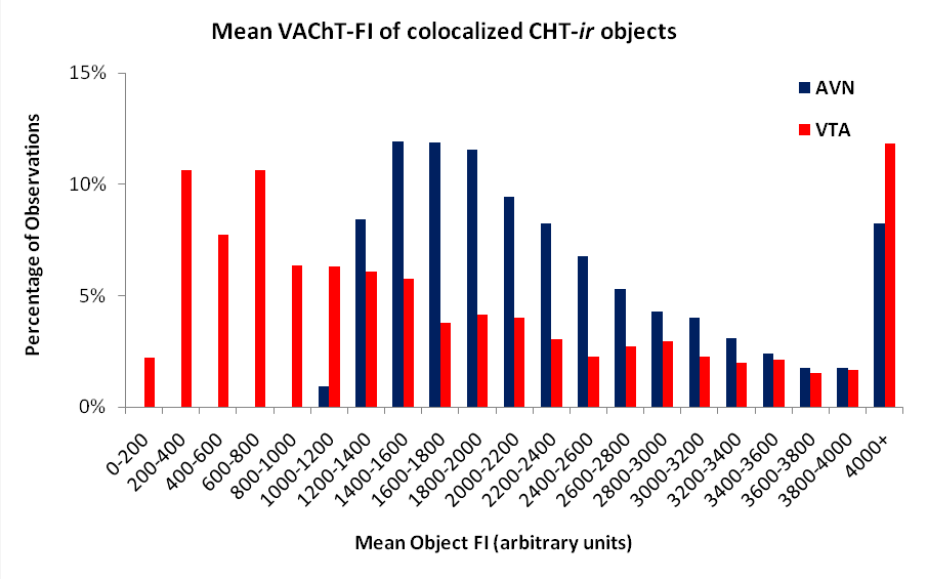

Figure 28 Frequency distributions of mean object fluorescence intensities – secondary immunofluorescent marker

Mean CHT FI of VAChT-*ir* objects (*top panel*) and mean VAChT FI of CHT-*ir* objects (*bottom panel*) sampled from the AVN and VTA. The VTA population displayed a greater range of values, both on the lower end of the range, which was lower for the VTA sample than for the AVN, and at the upper end of the range, where a higher percentage of VTA objects were represented.

iii. Comparison of relative levels of CHT and VAChT fluorescence intensities within colocalized puncta

Within colocalized boutons, the change in statistical analysis from using the ratio of the log mean FIs to using the difference of the log mean FI did not result in any change to our conclusions. For the difference of log mean CHT FI – log mean VAChT FI of colocalized VAChT-*ir* puncta, there was no significant effect of region ($F_{(1,\ 45.09)} = 0.275$, $p = 0.603$). Similarly, in colocalized CHT-*ir* puncta, the difference of log mean VAChT FI – log mean CHT FI was not significantly different across regions ($F_{(1,\ 44.94)} = 2.420$, $p = 0.127$). By either method used to examine the relationship between VAChT FI and CHT FI in individual puncta, there does not appear to be any regional differences in the relative expression of these two proteins.

c. Conclusions

Only one substantive change to the conclusions presented in Chapter 3 has resulted from the alternative statistical analysis of these data. Concerning the colocalization of significant CHT-immunoreactivity (i.e. above-threshold fluorescence for CHT) in objects identified on the basis of VAChT-immunoreactivity, the more precise analysis presented in this appendix indicates that there is no difference in the frequency of colocalization between the brain regions examined. However, colocalization of VAChT- immunoreactivity in CHT-*ir* objects was significantly less common in the VTA population of boutons than in the AVN. The preservation of this difference, even when the section related variability was accounted for, further supports

the notion that the singly labeled CHT-*ir* objects in our sample are real examples of axonal compartments that contain appreciable levels of CHT, but little or no VAChT.

BIBLIOGRAPHY

Aggleton J, Poirer G, Aggleton H, Vann S, Pearce J. 2009. Lesions of the fornix and anterior thalamic nuclei dissociate different aspects of hippocampal-dependent spatial learning: implications for the neural basis of scene learning. *Behavioral Neuroscience* 123:504-19

Aggleton JP, Hunt PR, Nagle S, Neave N. 1996. The effects of selective lesions within the anterior thalamic nuclei on spatial memory in the rat. *Behavioural Brain Research* 81:189-98

Agnati LF, Zoli M, Stromberg I, Fuxe K. 1995. Intercellular communication in the brain: wiring versus volume transmission. *Neuroscience* 69:711-26

Ainge JA, Jenkins TA, Winn P. 2004. Induction of c-fos in specific thalamic nuclei following stimulation of the pedunculopontine tegmental nucleus. *European Journal of Neuroscience* 20:1827-37

Alderson HL, Latimer MP, Winn P. 2008. A functional dissociation of the anterior and posterior pedunculopontine tegmental nucleus: excitotoxic lesions have differential effects on locomotion and the response to nicotine. *Brain Structure and Function* 213:247-53

Alelú-Paz R, Gimenéz-Amaya JM. 2007. Chemical parcellation of the anterior thalamic nuclei in the human brain. *Journal of Neural Transmission* 114:969-81

Alkondon M, Albuquerque EX. 2006. Subtype-specific inhibition of nicotinic acetylcholine receptors by choline: a regulatory pathway. *Journal of Pharmacology and Experimental Therapeutics* 318:268-75

Alkondon M, Pereira EFR, Cortes WS, Maelicke A, Albuquerque EX. 1997. Choline is a selective agonist of $\alpha 7$ nicotinic acetylcholine receptors in the rat brain neurons. *European Journal of Neuroscience* 9:2734-42

Amadeo A, Arcelli P, Spreafico R, De Biasi S. 1995. Ultrastructural immunolocalization of muscarinic actylcholine receptor in the dorsal thalamus of rat. *Neuroscience Letters* 184:161-4

Angelucci A, Clascá F, Sur M. 1996. Anterograde axonal tracing with the subunit B of cholera toxin: a highly sensitive immunohistochemical protocol for revealing fine axonal morphology in adult and neonatal brains. *Journal of Neuroscience Methods* 65

Antonelli T, Beani L, Bianchi C, Pedata F, Pepeu G. 1981. Changes in synaptosomal high affinity choline uptake following electrical stimulation of guinea-pig cortical slices: effect of atropine and physostigmine. *British Journal of Pharmacology* 74:525-31

Apparsundaram S, Ferguson S, George AJ, Blakely R. 2000. Molecular cloning of a human, hemicholinium-3 sensitive choline transporter. *Biochemical & Biophysical Research Communications* 276:862-7

Apparsundaram S, Martinez V, Parikh V, Kozak R, Sarter M. 2005. Increased capacity and density of choline transporters situated in synaptic membranes of the right medial prefrontal cortex of attentional task-performing rats. *Journal of Neuroscience* 25:3851-6

Argyropoulos SV, Wilson SJ. 2005. Sleep disturbances in depression and the effects of antidepressants. *International Review of Psychiatry* 17:237-45

Arvidsson U, Riedl M, Elde R, Meister B. 1997. Vesicular acetylcholine transporter (VAChT) protein: a novel and unique marker for cholinergic neurons in the central and peripheral nervous systems. *Journal of Comparative Neurology* 378:454-67

Bales KR, Tzavara ET, Wu S, Wade MR, Bymaster FB, Paul SM, Nomikos GG. 2006. Cholinergic dysfunction in a mouse model of Alzheimer disease is reversed by an anti-A beta antibody. *Journal of Clinical Investigation* 116:825-32

Bamford NS, Robinson S, Palmiter RD, Joyce JA, Moore C, Meshul CK. 2004a. Dopamine modulates release from corticostriatal terminals. *Journal of Neuroscience* 24:9541-52

Bamford NS, Zhang H, Schmitz Y, Wu NP, Cepeda C, Levine MS, Schmauss C, Zakharenko SS, Zablow L, Sulzer D. 2004b. Heterosynaptic dopamine neurotransmission selects sets of corticostriatal terminals. *Neuron* 42:653-63

Barbas H, Henion TH, Dermon CR. 1991. Diverse thalamic projections to the prefrontal cortex in the rhesus monkey. *Journal of Comparative Neurology* 313:65-94

Baude A, Nusser Z, Molnar E, McIlhinney RA, Somogyi P. 1995. High-resolution immunogold localization of AMPA type glutamate receptor subunits at synaptic and non-synaptic sites in rat hippocampus. *Neuroscience* 69:1031-55

Bazalakova MH, Wright J, Schneble EJ, McDonald MP, Heilman CJ, Levey AI, Blakely RD. 2007. Deficits in acetylcholine homeostasis, receptors and behaviors in choline transporter heterozygous mice. *Genes, Brain and Behavior* 6:411-24

Beaudet A, Sotelo C. 1981. Synaptic remodeling of serotonin axon terminals in rat agranular cerebellum. *Brain Research* 206:305-29

Beckstead RM. 1976. Convergent thalamic and mesencephalic projections to the anterior medial cortex in the rat. *Journal of Comparative Neurology* 166:403-16

Beckstead RM, Domesick VB, Nauta WJ. 1979. Efferent connections of the substantia nigra and ventral tegmental area in the rat. *Brain Research* 175:191-217

Beninato M, Spencer RF. 1987. A cholinergic projection to the rat substantia nigra from the pedunculopontine nucleus. *Brain Research* 412:169-74

Bentivoglio M, Kultas-Ilinsky K, Ilinsky I. 1993. Limbic thalamus: structure, intrinsic organization, and connections. In *Neurobiology of Cingulate Cortex and Limbic Thalamus*, ed. BA Vogt, M Gabriel, pp. 71-122. Boston: Birkhauser

Berendse H, Groenewegen H. 1990. Organization of the thalamostriatal projections in the rat, with special emphasis on the ventral striatum. *Journal of Comparative Neurology* 299:187-228

Berendse H, Groenewegen H. 1991. Restricted cortical termination fields of the midline and intralaminar thalamic nuclei. *Neuroscience* 42:73-102

Berger B, Gaspar P, Verney C. 1991. Dopaminergic innervation of the cerebral cortex: unexpected differences between rodents and primates. *Trends in Neurosciences* 14:21-7

Berger B, Verney C, Alvarez C, Vigny A, Helle K. 1985. New dopaminergic terminal fields in the motor, visual (Area 18b) and retrosplenial cortex in the young and adult rat. Immunocytochemical and catecholamine histochemical analyses. *Neuroscience* 15:983-98

Bernard V, Somogyi P, Bolam J. 1997. Cellular, subcellular, and subsynaptic distribution of AMPA-type glutamate receptor subunits in the neostriatum of the rat. *Journal of Neuroscience* 17:819-33

Berse B, Szczecinska W, Lopez-Coviella I, Madziar B, Zemelko V, Kaminski R, Kozar K, Lisp KS, Pfeil U, Blusztajn JK. 2005. Expression of high affinity choline transporter during mouse development in vivo and its upregulation by NGF and BMP-4 in vitro. *Brain Research. Developmental Brain Research* 157:132-40

Billet S, Cant NB, Hall WC. 1999. Cholinergic projections to the visual thalamus and superior colliculus. *Brain Research* 847:121-3

Bina K, Rusak B, Semba K. 1993. Localization of cholinergic neurons in the forebrain and brainstem that project to the suprachiasmatic nucleus of the hypothalamus in rat. *Journal of Comparative Neurology* 335:295-307

Bissette G, Seidler F, Nemeroff C, Slotkin T. 1996. High affinity choline transporter status in Alzheimer's disease tissue from rapid autopsy. *Annals of the New York Academy of Sciences* 777:197-204

Bjelke B, England R, Nicholson C, Rice ME, Lindberg J, Zoli M, Agnati LF, Fuxe K. 1995. Long distance pathways of diffusion for dextran along fibre bundles in brain. Relevance for volume transmission. *Neuroreport* 6:1005-9

Bolton RF, Cornwall J, Phillipson OT. 1993. Collateral axons of cholinergic pontine neurones projecting to midline, mediodorsal and parafascicular thalamic nuclei in the rat. *Journal of Chemical Neuroanatomy* 6:101-14

Boucetta S, Jones BE. 2009. Activity profiles of cholinergic and intermingled GABAergic and putative glutamatergic neurons in the pontomesencephalic tegmentum of urethane-anesthetized rats. *Journal of Neuroscience* 29:4664-74

Brandon E, Mellott T, Pizzo D, Coufal N, D'Amour K, Gobeske K, Lortie M, Lopez-Coviella I, Berse B, Thal L, Gage F, Blusztajn J. 2004. Choline transporter 1 maintains cholinergic function in choline acetyltransferase haploinsufficiency. *Journal of Neuroscience* 24:5459-66

Breer H, Knipper M. 1990. Regulation of high affinity choline uptake. *Journal of Neurobiology* 21:269-75

Brock M, Nickel A-C, Madziar B, Blusztajn JK, Berse B. 2007. Differential regulation of the high affinity choline transporter and the cholinergic locus by cAMP signaling pathways. *Brain Research* 1145:1-10

Brodin L, Löw P, Gad H, Gustafsson J, Pieribone VA, Shupliakov O. 1997. Sustained neurotransmitter release: new molecular clues. *European Journal of Neuroscience* 9:2503-11

Chen S, Aston-Jones G. 1995. Evidence that cholera toxin B subunit (CTb) can be avidly taken up and transported by fibers of passage. *Brain Research* 674:107-11

Chilton M, Mastropaolo J, Rosse RB, Bellack AS, Deutsch SI. 2004. Behavioral consequences of methyllycaconitine in mice: a model of α7 nicotinic acetylcholine receptor deficiency. *Life Sciences* 74:3133-9

Clarke PBS, Hommer DW, Pert A, Skirboll LR. 1987. Innervation of substantia nigra neurons by cholinergic afferents from pedunculopontine nucleus in the rat: neuroanatomical and electrophysiological evidence. *Neuroscience* 23:1011-9

Clements JR, Grant S. 1990. Glutamate-like immunoreactivity in neurons of the laterodorsal tegmental and pedunculopontine nuclei in the rat. *Neuroscience Letters* 120:70-3

Cooper DC. 2002. The significance of action potential bursting in the brain reward circuit. *Neurochemistry International* 41:333-40

Cooper JR, Bloom FE, Roth RH. 2003. Acetylcholine. In *The Biochemical Basis of Neuropharmacology*, ed. JR Cooper, FE Bloom, RH Roth, pp. 151-78. New York: Oxford University Press

Cornwall J, Cooper JD, Phillipson OT. 1990. Afferent and efferent connections of the laterodorsal tegmental nucleus in the rat. *Brain Research Bulletin* 25:271-84

Cornwall J, Phillipson O. 1988a. Quantitative analysis of axonal branching using the retrograde transport of fluorescent latex microspheres. *Journal of Neuroscience Methods* 24:1-9

Cornwall J, Phillipson O. 1989. Single neurones of the basal forebrain and laterodorsal tegmental nucleus project by collateral axons to the olfactory bulb and the mediodorsal nucleus in the rat. *Brain Research* 491:194-8

Cornwall J, Phillipson OT. 1988b. Mediodorsal and reticular thalamic nuclei receive collateral axons from prefrontal cortex and laterodorsal tegmental nucleus in the rat. *Neuroscience Letters* 88:121-6

Corrigall WA, Coen KM, Zhang J, Adamson LK. 2002. Pharmacological manipulations of the pedunculopontine tegmental nucleus in the rat reduce self-administration of both nicotine and cocaine. *Psychopharmacology* 160:198-205

Crawley J, Olschowka J, Diz D, Jacobowitz D. 1985. Behavioral significance of the coexistence of substance P, corticotropin releasing factor, and acetylcholinesterase in lateral dorsal tegmental neurons projecting to the medial frontal cortex of the rat. *Peptides* 6:891-901

Curro Dossi R, Pare D, Steriade M. 1991. Short-lasting nicotinic and long-lasting muscarinic depolarizing responses of thalamocortical neurons to stimulation of mesopontine cholinergic nuclei. *Journal of Neurophysiology* 65:393-406

Curro Dossi R, Pare D, Steriade M. 1992. Various types of inhibitory postsynaptic potentials in anterior thalamic cells are differentially altered by stimulation of laterodorsal tegmental cholinergic nucleus. *Neuroscience* 47:279-89

Darvesh S, Hopkins DA. 2003. Differential distribution of butylcholinesterase and acetylcholinesterase in the human thalamus. *Journal of Comparative Neurology* 463:25-43

Datta S, Siwek DF. 2002. Single cell activity patterns of pedunculopontine tegmentum neurons across the sleep-wake cycle in the freely moving rats. *Journal of Neuroscience Research* 70:611-21

de Castro BM, De Jaeger X, Martins-Silva C, Lima RD, Amaral E, Menezes C, Lima P, Neves CM, Pires RG, Gould TW, Welch I, Kushmerick C, Guatimosim C, Izquierdo I, Cammarota M, Rylett RJ, Gomez MV, Caron MG, Oppenheim RW, Prado MA, Prado VF. 2009. The vesicular acetylcholine transporter is required for neuromuscular development and function. *Molecular & Cellular Biology* 29:5238-50

Dekker JJ, Kuypers HG. 1976. Quantitative EM study of projection terminals in the rat's AV thalamic nucleus. Autoradiographic and degeneration techniques compared. *Brain Research* 117:399-422

Descarries L, Gisiger V, Steriade M. 1997. Diffuse transmission by acetylcholine in the CNS. *Progress in Neurobiology* 53:603-25

Ding JB, Guzman JN, Peterson JD, Goldberg JA, Surmeier DJ. 2010. Thalamic gating of corticostriatal signaling by cholinergic interneurons. *Neuron* 67:294-307

Doerr JP, Spiegelhalder K, Petzold F, Feige B, Hirscher V, Kaufmann R, Riemann D, Voderholzer U. 2010. Impact of escitalopram on nocturnal sleep, day-time sleepiness and performance compared to amitriptyline: a randomized, double-blind, placebo-controlled study in healthy male subjects. *Pharmacopsychiatry* 43:166-73

Domesick VB. 1969. Projections from the cingulate cortex in the rat. *Brain Research* 12:296-320

Eiden L. 1998. The cholinergic gene locus. *Journal of Neurochemistry* 70:2227-40

Emre M. 2003. What causes mental dysfunction in Parkinson's disease? *Movement Disorders* 18:S63-S71

Erb C, Troost J, Kopf S, Schmitt U, Loffelholz K, Soreq H, Klein J. 2001. Compensatory mechanisms enhance hippocampal acetylcholine release in transgenic mice expressing human acetylcholinesterase. *Journal of Neurochemistry* 77:638-46

Erickson JD, Varoqui H, Schafer M, Diebler MF, Weihe E, Modi W, Rand J, Eiden LE, Bonner TI, Usdin T. 1994. Functional characterization of the mammalian vesicular acetylcholine transporter and its expression from a "cholinergic" gene locus. *Journal of Biological Chemistry* 269:21929-32

Erro E, Lanciego JL, Giménez-Amaya JM. 1999. Relationships between thalamostriatal neurons and pedunculopontine projections to the thalamus: a neuroanatomical tract-tracing study in the rat. *Experimental Brain Research* 127:162-70

Erro ME, Lanciego JL, Giménez-Amaya JM. 2002. Re-examination of the thalamostriatal projections in the rat with retrograde tracers. *Neuroscience Research* 42:45-55

Farber S, Savci V, Wei A, Slack B, Wurtman R. 1996. Choline's phosphorylation in rat striatal slices is regulated by the activity of cholinergic neurons. *Brain Research* 723:90-9

Ferguson S, Bazalakova M, Savchenko V, Tapia J, Wright J, Blakely R. 2004. Lethal impairment of cholinergic neurotransmission in hemicholinium-3-sensitive choline transporter knockout mice. *Proceedings of the National Academy of Sciences of the United States of America* 101:8762-7

Ferguson S, Savchenko V, Apparsundaram S, Zwick M, Wright J, Heilman C, Yi H, Levey A, Blakely R. 2003. Vesicular localization and activity-dependent trafficking of presynaptic choline transporters. *Journal of Neuroscience* 23:9697-709

Ferguson SM, Blakely RD. 2004. The choline transporter resurfaces: new roles for synaptic vesicles? *Molecular Interventions* 4:22-37

Floresco SB, West AR, Ash B, Moore H, Grace AA. 2003. Afferent regulation of dopamine neuron firing differentially regulates tonic and phasic dopamine transmission. *Nature Neuroscience* 6:968-73

Florio T, Capozzo A, Puglielli E, Pupillo R, Pizzuti G, Scarnati E. 1999. The function of the pedunculopontine nucleus in the preparation and execution of an externally-cued bar pressing task in the rat. *Behavioural Brain Research* 104:95-104

Ford B, Holmes CJ, Mainville L, Jones BE. 1995. GABAergic neurons in the rat pontomesencephalic tegmentum: Codistribution with cholinergic and other tegmental neurons projecting to the posterior lateral hypothalamus. *Journal of Comparative Neurology* 363:177-96

Forster G, Blaha C. 2000. Laterodorsal tegmental stimulation elicits dopamine efflux in the rat nucleus accumbens by activation of acetylcholine and glutamate receptors in the ventral tegmental area. *European Journal of Neuroscience* 12:3596-604

Forster GL, Blaha CD. 2003. Pedunculopontine tegmental stimulation evokes striatal dopamine efflux by activation of acetylcholine and glutamate receptors in the midbrain and pons of the rat. *European Journal of Neuroscience* 17:751-62

Forster GL, Falcon AJ, Miller AD, Heruc GA, Blaha CD. 2002. Effects of laterodorsal tegmentum excitotoxic lesions on behavioral and dopamine responses evoked by morphine and d-amphetamine. *Neuroscience* 114:817-23

Fuxe K, Cintra A, Agnati LF, Harfstrand A, Goldstein M. 1988. Studies on the relationship of tyrosine hydroxylase, dopamine and cyclic amp-regulated phosphoprotein-32 immunoreactive neuronal structures and d1 receptor antagonist binding sites in various brain regions of the male rat-mismatches indicate a role of d1 receptors in volume transmission. *Neurochemistry International* 13:179-97

Fuxe K, Dahlstrom AB, Jonsson G, Marcellino D, Guescini M, Dam M, Manger P, Agnati L. 2010. The discovery of central monoamine neurons gave volume transmission to the wired brain. *Progress in Neurobiology* 90:82-100

Gabbott PL, Warner TA, Jays PR, Salway P, Busby SJ. 2005. Prefrontal cortex in the rat: projections to subcortical autonomic, motor, and limbic centers. *Journal of Comparative Neurology* 492:145-77

Gabriel M, Foster K, Orona E. 1980. Interaction of laminae of the cingulate cortex with the anteroventral thalamus during behavioral learning. *Science* 208:1050-2

Garcia-Cabezas MA, Martinez-Sanchez P, Sanchez-Gonzalez MA, Garzon M, Cavada C. 2009. Dopamine innervation in the thalamus: monkey versus rat. *Cerebral Cortex* 19:424-34

Garzon M, Vaughan RA, Uhl GR, Kuhar MJ, Pickel VM, Garzon M, Vaughan RA, Uhl GR, Kuhar MJ, Pickel VM. 1999. Cholinergic axon terminals in the ventral tegmental area target a subpopulation of neurons expressing low levels of the dopamine transporter. *Journal of Comparative Neurology* 410:197-210

Gates J, Jr., Ferguson S, Blakely R, Apparsundaram S. 2004. Regulation of choline transporter surface expression and phosphorylation by protein kinase C and protein phosphatase 1/2A. *Journal of Pharmacology and Experimental Therapeutics* 310:536-45

Geisler S, Zahm DS. 2005. Afferents of the ventral tegmental area in the rat-anatomical substratum for integrative functions. *Journal of Comparative Neurology* 490:270-94

Geyer J, Fernandes CF, Doring B, Burger S, Godoy JR, Rafalzik S, Hubschle T, Gerstberger R, Petzinger E. 2008. Cloning and molecular characterization of the orphan carrier protein Slc10a4: expression in cholinergic neurons of the rat central nervous system. *Neuroscience* 152:990-1005

Gibb SJ, Wolff M, Dalrymple-Alford JC. 2006. Odour-place paired-associate learning and limbic thalamus: comparison of anterior, lateral and medial thalamic lesions. *Behavioural Brain Research* 172:155-68

Giménez-Amaya J, McFarland N, de Las Heras S, Haber S. 1995. Organization of thalamic projections to the ventral striatum in the primate. *Journal of Comparative Neurology* 354:127-49

Göder R, Boigs M, Braun S, Friege L, Fritzer G, Aldenhoff JB, Hinze-Selch D. 2004. Impairment of visuospatial memory is associated with decreased slow wave sleep in schizophrenia. *Journal of Psychiatric Research* 38:591-9

Gonzalo-Ruiz A, Lieberman AR. 1995. GABAergic projections from the reticular nucleus to the anteroventral and anterodorsal thalamic nuclei of the rat. *Journal of Chemical Neuroanatomy* 9:165-74

Gonzalo-Ruiz A, Sanz-Anquela MJ, Lieberman AR. 1995. Cholinergic projections to the anterior thalamic nuclei in the rat: a combined retrograde tracing and choline acetyl transferase immunohistochemical study. *Anatomy & Embryology* 192:335-49

Gould E, Woolf NJ, Butcher LL. 1989. Cholinergic projections to the substantia nigra from the pedunculopontine and laterodorsal tegmental nuclei. *Neuroscience* 28:611-23

Grace AA, Bunney BS. 1984. The control of firing pattern in nigral dopamine neurons: burst firing. *Journal of Neuroscience* 4:2877-90

Grailhe R, Cardona A, Even N, Seif I, Changeux J, Cloëz-Tayarani I. 2009. Regional changes in the cholinergic system in mice lacking monoamine oxidase A. *Brain Research Bulletin* 78:283-9

Grant SJ, Highfield DA. 1991. Extracellular characteristics of putative cholinergic neurons in the rat laterodorsal tegmental nucleus. *Brain Research* 559:64-74

Grillner P, Berretta N, Bernardi G, Svensson TH, Mercuri NB. 2000. Muscarinic receptors depress GABAergic synaptic transmission in rat midbrain dopamine neurons. *Neuroscience* 96:299-307

Groenewegen HJ, Witter MP. 2004. Thalamus. In *The Rat Nervous System*, ed. G Paxinos, pp. 408-57. New York: Elsevier Academic Press

Grofova I, Zhou M. 1998. Nigral innervation of cholinergic and glutamatergic cells in the rat mesopontine tegmentum: light and electron microscopic anterograde tracing and immunohistochemical studies. *Journal of Comparative Neurology* 395:359-79

Gronier B, Perry KW, Rasmussen K. 2000. Activation of the mesocorticolimbic dopaminergic system by stimulation of muscarinic cholinergic receptors in the ventral tegmental area. *Psychopharmacology (Berl)* 147:347-55

Gronier B, Rasmussen K. 1998. Activation of midbrain presumed dopaminergic neurones by muscarinic cholinergic receptors: an in vivo electrophysiological study in the rat. *British Journal of Pharmacology* 124:455-64

Grove E. 1988. Efferent connections of the substantia innominata in the rat. *Journal of Comparative Neurology* 277:347-64

Guseva MV, Hopkins DM, Pauly JR. 2006. An autoradiographic analysis of rat brain nicotinic receptor plasticity following dietary choline modification. *Pharmacology, Biochemistry and Behavior* 84:26-34

Guyenet P, Lefresne P, Rossier J, Beaujouan J-C, Glowinski J. 1973. Effect of sodium, hemicholinium-3 and antiparkinson drugs on [^{14}C]acetylcholine synthesis and [^{3}H]choline uptake in rat striatal synaptosomes. *Brain Research* 62:523-9

Haberberger R, U P, Lips K, Kummer W. 2002. Expression of the high-affinity choline transporter, CHT1, in the neuronal and non-neuronal cholinergic system of human and rat skin. *Journal of Investigative Dermatology* 119:943–8

Haga T, Noda H. 1973. Choline uptake systems of rat brain synaptosomes. *Biochemica et Biophysica Acta* 291:564-75

Hahn MK, Blackford JU, Haman K, Mazei-Robison M, English BA, Prasad HC, Steele A, Hazelwood L, Fentress HM, Myers R, Blakely RD, Sanders-Bush E, Shelton R. 2008. Multivariate permutation analysis associates multiple polymorphisms with subphenotypes of major depression. *Genes, Brain & Behavior* 7:487-95

Hallanger AE, Levey AI, Lee HJ, Rye DB, Wainer BH. 1987. The origins of cholinergic and other subcortical afferents to the thalamus in the rat. *Journal of Comparative Neurology* 262:105-24

Hallanger AE, Price SD, Lee HJ, Steininger TL, Wainer BH. 1990. Ultrastructure of cholinergic synaptic terminals in the thalamic anteroventral, ventroposterior, and dorsal lateral geniculate nuclei of the rat. *Journal of Comparative Neurology* 299:482-92

Hallanger AE, Wainer BH. 1988. Ascending projections from the pedunculopontine tegmental nucleus and the adjacent mesopontine tegmentum in the rat. *Journal of Comparative Neurology* 274:483-515

Halliday GM, Li YW, Blumbers PC, Joh TH, Cotton RG, Howe PR, Blessing WW, Geffen LB. 1990. Neuropathology of immunohistochemically identified brainstem neurons in Parkinson's disease. *Annals of Neurology* 27

Heckers S, Geula C, Mesulam MM. 1992. Cholinergic innervation of the human thalamus: dual origin and differential nuclear distribution. *Journal of Comparative Neurology* 325:68-82

Himmelheber AM, Sarter M, Bruno JP. 2000. Increases in cortical acetylcholine release during sustained attention performance in rats. *Brain Research. Cognitive Brain Research.* 9:313-25

Himmelheber AM, Sarter M, Bruno JP. 2001. The effects of manipulations of attentional demand on cortical acetylcholine release. *Brain Research. Cognitive Brain Research.* 12:353-70

Hinton JM. 1963. Patterns of insomnia in depressive states. *Journal of Neurology, Neurosurgery, and Psychiatry* 26:184-9

Hofer SB, Bonhoeffer T. 2010. Dendritic spines: the stuff that memories are made of? *Current Biology* 20:R157-9

Hohlbein J, Gryte K, Heilemann M, Kapanidis AN. 2010. Surfing on a new wave of single-molecule fluorescence methods. *Physical Biology* 7:031001

Hökfelt T, Ljungdahl Å, Fuxe K, Johansson O. 1974. Dopamine nerve terminals in the rat limbic cortex: Aspects of the dopamine hypothesis of schizophrenia. *Science* 184:177-9

Holmstrand E, Asafu-Adjei J, Sampson A, Blakely R, Sesack S. 2010. Ultrastructural localization of high-affinity choline transporter in the rat anteroventral thalamus and ventral tegmental area: Differences in axon morphology and transporter distribution. *Journal of Comparative Neurology* 518:1908-24

Holmstrand EC, Sesack S, Blakely R. 2006. Ultrastructural characterization of the expression of the high-affinity choline transporter in the rat ventral tegmental area. In *2006 Society for Neuroscience Meeting*. Atlanta, GA: Society for Neuroscience

Holmstrand EC, Sesack SR. 2004. Cholinergic neurons in the rat mesopontine tegmentum comprise about one quarter of the projection to the ventral tegmental area. In *2004 Society for Neuroscience Annual Meeting*. San Diego, CA: Society for Neuroscience

Holmstrand EC, Sesack SR, Blakely RD. 2008. High affinity choline transporter in the rat ventral tegmental area and anteroventral thalamus: colocalization with the vesicular acetylcholine transporter and subcellular distribution to the plasma membrane. In *2008 Society for Neuroscience Annual Meeting*. Washington, DC: Society for Neuroscience

Hu B, Bouhassira D, Steriade M, Deschenes M. 1988. The blockage of ponto-geniculo-occipital waves in the cat lateral geniculate nucleus by nicotinic antagonists. *Brain Research* 473:394-7

Huitron-Resendiz S, Kristensen MP, Sanchez-Alavez M, Clark SD, Grupke SL, Tyler C, Suzuki C, Nothacker HP, Civelli O, Criado JR, Henriksen SJ, Leonard CS, de Lecea L. 2005. Urotensin II modulates rapid eye movement sleep through activation of brainstem cholinergic neurons. *Journal of Neuroscience* 25:5465-74

Hur EE, Zaborszky L. 2005. Vglut2 afferents to the medial prefrontal and primary somatosensory cortices: a combined retrograde tracing in situ hybridization study *Journal of Comparative Neurology* 483:351-73

Ichikawa T, Ajiki K, Matsuura J, Misawa H. 1997. Localization of two cholinergic markers, choline acetyltransferase and vesicular acetylcholine transporter in the central nervous system of the rat: in situ hybridization histochemistry and immunohistochemistry. *Journal of Chemical Neuroanatomy* 13:23-39

Ikemoto S, Panskepp J. 1996. Dissociations between appetitive and consummatory responses by pharmacological manipulations of reward-relevant brain regions. *Behavioral Neuroscience* 110:331-45

Inglis WI, Winn P. 1995. The pedunculopontine tegmental nucleus: Where the striatum meets the reticular formation. *Progress in Neurobiology* 47:1-29

Ivy M, Newkirk R, Karim M, Mtshali C, Townsel J. 2001. Hemicholinium-3 mustard reveals two populations of cycling choline cotransporters in *Limulus*. *Neuroscience* 102:969-78

Jellinger KA. 1991. Pathology of Parkinson's disease. Changes other than the nigrostriatal pathway. *Molecular and Chemical Neuropathology* 14:153-97

Jenkins TA, Dias R, Amin E, Aggleton JP. 2002. Changes in Fos expression in the rat brain after unilateral lesions of the anterior thalamic nuclei. *European Journal of Neuroscience* 16:1425-32

Jia H-G, Yamuy J, Sampogna S, Morales FR, Chase MH. 2003. Colocalization of γ-aminobutyric acid and acetylcholine in neurons in the laterodorsal and pedunculopontine tegmental nuclei in the cat: a light and electron microscopic study. *Brain Research* 992:205-19

Jones BE. 1995. Reticular formation: cytoarchitecture, transmitters, and projections. In *The Rat Nervous System*, ed. G Paxinos, pp. 155-71: Academic Press, Inc.

Jones BE, Beaudet A. 1987. Retrograde labeling of neurones in the brain stem following injections of [^{3}H]choline into the forebrain of the rat. *Experimental Brain Research* 65:437-48

Jones BE, Webster HH. 1988. Neurotoxic lesions of the dorsolateral pontomesencephalic tegmentum-cholinergic cell area in the cat. I. Effects upon the cholinergic innervation of the brain. *Brain Research* 451:13-32

Jones I, Wonnacott S. 2004. Precise localization of α7 nicotinic acetylcholine receptors on glutamatergic axon terminals in the rat ventral tegmental area. *Journal of Neuroscience* 24:11244-52

Jourdain A, Semba K, Fibiger HC. 1989. Basal forebrain and mesopontine tegmental projections to the reticular thalamic nucleus: an axonal collateralization and immunohistochemical study in the rat. *Brain Research* 505:55-65

Kang Y, Kitai ST, Kang Y, Kitai ST. 1990. Electrophysiological properties of pedunculopontine neurons and their postsynaptic responses following stimulation of substantia nigra reticulata. *Brain Research* 535:79-95

Karson CN, Garcia-Rill E, Biedermann J, Mrak RE, Husain MM, Skinner RD. 1991. The brain stem reticular formation in schizophrenia. *Psychiatry Research* 40:31-48

Katz L, Burkhalter A, Dreyer W. 1984. Fluorescent latex microspheres as a retrograde neuronal marker for in vivo and in vitro studies of visual cortex. *Nature* 310:498-500

Kayalioglu G, Balkan B. 2004. Expression of c-Fos and NADPH-d after peripheral noxious stimulation in the pedunculopontine tegmental nucleus. *Neuroreport* 15:421-3

Kehagia AA, Murray GK, Robbins TW. 2010. Learning and cognitive flexibility: frontostriatal function and monoaminergic modulation. *Current Opinion in Neurobiology* 20:199-204

Keller JJ, Keller AB, Bowers BJ, Wehner JM. 2005. Performance of α7 nicotinic receptor null mutants is impaired in appetitive learning measured in a signaled nose poke task. *Behavioural Brain Research* 162:143-52

Kelley A, Stinus L. 1984. The distribution of the projections from the parataenial nucleus of the thalamus to the nucleus accumbens in the rat: an autoradiographic study. *Experimental Brain Research* 54:499-512

Klein J, Gonzalez R, Koppen A, Loffelholz K. 1993a. Free choline and choline metabolites in rat brain and body fluids: sensitive determination and implications for choline supply to the brain. *Neurochemistry International* 22:293-300

Klein J, Holler T, Cappel E, Köppen A, Löffelholz K. 1993b. Release of choline from rat brain under hypoxia: contribution from phospholipase A2 but not from phospholipase D. *Brain Research* 630:337-40

Klein J, Köppen A, Löffelholz K, Schmitthenner J. 1992. Uptake and metabolism of choline by rat brain after acute choline administration. *Journal of Neurochemistry* 58:870-6

Kobayashi Y, Isa T. 2002. Sensory-motor gating and cognitive control by the brainstem cholinergic system. *Neural Networks* 15:731-41

Kolmac C, Mitrofanis J. 1998. Patterns of brainstem projection to the thalamic reticular nucleus. *Journal of Comparative Neurology* 396:531-43

Köppen A, Klein J, Erb C, Löffelholz K. 1997. Acetylcholine release and choline availability in rat hippocampus: Effects of exogenous choline and nicotinamide. *The Journal of Pharmacology and Experimental Therapeutics* 282:1139-45

Koyama Y, Jodo E, Y K. 1994. Sensory responsiveness of "broad-spike" neurons in the laterodorsal tegmental nucleus, locus coeruleus and dorsal raphe of awake rats: implication for cholinergic and monoaminergic neuron-specific responses. *Neuroscience* 63:1021-31

Krettek J, Price J. 1977. The cortical projections of the mediodorsal nucleus and adjacent thalamic nuclei in the rat. *Journal of Comparative Neurology* 171:157-92

Krishnaswamy A, Cooper E. 2009. An activity-dependent retrograde signal induces the expression of the high-affinity choline transporter in cholinergic neurons. *Neuron* 61:272-86

Krištofiková Z, Klaschka J, Tejkalová H. 1998. Effects of K^+-depolarization, arachidonic acid, ethanol, and aging on the high-affinity choline transport in rat hippocampus. *Neurochemical Research* 23:923-9

Kroener S, Chandler LJ, Phillips PE, Seamans JK. 2009. Dopamine modulates persistent synaptic activity and enhances the signal-to-noise ratio in the prefrontal cortex. *PLoS One* 4:e6507

Kus L, Borys E, Chu Y, Ferguson S, Blakely R, Emborg M, Kordower J, Levey A, Mufson E. 2003. Distribution of high affinity choline transporter immunoreactivity in the primate central nervous system. *Journal of Comparative Neurology* 463:341-57

Lammel S, Hetzel A, Häckel O, Jones I, Liss B, Roeper J. 2008. Unique properties of mesoprefrontal neurons within a dual mesocorticolimbic dopamine system. *Neuron* 57:760-73

Lança AJ, Adamson KL, Coen KM, Chow BL, Corrigall WA. 2000. The pedunculopontine tegmental nucleus and the role of cholinergic neurons in nicotine self-administration in the rat: a correlative neuroanatomical and behavioral study. *Neuroscience* 96:735-42

Laviolette SR, Priebe RP, Yeomans JS. 2000. Role of the laterodorsal tegmental nucleus in scopolamine- and amphetamine-induced locomotion and stereotypy. *Pharmacology, Biochemistry & Behavior* 65:163-74

Laviolette SR, van der Kooy D. 2003. The motivational valence of nicotine in the rat ventral tegmental area is switched from rewarding to aversive following blockade of the alpha7-subunit-containing nicotinic acetylcholine receptor. *Psychopharmacology (Berl)* 166:306-13

Lavoie B, Parent A. 1994. Pedunculopontine nucleus in the squirrel monkey: distribution of cholinergic and monoaminergic neurons in the mesopontine tegmentum with evidence for the presence of glutamate in cholinergic neurons. *Journal of Comparative Neurology* 344:190-209

Lecomte M, De Gois S, Guerci A, Ravassard P, Faucon Biguet N, Mallet J, Berrard S. 2005. Differential expression and regulation of the high-affinity choline transporter CHT1 and choline acetyltransferase in neurons of superior cervical ganglion. *Molecular & Cellular Neuroscience* 28:303-13

Lee R-S, Steffensen SC, Henricksen SJ. 2001. Discharge profiles of ventral tegmental area GABA neurons during movement, anesthesia, and the sleep-wake cycle. *Journal of Neuroscience* 21:1757-66

Leonard CS, Llinás RR. 1990. Electrophysiology of mammalian pedunculopontine and laterodorsal tegmental neurons *in vitro*: Implications for the control of REM sleep. In *Brain Cholinergic Systems*, ed. M Steriade, D Biesold, pp. 205 - 23. New York: Oxford University Press

Lepore M, Franklin KBJ. 1996. N-Methyl-D-Aspartate lesions of the pedunculopontine nucleus block acquisition and impair maintenance of responding reinforced with brain stimulation. *Neuroscience* 71:147-55

Levey AI, Hallanger AE, Wainer BH. 1987. Choline acetyltransferase immunoreactivity in the rat thalamus. *Journal of Comparative Neurology* 257:317-32

Lima RdF, Prado VF, Prado MA, Kushmerick C. 2010. Quantal release of acetylcholine in mice with reduced levels of the vesicular acetylcholine transporter. *Journal of Neurochemistry* 113:943-51

Lindvall O, Björklund A, Moore R, Stenevi U. 1974. Mesencephalic dopamine neurons projecting to neocortex. *Brain Research* 81:325-31

Lips K, Pfeil U, Haberberger R, Kummer W. 2002. Localisation of the high-affinity choline transporter-1 in the rat skeletal motor unit. *Cell & Tissue Research* 307:275-80

Lips K, Pfeil U, Reiners K, Rimasch C, Kuchelmeister K, Braun-Dullaeus R, Haberberger R, Schmidt R, Kummer W. 2003. Expression of the high-affinity choline transporter CHT1 in rat and human arteries. *Journal of Histochemistry and Cytochemistry* 51:1645-54

Lisman JE, Harris KM. 1993. Quantal analysis and synaptic anatomy - integrating two views of hippocampal plasticity. *Trends in Neurosciences* 16:141-7

Littell RC, Nilliken GA, Stroup WW, Wolfinger RD, Schabenberger O. 2006. *SAS for Mixed Models*. Cary, NC: SAS Institute, Inc.

Liu Y, Edwards RH. 1997. Differential localization of vesicular acetylcholine and monoamine transporters in PC12 cells but not CHO cells. *Journal of Cell Biology* 139:907-16

Ljungberg T, Apicella P, Schultz W. 1992. Responses of monkey dopamine neurons during learning of behavioral reactions. *Journal of Neurophysiology* 67:145-63

Lodge D, Grace A. 2006. The laterodorsal tegmentum is essential for burst firing of ventral tegmental area dopamine neurons. *Proceedings of the National Academy of Sciences of the United States of America* 103:5167-72

Löffelholz K, Klein J. 2006. Precursors: choline and glucose. In *The Brain Cholinergic System in Health and Disease*, ed. E Giacobini, G Pepeu, pp. 75-84. Boca Raton: Informa Healthcare

Löffelholz K, Klein J, Köppen A. 1993. Choline, a precursor of acetylcholine and phospholipids in the brain. *Progress in Brain Research* 98:197-200

Lolova IS, Lolov SR, Itzev DE. 1996. Changes in NADPH-diaphorase neurons of the rat laterodorsal and pedunculopontine tegmental nuclei in aging. *Mechanisms of ageing and development* 90:111-28

Losier BJ, Semba K. 1993. Dual projections of single cholinergic and aminergic brainstem neurons to the thalamus and basal forebrain in the rat. *Brain Research* 604:41-52

Loughlin S, Fallon J. 1984. Substantia nigra and ventral tegmental area projections to cortex: topography and collateralization. *Neuroscience* 11:425-35

Luppi P-H, Fort P, Jouvet M. 1990. Iontophoretic application of unconjugated cholera toxin B subunit (CTb) combined with immunohistochemistry of neurochemical substances: a method for transmitter identification of retrogradely labeled neurons *Brain Research* 534:209-24

MacDermott A, Role L, Sigelbaum S. 1999. Presynaptic ionotropic receptors and the control of transmitter release. *Annual Review of Neuroscience* 22:443-85

Madziar B, Shah S, Brock M, Burke R, Lopez-Coviella I, Nickel AC, Cakal EB, Blusztajn JK, Berse B. 2008. Nerve growth factor regulates the expression of the cholinergic locus and the high-affinity choline transporter via the Akt/PKB signaling pathway. *Journal of Neurochemistry* 107:1284-93

Mansvelder HD, De Rover M, McGehee DS, Brussaard AB. 2003. Cholinergic modulation of dopaminergic reward areas: upstream and downstream targets of nicotine addiction. *European Journal of Pharmacology* 480:117-23

Mansvelder HD, McGehee DS. 2000. Long-term potentiation of excitatory inputs to brain reward areas by nicotine. *Neuron* 27:349-57

Masland RH, Mills JW. 1980. Choline accumulation by photoreceptor cells of the rabbit retina. *Proceedings of the National Academy of Sciences of the United States of America* 77:1671-5

Mathiisen TM, Nagelhus EA, Jouleh B, Torp R, Frydenlund DS, Mylonakou M-N, Amiry-Moghaddam M, Covolan L, Utvik JK, Riber B, Gujord KM, Knutsen J, Skare Ø, Laake P, Davanger S, Haug F-M, Rinvik E, Ottersen OP. 2005. Postembedding immunogold cytochemistry of membrane molecules and amino acid transmitters in the central nervous system . In *Neuroanatomical Tract-Tracing 3: Molecules, Neurons, and Systems*, ed. L Zaborszky, FG Wouterlood, JL Lanciego, pp. 72-108. New York: Springer

Matthies DS, Fleming PA, Wilkes DM, Blakely RD. 2006. The Caenorhabditis elegans choline transporter CHO-1 sustains acetylcholine synthesis and motor function in an activity-dependent manner. *Journal of Neuroscience* 26:6200-12

McGehee DS, Heath MJ, Gelber S, Devay P, Role LW. 1995. Nicotine enhancement of fast excitatory synaptic transmission in CNS by presynaptic receptors. *Science* 269:1692-6

Mclean IW, Nakane PK. 1974. Periodate-lysine-paraformaldehyde fixative. A new fixation for immunoelectron microscopy. *Journal of Histochemistry and Cytochemistry* 22:1077-83

Melchitzky DS, Erickson SL, Lewis DA. 2006. Dopamine innervation of the monkey mediodorsal thalamus: Location of projection neurons and ultrastructural characteristics of axon terminals. *Neuroscience* 143:1021-30

Mellott T, Kowall N, Lopez-Coviella I, Blusztajn JK. 2007. Prenatal choline deficiency increases choline transporter expression in the septum and hippocampus during postnatal development and in adulthood in rats. *Brain Research* 1151:1-11

Mena-Segovia J, Winn P, Bolam JP. 2008. Cholinergic modulation of midbrain dopaminergic systems. *Brain Research Reviews* 58:265-71

Mesulam M-M. 1995a. Structure and function of cholinergic pathways in the cerebral cortex, limbic system, basal ganglia, and thalamus of the human brain. In *Psychopharmacology: The Fourth Generation of Progress*, ed. FE Bloom, DJ Kupfer. New York: Raven Press

Mesulam M. 1995b. Cholinergic pathways and the ascending reticular activating system of the human brain. *Annals of the New York Academy of Sciences* 757:169-79

Mesulam M, Mufson E, Wainer B, Levey A. 1983. Central cholinergic pathways in the rat: an overview based on an alternative nomenclature (Ch1-Ch6). *Neuroscience* 10:1185-201

Michel V, Yuan Z, Ramsubur S, Bakovic M. 2006. Choline transport for phospholipid synthesis. *Experimental Biology and Medicine* 231:490-504

Mike A, Castro NG, Albuquerque EX. 2000. Choline and acetylcholine have similar kinetic properties of activation and desensitization on the α7 nicotinic receptors in rat hippocampal neurons. *Brain Research* 882:155-68

Miller A, Blaha C. 2004. Midbrain muscarinic receptor mechanisms underlying regulation of mesoaccumbens and nigrostriatal dopaminergic transmission in the rat. *European Journal of Neuroscience* 21:1837-46

Miner LH, Jedema HP, Moore FW, Blakely RD, Grace AA, Sesack SR. 2006. Chronic stress increases the plasmalemmal distribution of the norepinephrine transporter and the coexpression of tyrosine hydroxylase in norepinephrine axons in the prefrontal cortex. *Journal of Neuroscience* 26:1571-8

Misawa H, Fujigaya H, Nishimura T, Moriwaki Y, Okuda T, Kawshima K, Nakata K, Ruggiero AM, Blakely RD, Nakatsu F, Ohno H. 2008. Aberrant trafficking of the high-affinity choline transporter in AP-3-deficient mice. *European Journal of Neuroscience* 27:3109-17

Misawa H, Nakata K, Matsuura J, Nagao M, Okuda T, Haga T. 2001. Distribution of the high-affinity choline transporter in the central nervous system of the rat. *Neuroscience* 105:87-98

Mitchell AS, Dalrymple-Alford JC. 2006. Lateral and anterior thalamic lesions impair independent memory systems. *Learning & Memory* 13:388-96

Monti JM, Monti D. 2007. The involvement of dopamine in the modulation of sleep and waking. *Sleep Medicine Reviews* 11:113-33

Morgane PJ, Galler JR, Mokler DJ. 2005. A review of systems and networks of the limbic forebrain/limbic midbrain. *Progress in Neurobiology* 75:143-60

Morley BJ, Garner LL. 1986. Increases in the concentrations of brain α-Bungarotoxin binding sites induced by dietary choline are age-dependent. *Brain Research* 378:315-9

Morley BJ, Garner LL. 1990. AF64A depletes hippocampal high-affinity choline uptake but does not alter the density of α-BgTx binding sites or modify the effect of exogenous choline. *Brain Research* 519:1-5

Morley BJ, Robinson GR, Brown GB, Kemp GE, Bradley RJ. 1977. Effects of dietary choline on nicotinic acetylcholine receptors in brain. *Nature* 266:848-50

Mulder AH, Yamamura HI, Kuhar MJ, Snyder SH. 1974. Release of acetylcholine from hippocampal slices by potassium depolarization: dependence on high affinity choline uptake. *Brain Research* 70:372-6

Murrin LC, Kuhar MJ. 1976. Activation of high-affinity choline uptake in vitro by depolarizing agents. *Molecular Pharmacology* 12:1082-90

Nakata K, Okuda T, Misawa H. 2004. Ultrastructural localization of high-affinity choline transporter in the rat neuromuscular junction: enrichment on synaptic vesicles. *Synapse* 53:53-6

Nemcova V, Petrovicky P, ten Donkelaar HJ. 2000. The effect of electrolytic thalamic lesions on the NADPH-diaphorase activity of neurons of the laterodorsal tegmental and pedunculopontine nuclei in rats. *Journal of Chemical Neuroanatomy* 17:227-32

Neumann SA, Brown SM, Ferrell RE, Flory JD, Manuck SB, Hariri AR. 2006. Human choline transporter gene variation is associated with corticolimbic reactivity and autonomic-cholinergic function. *Biological Psychiatry* 60:1155-62

Niimi K, Niimi M, Okada Y. 1978. Thalamic afferents to the limbic cortex in the cat studied with the method of retrograde axonal transport of horseradish peroxidase. *Brain Research* 145:225-38

Oades R, Halliday G. 1987. Ventral tegmental (A10) system: neurobiology. 1. Anatomy and connectivity. *Brain Research* 434:117-65

Oakman S, Faris P, Cozzari C, Hartman BK. 1999. Characterization of the extent of pontomesencephalic cholinergic neurons' projections to the thalamus: comparison with projections to midbrain dopaminergic groups. *Neuroscience* 94:529-47

Oakman S, Faris P, Kerr P, Cozzari C, Hartman B. 1995. Distribution of pontomesencephalic cholinergic neurons projecting to substantia nigra differs significantly from those projecting to ventral tegmental area. *Journal of Neuroscience* 15:5859-69

Oda S. 1997. Ultrastructure and distribution of corticothalamic fiber terminals from the posterior cingulate cortex and the presubiculum to the anteroventral thalamic nucleus of the rat. *Brain Research Bulletin* 42:485-91

Oda S, Kuroda M, Kakuta S, Tanihata S, Ishikawa Y, Kishi K. 2003. Ultrastructure of ascending cholinergic terminals in the anteroventral thalamic nucleus of the rat: A comparison with the mammillothalamic terminals. *Brain Research Bulletin* 59:473-83

Oda S, Sato F, Okada A, Akahane S, Igarashi H, Yokofujita J, Yang J, Kuroda M. 2007. Immunolocalization of muscarinic receptor subtypes in the reticular thalamic nucleus of rats. *Brain Research Bulletin* 74:376-84

Okada K, Toyama K, Inoue Y, Isa T, Kobayashi Y. 2009. Different pedunculopontine tegmental neurons signal predicted and actual task rewards. *Journal of Neuroscience* 29:4858-70

Okuda T, Haga T. 2003. High-affinity choline transporter. *Neurochemical Research* 28:483-8

Okuda T, Haga T, Kanai Y, Endou H, Ishihara T, Katsura I. 2000. Identification and characterization of the high-affinity choline transporter. *Nature* 3:120-5

Omelchenko N, Sesack S. 2005. Laterodorsal tegmental projections to identified cell populations in the rat ventral tegmental area. *Journal of Comparative Neurology* 483:217-35

Omelchenko N, Sesack S. 2006. Cholinergic axons in the rat ventral tegmental area synapse preferentially onto mesoaccumbens dopamine neurons. *Journal of Comparative Neurology* 494:863-75

Oosawa H, Fujii T, Kawashima K. 1999. Nerve growth factor increases the synthesis and release of acetylcholine and the expression of vesicular acetylcholine transporter in primary cultured rat embryonic septal cells. *Journal of Neuroscience Research* 57:381-7

Oshima S, Yamada K, Shirakawa T, Watanabe M. 2004. Changes of high-affinity choline transporter CHT1 mRNA expression during degeneration and regeneration of hypoglossal nerves in mice. *Neuroscience Letters* 365:97-101

Otake K, Nakamura Y. 1998. Single midline thalamic neurons projecting to both the ventral striatum and the prefrontal cortex in the rat. *Neuroscience* 86:635-49

Overton PG, Clark D. 1997. Burst firing in midbrain dopaminergic neurons. *Brain Research Reviews* 25:312-34

Pakan J, Graham D, Iwaniuk A, Wylie D. 2008. Differential projections from the vestibular nuclei to the flocculus and uvula-nodulus in pigeons (Columba livia). *Journal of Comparative Neurology* 508:402-17

Pan W, Hyland B. 2005. Pedunculopontine tegmental nucleus controls conditioned responses of midbrain dopamine neurons in behaving rats. *Journal of Neuroscience* 25:4725-32

Pape HC, Eysel UT. 1988. Cholinergic excitation and inhibition in the visual thalamus of the cat--influences of cortical inactivation and barbiturate anesthesia. *Brain Research* 440:79-86

Paré D, Steriade M, Deschenes M, Bouhassira D. 1990. Prolonged enhancement of anterior thalamic synaptic responsiveness by stimulation of a brain-stem cholinergic group. *Journal of Neuroscience* 10:20-33

Parent A, Paré D, Smith Y, Steriade M. 1988. Basal forebrain cholinergic and noncholinergic projections to the thalamus and brainstem in cats and monkeys. *Journal of Comparative Neurology* 277:281-301

Parent A, Parent M, Charara A. 1999. Glutamatergic inputs to midbrain dopaminergic neurons in primates. *Parkinsonism and Related Disorders* 5:193-201

Parent M, Descarries L. 2008. Acetylcholine innervation of the adult rat thalamus: distribution and ultrastructural features in dorsolateral geniculate, parafascicular, and reticular thalamic nuclei. *Journal of Comparative Neurology* 511:678-91

Parikh V, Apparsundaram S, Kozak R, Richards JB, Sarter M. 2006. Reduced expression and capacity of the striatal high-affinity choline transporter in hyperdopaminergic mice. *Neuroscience* 141:379-89

Pascoe JP, Kapp BS. 1993. Electrophysiology of the dorsolateral mesopontine reticular formation during pavlovian conditioning in the rabbit. *Neuroscience* 54:753-72

Paxinos G, Watson C. 1986. *The Rat Brain in Stereotaxic Co-ordinates*. Sydney: Academic Press

Paxinos G, Watson C. 1997. The Rat Brain in Stereotaxic Co-ordinates. In *Compact 3rd Edition*. San Diego, CA: Academic Press, Inc.

Pidoplichko VI, Noguchi J, Areola OO, Liang Y, Peterson J, Zhang T, Dani JA. 2004. Nicotinic cholinergic synaptic mechanisms in the ventral tegmental area contribute to nicotine addiction. *Learning & Memory* 11:60-9

Pierce J, Lewin G. 1994. An ultrastructural size principle. *Neuroscience* 58:441-6

Pieribone VA, Shuliakov O, Brodin L, Hilfiker-Rothenfluh S, Czernik AJ, Greengard P. 1995. Distinct pools of synaptic vesicles in neurotransmitter release. *Nature* 375:493-7

Pinthong M, Black SAG, Ribeiro FM, Pholpramool C, Ferguson SSG, Rylett RJ. 2008. Activity and subcellular trafficking of the sodium-coupled choline transporter CHT is regulated acutely by peroxynitrite. *Molecular Pharmacology* 73:801-12

Rasmussen BA, Perry DC. 2006. An autoradiographic analysis of [^{125}I]α-bungarotoxin binding in rat brain after chronic nicotine exposure. *Neuroscience Letters* 404:9-14

Redgrave P, Gurney K, Reynolds J. 2008. What is reinforced by phasic dopamine signals? *Brain Research Reviews* 58:322-39

Reep R. 1984. Relationship between prefrontal and limbic cortex: a comparative anatomical review. *Brain, Behavior and Evolution* 25:5-80

Reese NB, Garcia-Rill E, Skinner RD. 1995a. Auditory input to the pedunculopontine nucleus: II. Unit Responses. *Brain Research Bulletin* 37:265-73

Reese NB, Garcia-Rill E, Skinner RD. 1995b. The pedunculopontine nucleus - Auditory input, arousal and pathophysiology. *Progress in Neurobiology* 42:105-33

Ribeiro F, Alves-Silva J, Volknandt W, Martins-Silva C, Mahmud H, Wilhelm A, Gomez M, Rylett R, Ferguson S, Prado V, Prado M. 2003. The hemicholinium-3 sensitive high affinity choline transporter is internalized by clathrin-mediated endocytosis and is present in endosomes and synaptic vesicles. *Journal of Neurochemistry* 87:136-46

Ribeiro F, Pinthong M, Black S, Gordon A, Prado V, Prado M, Rylett R, Ferguson S. 2007a. Regulated recycling and plasma membrane recruitment of the high-affinity choline transporter. *European Journal of Neuroscience* 26:3437-48

Ribeiro FM, Black SAG, Cregan SP, Prado VF, Prado MAM, Rylett RJ, Ferguson SSG. 2005. Constitutive high-affinity choline transporter endocytosis is determined by a carboxyl-terminal tail dileucine motif. *Journal of Neurochemistry* 94:86-96

Ribeiro FM, Black SAG, Prado VF, Rylett RJ, Ferguson SSG, Prado MAM. 2006. The "ins" and "outs" of the high-affinity choline tranpsorter CHT1. *Journal of Neurochemistry* 97:1-12

Ribeiro FM, Ferreira LT, Marion S, Fontes S, Gomez M, Ferguson SS, Prado MA, Prado VF. 2007b. SEC14-like protein 1 interacts with cholinergic transporters. *Neurochemistry International* 50:356-64

Robinson TE, Kolb B. 2004. Structural plasticity associated with exposure to drugs of abuse. *Neuropharmacology* 47:33-46

Roghani A, Carroll PT. 2002. Analysis of uptake and release of newly synthesized acetylcholine in PC12 cells overexpressing the rat vesicular acetylcholine transporter (VAChT). *Brain Research. Molecular Brain Research.* 100:21-30

Roskoski RJ. 1978. Acceleration of choline uptake after depolarization-induced acetylcholine release in rat cortical synaptosomes. *Journal of Neurochemistry* 30:1357-61

Russo SJ, Dietz DM, Dumitriu D, Morrison JH, Malenka RC, Nestler EJ. 2010. The addicted synapse: mechanisms of synaptic and structural plasticity in nucleus accumbens. *Trends Neurosci* 33:267-76

Rye DB, Saper CB, Lee HJ, Wainer BH. 1987. Pedunculopontine tegmental nucleus of the rat: cytoarchitecture, cytochemistry, and some extrapyramidal connections of the mesopontine tegmentum. *Journal of Comparative Neurology* 259:483-528

Sanchez-Gonzalez MA, Garcia-Cavezas MA, Rico B, Cavada C. 2005. The primate thalamus is a key target for brain dopamine. *Journal of Neuroscience* 25:6076-83

Satoh K, Fibiger HC. 1986. Cholinergic neurons of the laterodorsal tegmental nucleus: efferent and afferent connections. *Journal of Comparative Neurology* 253:277-302

Scherer-Singler U, Vincent SR, Kimura H, McGeer EG. 1983. Demonstration of a unique population of neurons with NADPH-diaphorase histochemistry. *Journal of Neuroscience Methods* 9:229-34

Schilström B, Fagerquist MV, Zhang X, Hertel P, Panagis G, Nomikos GG, Svensson TH. 2000. Putative role of presynaptic α7* nicotinic receptors in nicotine stimulated increases of extracellular levels of glutamate and aspartate in the ventral tegmental area. *Synapse* 38:375-83

Schilström B, Svensson HM, Svensson TH, Nomikos GG. 1998. Nicotine and food induced dopamine release in the nucleus accumbens of the rat: putative role of α7 nicotinic receptors in the ventral tegmental area. *Neuroscience* 85:1005-9

Schmidt HD, Famous KR, Pierce RC. 2009. The limbic circuitry underlying cocaine seeking encompasses the PPTg/LDT. *European Journal of Neuroscience* 30:1358-69

Schofield BR. 2001. Retrograde axonal tracing with fluorescent markers. *Current Protocols in Neuroscience* 43:1-24

Schultz W. 2002. Getting formal with dopamine and reward. *Neuron* 36:241-63

Schultz W. 2007. Behavioral dopamine signals. *Trends in Neurosciences* 30:203-10

Schultz W, Apicella P, Ljungberg T. 1993. Responses of monkey dopamine neurons to reward and conditioned stimuli during successive steps of learning a delayed response task. *Journal of Neuroscience* 13:900-13

Semba K, Fibiger HC. 1992. Afferent connections of the laterodorsal and the pedunculopontine tegmental nuclei in the rat: a retro- and antero-grade transport and immunohistochemical study. *Journal of Comparative Neurology* 323:387-410

Semba K, Reiner PB, Fibiger HC. 1990. Single cholinergic mesopontine tegmental neurons project to both the pontine reticular formation and the thalamus in the rat. *Neuroscience* 38:643-54

Sesack S, Miner L, Omelchenko N. 2006. Preembedding immunoelectron microscopy: applications for studies of the nervous system. In *Neuroanatomical Tract-Tracing 3: Molecules, Neurons, and Systems*, ed. L Zaborszky, F Wouterlood, J Lanciego, pp. 6-71. New York: Springer

Sesack SR, Carr DB, Omelchenko N, Pinto A. 2003. Anatomical substrates for glutamate-dopamine interactions: evidence for specificity of connections and extrasynaptic actions. *Annals of the New York Academy of Sciences* 1003:36-52

Sherman KA, Friedman E. 1990. Pre- and post-synaptic cholinergic dysfunction in aged rodent brain regions: new findings and an interpretative review. *International Journal of Developmental Neuroscience* 8:689-708

Shibata H. 1992. Topographic organization of subcortical projections to the anterior thalamic nuclei in the rat. *Journal of Comparative Neurology* 323:117-27

Shibata H. 1993. Efferent projections from the anterior thalamic nuclei to the cingulate cortex in the rat. *Journal of Comparative Neurology* 330:533-42

Shibata H, Naito J. 2005. Organization of anterior cingulate and frontal cortical projections to the anterior and laterodorsal thalamic nuclei in the rat. *Brain Research* 1059:93-103

Sikes RW, Vogt BA. 1987. Afferent connections of anterior thalamus in rats: sources and association with muscarinic acetylcholine receptors. *Journal of Comparative Neurology* 256:538-51

Simon H, Le Moal M, Calas A. 1979. Efferents and afferents of the ventral tegmental A10 region studied after local injection of [^{3}H] leucine and horseradish peroxidase. *Brain Research* 178:17-40

Simon JR, Atweh S, Kuhar MJ. 1976. Sodium-dependent, high affinity choline uptake: a regulatory step in the synthesis of acetylcholine. *Journal of Neurochemistry* 26:909-22

Simon JR, Kuhar MJ. 1975. Impulse-flow regulation of high affinity-choline uptake in brain cholinergic terminals. *Nature* 255:162-3

Slotkin T, Nemeroff C, Bisette G, Seidler F. 1994. Overexpression of the high affinity choline transporter in cortical regions affected by Alzheimer's disease. *Journal of Clinical Investigation* 94:696-702

Slotkin T, Seidler F, Crain B, Bell J, Bisette G, Nemeroff C. 1990. Regulatory changes in presynaptic cholinergic function assessed in rapid autopsy material from patients with Alzheimer disease: Implications for etiology and therapy. *Proceedings of the National Academy of Sciences of the United States of America* 87:2452-5

Small SV. 1968. Measurement of section thickness. In *Tipografia*, ed. DS Bocciarelli, pp. 609-10. Rome: Poliglotta Vaticana

Smith Y, Raju D, Nanda B, Pare J, Galvan A, Wichmann T. 2009. The thalamostriatal systems: anatomical and functional organization in normal and parkinsonian states. *Brain Research Bulletin* 78:60-8

Sofroniew M, Priestley J, Consolzaione A, Eckenstein F, Cuello A. 1985. Cholinergic projections from the midbrain and pons to the thalamus in the rat, identified by combined retrograde tracing and choline acetyltransferase immunohistochemistry. *Brain Research* 329:213-23

Song H, Ming G, Fon E, Bellocchio E, Edwards RH, Poo M. 1997. Expression of a putative vesicular acetylcholine transporter facilitates quantal transmitter packaging. *Neuron* 18:815-26

Sparenborg S, Gabriel M. 1992. Local norepinephrine depletion and learning-related neuronal activity in cingulate cortex and anterior thalamus of rabbits. *Experimental Brain Research* 92:267-85

Standaert D, Saper C, Rye D, Wainer B. 1986. Colocalization of atriopeptin-like immunoreactivity with choline acetyltransferase and substance P-like immunoreactivity in the pedunculopontine and laterodorsal tegmental nuclei in the rat. *Brain Research* 382:163-9

Stanton TL, Johnson GV. 1987. In vitro measurements of cholinergic activity in brain regions of hibernating ground squirrels. *Brain Research Bulletin* 18:663-7

Steininger TL, Rye DB, Wainer BH. 1992. Afferent projections to the cholinergic pedunculopontine tegmental nucleus and adjacent midbrain extrapyramidal area in the albino rat. I. Retrograde tracing studies. *Journal of Comparative Neurology* 321:515-43

Steriade M, Datta S, Paré D, Oakson G, Curró Dossi R. 1990a. Neuronal activities in brain-stem cholinergic nuclei related to tonic activation processes in thalamocortical systems. *Journal of Neuroscience* 10:2541-59

Steriade M, Jones E, McCormick D. 1997. *Thalamus*. New York: Elsevier

Steriade M, Paré D, Datta S, Oakson G, Curro Dossi R. 1990b. Different cellular types in mesopontine cholinergic nuclei related to ponto-geniculo-occipital waves. *Journal of Neuroscience* 10:2560-79

Suaud-Chagny MF, Chergui K, Chouvet G, Gonon F. 1992. Relationship between dopamine release in the rat nucleus accumbens and the discharge activity of dopaminergic neurons during local in vivo application of amino acids in the ventral tegmental area. *Neuroscience* 49:63-72

Sutin E, Jacobowitz D. 1990. Localization of substance P mRNA in cholinergic cells of the rat laterodorsal tegmental nucleus: *in situ* hybridization histochemistry and immunocytochemistry. *Cellular and Molecular Neurobiology* 10:19-31

Sziklas V, Petrides M. 2007. Contribution of the anterior thalamic nuclei to conditional learning in rats. *Hippocampus* 17:456-61

Takashina K, Bessho T, Mori R, Eguchi J, Saito K-I. 2008. MKC-231, a choline uptake enhancer: (2) Effect on synthesis and release of acetylcholine in AF64A-treated rats. *Journal of Neural Transmission* 115:1027-35

Tandon R, Shipley JE, Greden JF, Mann NA, Eisner WH, Goodson JA. 1991. Muscarinic cholinergic hyperactivity in schizophrenia. Relationship to positive and negative symptoms. *Schizophrenia Research* 4:23-30

Theirry A, Stinus L, Blanc G, Glowinski J. 1973. Some evidence for the existence of dopaminergic neurons in the rat cortex. *Brain Research* 50:230-4

Thierry A, Blanc G, Sobel A, Stinus L, Glowinski J. 1973. Dopaminergic terminals in the rat cortex. *Science* 182:499-501

Tomimoto H, Kamo H, Kameyama M, McGeer P, Kimura H. 1987. Descending projections of the basal forebrain in the rat demonstrated by the anterograde neural tracer *Phaseolus vulgaris* leucoagglutinin (PHA-L). *Brain Research* 425:248-55

Tribollet E, Bertrand D, Marguerat A, Raggenbass M. 2004. Comparative distribution of nicotinic receptor subtypes during development, adulthood, and aging: an autoradioraphic study in the rat brain. *Neuroscience* 12:405-20

Trulson ME, Preussler DW. 1984. Dopamine-containing ventral tegmental area neurons in freely moving cats: activity during the sleep-waking cycle and effects of stress. *Experimental Neurology* 83:367-77

Turrini P, Casu MA, Wong TP, De Koninck Y, Ribeiro-da-Silva A, Cuello AC. 2001. Cholinergic nerve terminals establish classical synapses in the rat cerebral cortex: synaptic pattern and age-related atrophy. *Neuroscience* 105:277-85

Umbriaco D, Watkins K, Descarries L, Cozzari C, Hartman B. 1982. Ultrastructural and morphometric features of the acetylcholine innervation in adult rat parietal cortex: an electron microscopic study in serial sections. *Journal of Comparative Neurology* 348:351-73

Umeda A, Torikata C, Takasugi T, Tanaka M, Yamaguchi K, Kanazawa M, Yoshida T. 1997. Displacement of gold marker in immunoelectron microscopy of human respiratory cilia. *Microscopy Research and Technique* 38:500-4

Uteshev V, Meyer E, Papke R. 2003. Regulation of neuronal function by choline and 4OH-GTS-21 through α7 nicotinic receptors. *Journal of Neurophysiology* 89:1797-806

Van der Kloot W. 2003. Loading and recycling of synaptic vesicles in the Torpedo electric organ and the vertebrate neuromuscular junction. *Progress in Neurobiology* 71:269-303

Van der Kloot W, Colasante C, Cameron R, Molgó J. 2000. Recycling and refilling of transmitter quanta at the frog neuromuscular junction. *Journal of Physiology* 523:247-58

Van der Kloot W, Molgó J, Cameron R, Colasante C. 2002. Vesicle size and transmitter release at the frog neuromuscular junction when quantal acetylcholine content is increased or decreased. *Journal of Physiology* 541:385-93

Vertes R. 2006. Interactions among the medial prefrontal cortex, hippocampus and midline thalamus in emotional and cognitive processing in the rat. *Neuroscience* 142:1-20

Vertes R, Hoover W, Do Valle A, Sherman A, Rodriguez J. 2006. Efferent projections of reuniens and rhomboid nuclei of the thalamus in the rat. *Journal of Comparative Neurology* 499:768-96

Vertes RP, Hoover WB. 2008. Projections of the paraventricular and paratenial nuclei of the dorsal midline thalamus in the rat. *Journal of Comparative Neurology* 508:212-37

Veznedaroglu E, Milner TA. 1992. Elimination of artifactual labeling of hippocampal mossy fibers seen following pre-embedding immunogold-silver technique by pretreatment with zinc chelator. *Microscopy Research and Technique* 23

Vincent S, Satoh K, Armstrong D, Fibiger H. 1983. Substance P in the ascending cholinergic reticular system. *Nature* 306:688-91

Vogelsberg V, Neff NH, Hadjiconstatntinov M. 1997. Cyclic AMP-mediated enhancement of high-affinity choline transport and acetylcholine synthesis in brain. *Journal of Neurochemistry* 68:1062-70

Vogt LJ, Vogt BA, Sikes RW. 1992. Limbic thalamus in rabbit: architecture, projections to cingulate cortex and distribution of muscarinic acetylcholine, GABAA, and opioid receptors. *Journal of Comparative Neurology* 319:205-17

Wada E, Wada K, Boulter J, Deneris E, Heinemann S, Patrick J, Swanson LW. 1989. Distribution of alpha2, alpha3, alpha4, and beta2 neuronal nicotinic receptor subunit mRNAs in the central nervous system: a hybridization histochemical study in the rat. *Journal of Comparative Neurology* 284:314-35

Wainer BH, Mesulam MM. 1990. Ascending cholinergic pathways in the rat brain. In *Brain Cholinergic Systems*, ed. M Steriade, D Biesold, pp. 63-119. New York: Oxford University Press

Wang B, Gonzalo-Ruiz A, Sanz J, Campbell G, Lieberman A. 1999. Immunoelectron microscopic study of γ–aminobutyric acid inputs to identified thalamocortical projection neurons in the anterior thalamus of the rat. *Experimental Brain Research* 126:369-82

Wang B, Yang L, Wang Z, Zheng H. 2007. Amyloid precursor protein mediates presynaptic localization and activity of the high-affinity choline transporter. *Proceedings of the National Academy of Sciences of the United States of America* 104:14140-5

Warburton EC, Aggleton JP. 1999. Differential deficits in the Morris water maze following cytotoxic lesions of the anterior thalamus and fornix transection. *Behavioural Brain Research* 98:27-38

Wecker L, Dettbarn W-D. 1979. Relationship between choline availability and acetylcholine synthesis in discrete regions of rat brain. *Journal of Neurochemistry* 32:961-7

Weiss F, Koob GF. 2001. Drug addiction: functional neurotoxicity of the brain reward systems. *Neurotoxicity Research* 3:145-56

Whiteaker P, Davies ARL, Marks MJ, Blagbrough IS, Potter BVL, Wolstenholme AJ, Collins AC, Wonnacott S. 1999. An autoradiographic study of the distribution of binding sites for the novel a7-selective nicotinic radioligand [3H]-methyllycaconitine in the mouse brain. *European Journal of Neuroscience* 11:2689-96

Wilcox K, Grant S, Burkhart B, Christoph G. 1989. *In vitro* electrophysiology of neurons in the lateral dorsal tegmental nucleus. *Brain Research Bulletin* 22:557-60

Williams JA, Comisarow J, Day J, Fibiger HC, Reiner PB. 1994. State-dependent release of acetylcholine in rat thalamus measured by in vivo microdialysis. *Journal of Neuroscience* 14:5236-42

Williams JA, Vincent SR, Reiner PB. 1997. Nitric oxide production in rat thalamus changes with behavioral state, local depolarization, and brainstem stimulation. *Journal of Neuroscience* 17:420-7

Wilson D, MacLaren D, Winn P. 2009. Bar pressing for food: differential consequences of lesions to the anterior versus posterior pedunculopontine. *European Journal of Neuroscience* 30:504-13

Wilson S, Argyropoulos S. 2005. Antidepressants and sleep: a qualitative review of the literature. *Drugs* 65:927-47

Winn P. 1998. Frontal syndrome as a consequence of lesions in the pedunculopontine tegmental nucleus: a short theoretical review. *Brain Research Bulletin* 47:551-63

Winn P. 2008. Pedunculopontine functions: are they motor, sensory, or integrative? *Parkinsonism and Related Disorders* 14:S194-S8

Wolf ME, Sun X, Mangiavacchi S, Chao SZ. 2004. Psychomotor stimulants and neuronal plasticity. *Neuropharmacology* 47 Suppl 1:61-79

Wolff M, Loukavenko EA, Will BE, Dalrymple-Alford JC. 2008. The extended hippocampal-diencephalic memory system: enriched housing promotes recovery of the flexible use of spatial representations after anterior thalamic lesions. *Hippocampus* 18:996-1007

Wonnacott S. 1997. Presynaptic nicotinic ACh receptors. *Trends in Neuroscience* 20:92-8

Woolf N, Gould E, Butcher L. 1989. Nerve growth factor receptor is associated with cholinergic neurons of the basal forebrain but not the pontomesencephalon. *Neuroscience* 30:143-52

Woolf NJ. 1991. Cholinergic systems in mammalian brain and spinal cord. *Progress in Neurobiology* 37:475-524

Woolf NJ, Butcher LL. 1986. Cholinergic systems in the rat brain: III. Projections from the pontomesencephalic tegmentum to the thalamus, tectum, basal ganglia, and basal forebrain. *Brain Research Bulletin* 16:603-37

Woolf NJ, Butcher LL. 1989. Cholinergic systems in the rat brain: IV. Descending projections of the pontomesencephalic tegmentum. *Brain Research Bulletin* 23:519-40

Wouterlood F, G. 2006. Combined fluorescence methods to determine synapses in the light microscope: multilabel confocal laser scanning microscopy. In *Neuroanatomical Tract-Tracing 3: Molecules, Neurons, and Systems*, ed. L Zaborszky, FG Wouterlood, JL Lanciego, pp. 395-435. New York: Springer

Xiao D, Zikopoulos B, Barbas H. 2009. Laminar and modular organization of prefrontal projections to multiple thalamic nuclei. *Neuroscience* 161:1067-81

Xu L, Ryugo D, Pongstaporn T, Johe K, Koliatsos V. 2009. Human neural stem cell grafts in the spinal cord of SOD1 transgenic rats: differentiation and structural integration into the segmental motor circuitry. *Journal of Comparative Neurology* 514:297-309

Xuereb JH, Perry EK, Candy JM, Bonham JR, Perry RH, Marshall E. 1990. Parameters of cholinergic neurotransmission in the thalamus in Parkinson's disease and Alzheimer's disease. *Journal of the Neurological Sciences* 99:185-97

Yamamura HI, Snyder SH. 1972. Choline: High-affinity uptake by rat brain synaptosomes. *Science* 178: 626-628

Yamamura HI, Snyder SH. 1973. High affinity transport of choline into synaptosomes of rat brain. *Journal of Neurochemistry* 21:1355-74

Yan Q, Johnson Jr. EM. 1989. Immunohistochemical localization and biochemical characterization of nerve growth factor receptor in adult rat brain. *Journal of Comparative Neurology* 290:585-98

Yasoshima Y, Scott T, Yamamoto T. 2007. Differential activation of anterior and midline thalamic nuclei following retrieval of aversively motivated learning tasks. *Neuroscience* 146:922-30

Yeomans JS. 1995. Role of tegmental cholinergic neurons in dopaminergic activation, antimuscarinic psychosis and schizophrenia. *Neuropsychopharmacology* 12:3-16

Yeomans JS, Mathur A, Tampakeras M. 1993. Rewarding brain stimulation: role of the tegmental cholinergic neurons that activate dopamine neurons. *Behavioral Neuroscience* 107:1077-87

Yun IA, Wakabayashi KT, Fields HL, Nicola SM. 2004. The ventral tegmental area is required for the behavioral and nucleus accumbens neuronal firing responses to incentive cues. *Journal of Neuroscience* 24:2923-33

Zahalka E, Seidler F, Lappi S, Yanai J, Slotkin T. 1993. Differential devlopment of cholinergic nerve terminal markers in rat brain regions: implications for nerve terminal density, impulse activity and specific gene expression. *Brain Research* 601:221-9

Zapata A, Capdevila JL, Trullas R. 2000. Role of high-affinity choline uptake on extracellular choline and acetylcholine evoked by NMDA. *Synapse* 35:272-80

Zhang J-H, Sampogna S, Morales FR, Chase MH. 2005. Age-related changes in cholinergic neurons in the laterodorsal and the pedunculo-pontine tegmental nuclei of cats: a combined light and electron microscopic study. *Brain Research* 1052:47-55

Zhao D, Frohman MA, Blusztajn JK. 2001. Generation of choline for actylcholine synthesis by phospholipase D isoforms. *Biomed Central Neuroscience* 2:16

Zhou F-m, Wilson C, Dani JA. 2003. Muscarinic and nicotinic cholinergic mechanisms in the mesostriatal dopamine systems. *The Neuroscientist* 9:23-36

Zoli M, Torri C, Ferrari R, Jansson A, Zini I, Fuxe K, Agnati LF. 1998. The emergence of the volume transmission concept. *Brain Research Reviews* 26:136-47